TR 3954-S

Propositions (Stellingen)

Switching Three-Phase Distribution Transformers with a Vacuum Circuit Breaker
Analysis of Overvoltages and the Protection of Equipment

Marjan POPOV

Delft University of Technology
12 November 2002

1. Reignition in the circuit breaker is a phenomenon that can occur for any type of circuit breaker under specific network conditions.

   Herontsteking in de vermogenschakelaar is een verschijnsel dat bij ieder type schakelaar kan optreden en wordt bepaald door de netwerkcondities.

2. It is often better to invest in means to protect the transformer from switching surges rather than to cure the consequences of a potential transformer failure.

   Het is vaak beter om te investeren in een middel om de transformator tegen schakeloverspanningen te beveiligen dan de gevolgen van mogelijke transformatoruitval te bestrijden.

3. The study of transients in power systems is important for the safety of equipment and the lifetime of the insulation.

   Het bestuderen van transiënte verschijnselen in elektriciteitsvoorzieningssystemen is belangrijk voor de veiligheid van de componenten en de levensduur van de isolatie.

4. It is impossible to study accurately electrical transients without the combination of an adequate simulation software and adequate physical insight.

   Het is onmogelijk transiënte elektrische verschijnselen nauwkeurig te bestuderen zonder de combinatie van de juiste simulatiesoftware en het juiste fysische inzicht.

5. In vacuum circuit breakers, the arc resistance has little influence on the transient recovery voltage generated by switching off small inductive currents.

De boogweerstand in de vacuümschakelaar is nauwelijks van invloed op de transiënte wederkerende spanning die ontstaat na het afschakelen van kleine inductieve stromen.

6. In the transformer complicated physical processes occur and therefore the interaction with the system is not unambiguous. Therefore each type of disturbance needs a dedicated transformer model.

   In de transformator spelen zich gecompliceerde fysische processen af en de interactie met het net is vaak niet eenduidig. Daarom is voor elk type verstoring een aangepast transformatormodel noodzakelijk.

7. To improve the world, start with your own country.

   Verbeter de wereld. Begin met je eigen land.

8. Today, the salary of the researchers in electrical engineering is often inversely proportional to the acquired knowledge.

   Tegenwoordig is het verdiende salaris van de onderzoekers vaak omgekeerd evenredig met de vergaarde elektrotechnische kennis.

9. Electrical power systems are more reliable than people.

   Elektriciteitsvoorzieningssystemen zijn betrouwbaarder dan mensen.

10. People should put their faith in technology rather than in politics.

    Het is verstandiger om in de techniek te geloven dan in de politiek.

11. While financial support to the developing countries should be the number one issue, the interference in the internal politics is usually on top of the agenda.

    Hoewel financiële steun aan ontwikkelingslanden hoog in het ambtelijk vaandel zou moeten staan, neemt de inmenging in de binnenlandse politiek meestal toch een hogere plaats op de agenda in.

12. Never abandon great problems, otherwise you will miss great solutions.

    Ga grote problemen nooit uit de weg, anders mis je de grote oplossingen.

13. People should spend more time and energy on developing their creativity and less on criticising.

    Mensen moeten meer tijd en energie besteden aan het ontwikkelen van hun creativiteit en minder aan het leveren van kritiek.

14. One should strive for the satisfaction in the work, not for the hope of success.

    Het geluk moet gezocht worden in het werk zelf en niet in het resultaat ervan.

3954
TR 3954 781395
3107287

Switching Three-Phase Distribution Transformers with a Vacuum Circuit Breaker

Analysis of Overvoltages and the Protection of Equipment

Marjan POPOV

Switching Three-Phase Distribution Transformers with a Vacuum Circuit Breaker

Analysis of Overvoltages and the Protection of Equipment

BIBLIOTHEEK TECHNISCHE UNIVERSITEIT
Prometheusplein 1
2628 ZC
DELFT

PROEFSCHRIFT

ter verkrijging van de graad van doctor
aan de Technische Universiteit Delft
op gezag van de Rector Magnificus Prof. dr. ir. J.T. Fokkema,
in het openbaar te verdedigen ten overstaan van een commissie,
door het College voor Promoties aangewezen,
op dinsdag 12 november 2002 te 13:30 uur
door

Marjan POPOV

Elektrotechnisch ingenieur, University St. Cyril and Metodius, Skopje
Magister, University St. Cyril and Metodius, Skopje

geboren te Kavadarci, Macedonië

Dit proefschrift is goedgekeurd door de promotor:
Prof. ir. L. van der Sluis

Samenstelling Promotiecommissie:
Rector Magnificus(Voorzitter, Technische Universiteit Delft)
Prof. ir. L. van der Sluis (promotor, Technische Universiteit Delft)
Prof. ir. W.L. Kling (Technische Universiteit Delft/Eindhoven, Tennet)
Prof. dr. eng. J.A. Ferreira (Technische Universiteit Delft)
Prof. dr. ir. R.P.P. Smeets (KEMA, Technische Universiteit Eindhoven)
Prof. ir. G.C. Damstra (Technische Universiteit Eindhoven)
Prof. dr. ir. D. van Dommelen (Katholieke Universiteit Leuven)
Dr. ir. G.C. Paap (Technische Universiteit Delft)
Prof. dr. J.J. Smit, reservelid (Technische Universiteit Delft)

ISBN 90-9016124-4
Copyright © 2002 by M. Popov
All rights reserved.

No part of the material protected by this copyright notice may be reproduced or utilized in any form or by any means, electronic or mechanical, including photocopying, recording or by any information storage and retrievals system, without permission from the author.

Printed by:

Offsetdrukkerij Ridderprint B.V., Ridderkerk

Delft University of Technology
Faculty of Electrical Engineering,
Power Systems Laboratory,
Mekelweg 4, 2628 CD Delft,
The Netherlands

Tel. 015 278 2870
Fax: 015 278 1182

To my wife Elizabeta,
our daughter Veronika and our parents

"The world, I think, will long have to wait for a mind equal to Nikola Tesla's, a mind of such creative possibilities and such wealth of imagination"

E.H. Armstrong

Contents

1 **Introduction** 1

1.1 The application of the vacuum circuit breaker in modern power systems . 1

1.2 Duties and concerns 2

1.2.1 General network description 7

1.3 Overview of earlier research work 10

1.4 Aim of this work 12

1.5 Alternative Transient Program (ATP) 13

1.6 Outline of this Dissertation 19

2 **Modelling reignitions in vacuum circuit breakers** **23**

2.1 Introduction 23

2.2 Modelling circuit breaker reignitions 30

2.2.1 Description of the vacuum arc 30

2.2.2 Reignition in vacuum 31

2.3 Circuit breaker model 36

2.3.1 Chopping current 36

2.3.2 Dielectric and quenching capability 38

2.3.3 Modelling reignitions by taking into account the arc resistance . . 40

2.3.4 An algorithm for the vacuum circuit breaker 42

2.4 Simulation in a single-phase circuit 44

2.5 Analytical analysis of the reignition overvoltages 49

2.6 Conclusion 53

3 Modelling of the Supply Network 55
3.1 Introduction 55
3.2 Busbars 55
3.3 Cable Modelling 56

3.4 Single-phase cable model 59
3.5 Investigation of the cable's frequency dependency 65
3.6 Three-phase cable modelling 71
3.7 Conclusion 72

4 Transformer modelling 75
4.1 Introduction 75
4.2 A terminal impedance transformer model 79
4.3 The three-phase transformer model 83
4.4 The influence of the magnetic core 89
4.4.1 The theory behind the Jiles model 89
4.4.2 The application of the JM for calculating overvoltages after chopping 91
4.5 Conclusion 95

5 Modelling surge arresters and surge suppressors 98

5.1 Introduction 98
5.2 Surge arrester models for protection against fast surges 99
5.2.1 General properties of the metal-oxide surge arrester 99
5.2.2 A model of an arrester disk for fast surges 101
5.2.3 The IEEE surge arrester model 102
5.2.4 Generalised arrester model 106
5.2.5 The simplified IEEE arrester model 108
5.3 Developing an arrester model 108
5.3.1 The impulse function for the representation of the current sources 109
5.3.2 Modelling a surge arrester 111
5.4 Other methods for equipment protection 118

5.5 Conclusion 121

6 **Switching off an unloaded transformer** **123**

6.1 Description of the problem 123

6.2 A statistical approach to the estimated overvoltages 126

6.3 Investigation of the switching overvoltages 128

6.4 Protection of transformers against switching surges 137

6.4.1 Surge arresters connected phase-to-ground 137

6.4.2 Surge arresters connected between phases and phase-to-ground . . 138

6.4.3 R-C branch as a protective device 139

6.5 Conclusion 141

7 **Calculation of the Probability of Reignition** **143**

7.1 Introduction 143

7.2 Influence of the circuit parameters 144

7.2.1 Probability of a reignition 144

7.3 Computation methodology 146

7.3.1 Results 147

7.4 Determination of the overvoltage curves 155

7.5 Conclusion 160

8 **General Conclusions and Future Possible Work** **161**

8.1 Conclusion 161

8.2 Suggestions for future work 163

A **Statistical variation of the breaker parameters** **165**

B **Comparing different breaker models** **167**

Bibliography 173

List of published papers 182

Summary 183

Summary in Dutch 185

Summary in Macedonian 187

Acknowledgements 189
Curriculum vitae 191
Curriculum vitae in Macedonian 193

List of Figures

1-1 Description of the process of multiple reignition in a vacuum circuit breaker 4

1-2 Single-line diagram of a load supply network 8

1-3 Equivalent networks for R, L, C and lossless line 16

1-4 Description of the network connection 18

2-1 Size reduction of a 15 kV, 12 kA Vacuum Circuit Breaker between 1967 and 1995 [78] 24

2-2 Total number of medium voltage circuit breakers in operation in the world between 1980 and 2000 25

2-3 Survey of the chopping phenomena in a single-phase circuit 26

2-4 An induction motor for studying reignitions [15, 46] 32

2-5 Circuit breaker current when contacts open at 150 μs before current zero for the circuit in Figure 2-4 33

2-6 Reignition voltage when contacts open 150 μs for the circuit in Figure 2-4; upper trace: TRV; lower trace: load side voltage 33

2-7 Circuit breaker current when contacts open 250 μs before current zero for the circuit in Figure 2-4 34

2-8 Reignition voltage when contacts open 250 μs before current zero for the circuit in Figure 2-4; upper trace: TRV; lower trace: load side voltage . . 34

2-9 Arc voltage and post-arc current for different arc and load current . . . 40

2-10 Arc resistance calculated by the breaker's voltage and current 41

2-11 The ATP-EMTP circuit breaker model 42

2-12 Flow chart of the circuit breaker's reignition modelling 43

2-13 Single-phase circuit for reignition study 45

2-14 Simulated reignited current (upper trace) and voltage across the breaker contacts (lower trace) for the circuit in Figure 2-13 46
2-15 Simulated voltage (upper trace) and current (lower trace) at the load side for the circuit in Figure 2-13 47
2-16 Simulated reignited current (upper trace), voltage across the breaker contacts (middle trace) and load side voltage (lower trace) for the circuit in Figure 2-13 during the first reignition 47
2-17 Zoomed values of the last three current reignitions, circuit breaker voltage and load side voltage from Figure 2-14 48
2-18 An analytical calculation of reignitions a) Sample circuit for computation reignitions; b) Part of the circuit that determines the high frequency component 49
2-19 Calculated circuit breaker current (upper trace), circuit breaker voltage (upper middle trace), load side voltage (lower middle trace) and load side current (lower trace) from Figure 2-18a 50
2-20 Description of the first two reignitions from Figure 2-19; circuit breaker current (upper trace); circuit breaker voltage (middle trace); load side voltage (lower trace) 51
2-21 Calculated circuit breaker current (upper trace), circuit breaker voltage (upper middle trace), load side voltage (lower middle trace) and load side current (lower trace) from Figure 2-18a 51
2-22 Description of the first two reignitions from Figure 2-21; circuit breaker current (upper trace); circuit breaker voltage (middle trace); load side voltage (lower trace) 52

3-1 Cable system for busbar response testing 57
3-2 Switch current at the busbar from Figure 3-1 57
3-3 Voltage response at the load from Figure 3-1 58
3-4 Cable with a *RLC* load 61
3-5 Voltage at the receiving end of the cable from Figure 3-4 61
3-6 Current at the sending end of the cable from Figure 3-4 62
3-7 Phasor representation of the cable dielectric losses 62

3-8 Equivalent circuits for lossy capacitors 63

3-9 Lumped element representation of a single-phase cable Π-section 63

3-10 Comparison between voltage at the receiving end of the cable from Figure 3-4 with upgraded Π-section model 64

3-11 Cross section of a single-phase cable 66

3-12 Frequency scan of a single-phase cable 67

3-13 Test circuit for a voltage response study of the sending and receiving end of cable 2 67

3-14 Frequency response of the impedance amplitude and phase characteristic of a cable - receiving end open according to Figure 3-12 68

3-15 Frequency response of the impedance amplitude and phase characteristic of a cable - receiving end shorted to earth according to Figure 3-12 . . . 68

3-16 Comparison of the voltages at the sending end of cable 2 in Figure 3-13 when using ATP- and Π-section model 69

3-17 Comparison of the voltages at the receiving end of cable 2 in Figure 3-13 when using ATP- and Π-section model 69

3-18 Model for an unshielded three-phase cable 71

3-19 Position of the cable in soil 72

4-1 Foster circuit for representing the transformer charcteristic 81

4-2 Calculated and measured amplitude and phase characteristics of a 144 MVA, 230/16 kV generator step up transformer 83

4-3 Transformer model over a wide frequency range 85

4-4 Measured and calculated transformer magnetising curve 86

4-5 Terminal amplitude and phase characteristic of the studied transformer . 87

4-6 Approximation of the eddy current losses for a) frequency-dependent core losses; b) constant core losses 87

4-7 Comparison between the parameters of the core model with constant losses and frequency-dependent losses; upper trace: equivalent inductance of the core; lower trace: equivalent resistance of the core 88

4-8 Calculated steady-state hysteresis loops 90

4-9 A representation of a single-phase transformer circuit for low frequency transients . . . 92

4-10 Calculated and simulated magnetising current and magnetic flux for the circuit in Figure 4-9 . . . 93

4-11 The magnetising current and terminal voltage after de-energising a single-phase transformer for the circuit in Figure 4-9 . . . 93

4-12 The magnetic flux after de-energising a single-phase transformer for different types of hysteresis for the circuit in Figure 4-9 . . . 94

4-13 The magnetic fluxes (upper trace), magnetising currents in the leakage impedance (middle trace) and terminal voltages (lower trace) after de-energising a three-phase transformer . . . 94

5-1 Equivalent circuit of a disc of metal-oxide surge arrester . . . 100

5-2 Typical volt-ampere characteristic of an arrester at different temperatures (θ) . . . 101

5-3 Arrester model from *Schmidt* et al. [78] . . . 102

5-4 IEEE Frequency-dependent arrester model . . . 104

5-5 Volt-ampere relationship of a 20 kV ZnO arrester . . . 105

5-6 Volt-ampere relationship of a 20 kV ZnO arrester . . . 105

5-7 A general frequency-dependent metal-oxide arrester model . . . 107

5-8 Model by *Pinceti* and *Giannettoni* [59] . . . 107

5-9 General form of a surge current impulse 10 kA, 8/20 μs . . . 110

5-10 Current impulses with different shape for the parameter values in Table 5.2 112

5-11 A simplified surge arrester model . . . 113

5-12 Measured characteristic of an arrester with the parameters in Table 5.3 . 115

5-13 Response of the arrester (Table 5.3) after excitation by front-of-wave current impulses 0.5 μs . . . 115

5-14 Response of the arrester (Table 5.3) after excitation by a current impulse 1/5 μs . . . 116

5-15 Response of the arrester (Table 5.3) after excitation by a current impulse 8/20 μs . . . 116

5-16 Response of the arrester (Table 5.3) after excitation by a current impulse 30/60 μs . . . 117
5-17 Dynamic voltage-current characteristic for current impulses 0.5/3 μs and 8/20 μs . . . 117
5-18 Examples of surge suppression circuits . . . 119

6-1 System configuration for studying transients . . . 124
6-2 Calculated transformer inrush currents for the system in Figure 6-1, upper trace: initial phase 0^0, lower trace: initial phase 30^0 . . . 125
6-3 Calculated transformer magnetising currents for the system in Figure 6-1 125
6-4 Possible switching instants during the existence of inrush currents; It describes the first period for the currents shown in Figure 6-2 . . . 127
6-5 A histogram of the distribution of switching surge overvoltages . . . 127
6-6 Calculated transformer terminal and phase-to-phase voltages for the system in Figure 6-1 (the circuit breaker model is A_1 and the cable length is 30 m) . . . 128
6-7 Calculated transformer terminal voltages and phase-to-phase voltages for the system in Figure 6-1 (the circuit breaker model is A_2 and the cable length is 10 m) . . . 129
6-8 Cumulative occurrence of overvoltages during magnetising current switching for the system in Figure 6–1 (model A_2) for different cable lengths. . 130
6-9 Transformer terminal voltages during the inrush current switching for the system presented in Figure 6-1 with the breaker model B; upper trace: voltage in phase R; middle trace: voltage in phase S; lower trace: voltage in phase T . . . 131
6-10 Transformer terminal voltages during inrush current switching for the system in Figure 6-1 with the breaker model A_1; upper trace: voltage in phase R; middle trace: voltage in phase S; lower trace: voltage in phase T . . . 132
6-11 Transformer terminal voltages during inrush current switching for the system in Figure 6-1 with the breaker model A_2; upper trace: voltage in phase R; middle trace: voltage in phase S; lower trace: voltage in phase T . . . 133

6-12 Cumulative occurrence of the maximal overvoltage during inrush current switching for the system in Figure 6-1 for different cable lengths; the switching instants are randomly chosen within interval T_1 (Figure 6-4); circuit breaker model B 134

6-13 Cumulative occurrence of the maximal overvoltage during inrush current switching for the system in Figure 6-1 for different cable lengths; the switching instants are randomly chosen within interval T_1 (Figure 6-4); circuit breaker model A_1 134

6-14 Cumulative occurrence of the maximal overvoltage during inrush current switching for the system in Figure 6-1 for different cable lengths; the switching instants are randomly chosen within interval T_1 (Figure 6-4); circuit breaker model A_2 135

6-15 Cumulative occurrence of the maximal overvoltage during inrush current switching for the system in Figure 6-1 for different cable lengths; the switching instants are randomly chosen within the interval of the first period (Figure 6-4); circuit breaker model A_1 135

6-16 Cumulative occurrence of the maximal overvoltage during inrush current switching for the system in Figure 6-1 for different cable lengths; the switching instants are randomly chosen within the interval of the first period (Figure 6-4); circuit breaker model A_2 136

6-17 Cumulative occurrence of the maximal overvoltage during inrush current switching for the system in Figure 6-1 for different cable lengths; the switching instants are randomly chosen within the interval of the first period (Figure 6-4); circuit breaker model B 136

6-18 A way of protecting transformers against voltage surges 137

6-19 Simulation of the arrester effect when arresters are installed only phase-to-ground during inrush current switching for the system in Figure 6-1; upper trace: voltage in phase R; middle trace: voltage in phase S; lower trace: voltage between phases R and S 138

6-20 Simulation of the arrester effect when arresters are installed phase-to-ground and between each two phases during inrush current switching for the system in Figure 6-1; upper trace: voltage in phase R; middle trace: voltage in phase S; lower trace: voltage between phases R and S 139

6-21 The variation of the suppressed voltage when using R-C circuit during inrush current switching for the system in Figure 6-1 and for different values of the protective capacitors 140

6-22 The variation of the suppressed voltage when using R-C circuit during inrush current switching for the system in Figure 6-1 and for different values of the protective capacitors 140

6-23 Calculated suppression factor for different parameters of R and C 141

7-1 Time window of a reignition in relation to current chopping and the TRV 145

7-2 Standard motor circuit according to IEC 61233 145

7-3 Flow chart for reignition probability computation 147

7-4 Probability of total reignition P_{reig} as a function of the motor power and the cable length; the slope of the recovery curve is 20 V/μs and the chopping current is 3 A 148

7-5 Probability of total reignition P_{reig} as a function of the motor power and the cable length; the slope of the recovery curve is 20 V/μs and the chopping current is 3 A 149

7-6 Probability of reignition with a VCC P_{VCC} as a function of the motor power and the cable length; the slope of the recovery curve is 20 V/μs and the chopping current is 3 A 149

7-7 Probability of reignition with a VCC P_{VCC} as a function of the motor power and the cable length; the slope of the recovery curve is 20 V/μs and the chopping current is 3 A 150

7-8 Probability of total reignition P_{reig} as a function of the motor power and the cable length; the slope of the recovery curve is 50 V/μs and the chopping current is 3 A 150

7-9 Probability of reignition with a VCC P_{VCC} as a function of the motor power and the cable length; the slope of the recovery curve is 50 V/μs and the chopping current is 3 A 151
7-10 Probability of total reignition P_{reig} as a function of the motor power and the cable length; the slope of the recovery curve is 20 V/μs and the chopping current is 5 A 151
7-11 Probability of total reignition P_{reig} as a function of the motor power and the cable length; the slope of the recovery curve is 20 V/μs and the chopping current is 5 A 152
7-12 Probability of reignition with the VCC P_{VCC} as a function of the motor power and the cable length; the slope of the recovery curve is 20 V/μs and the chopping current is 5 A 152
7-13 Probability of reignition with the VCC P_{VCC} as a function of the motor power and the cable length; the slope of the recovery curve is 20 V/μs and the chopping current is 5 A 153
7-14 Probability of total reignition P_{reig} as a function of the motor power and the cable length; the slope of the recovery curve is 50 V/μs and the chopping current is 5 A 153
7-15 Probability of reignition with the VCC P_{VCC} as a function of the motor power and the cable length; the slope of the recovery curve is 50 V/μs and the chopping current is 5 A 154
7-16 Probability of total reignition (solid line) P_{reig} and the reignition with the VCC (dashed line) P_{VCC} as a function of the chopping current and the cable length; the slope of recovery curve is 30 V/μs and the motor power is 200 kW 154
7-17 The geometrical place of the combination between cable length and motor power resulting in an overvoltage of 3 p.u. or 5 p.u. 155
7-18 The geometrical place of the combination between cable length and motor power resulting in an overvoltage of 3 p.u. or 5 p.u. 156
7-19 The geometrical place of the combination between cable length and motor power resulting in an overvoltage of 3 p.u. or 5 p.u. 158

7-20 The geometrical place of the combination between cable length and motor power resulting in an overvoltage of 3 p.u. or 5 p.u. 158

7-21 The geometrical place of the combination between cable length and motor power resulting in an overvoltage of 3 p.u. or 5 p.u. 159

7-22 The geometrical place of the combination between cable length and motor power resulting in an overvoltage of 3 p.u. or 5 p.u. 159

A-1 Normal distribution of the withstand voltage 166

B-1 Three-phase system configuration used for the vacuum circuit breaker model validation 167

B-2 Representation of the motor by a lumped element 168

B-3 Voltage at the motor terminals for the system in Figure B-1 170

B-4 Current through the circuit breaker for the system in Figure B-1 using model A 170

B-5 Current through the circuit breaker for the system in Figure B-1 using model B 171

B-6 Reignited breaker's currents for models *A* and *B* for the system in Figure B-1; upper trace: Phase R; middle trace: Phase S; lower trace: Phase T . 171

B-7 Motor voltages for models *A* and *B*; upper trace: voltage in phase R; middle trace: voltage in phase S; lower trace: voltage in phase S 172

B-8 Motor terminal voltage in phase R from Figure B-7 (last three reignitions) 172

List of Tables

1.1 Relation between circuit breaker and disconnector performance and frequency interval 9

2.1 Chopping current constants 37
2.2 Characteristics parameters according to equation (2.5) 39
2.3 Circuit data 45

3.1 Data for a 20 kV cable, NA2XS2Y 66

4.1 Transformer models for different frequency intervals 78
4.2 Equivalent parameters for transformer measured characteristic from Figure 4-2 82
4.3 Equivalent parameters for transformer characteristic of Figure 4-5 84
4.4 Circuit and model parameters for the Jiles model 91

5.1 Volt-ampere characteristic for A0 and A1 with respect to Figure 5-5 and Figure 5-6 104
5.2 Calculated parameters for the Heidler function 111
5.3 Measured volt-ampere characteristic of 12 kV ZNO surge arrester 113
5.4 Calculated and measured residual voltages 113

6.1 Transformer data 124

B.1 Parameters for the system components 168
B.2 Calculated maximum overvoltages 169

List of Abbreviations

ATP - Alternative Transient Program
ANSI - American National Standard Institute
BIL - Basic Insulation Level
EMTP - Electro Magnetic Transient Program
IEC - International Electrotechnical Commission
IEEE - Institute of Electrical and Electronics Engineers
JM - Jiles Model
MCOV - Maximal Continuous Overvoltage
NSDD - Non-Sustained Disruptive Discharge
TACS - Transient Analysis Control System
MODELS - Newer TACS
SF6 - Sulphur Hexafluoride
TRV - Transient Recovery Voltage
VCC - Virtual Current Chopping

Chapter 1

Introduction

1.1 The application of the vacuum circuit breaker in modern power systems

For more than a hundred years, the circuit breaker has been one of the most important devices for the protection of power transmission and distribution systems, where the principle of arc extinguishing as an interrupting medium is used for current interruption. The history of the circuit breaker's technology starts with the early designs of circuit breakers which simply use air as a medium for arc interruption. The beginning of the 20th century was the period of air-blast forced cooling and oil-filled circuit breakers. Since the 1950s, the revolutionary development of SF6 and vacuum designs of circuit breaking has been in use. This implies a reduction of the volume of the chamber and improvement of the dielectric characteristics with respect to the first switching devices. Today, SF6 and vacuum circuit breakers represent almost 90% of the world market for high voltage and medium voltage switching equipment. For high and very high voltage levels, gas- and oil-insulated circuit breakers are still irreplaceable whereas in medium voltage power supply systems, vacuum switching devices dominate all power switching functions. Today, for example in Japan, vacuum circuit breakers command almost 80% of the medium voltage switchgear market.

Vacuum circuit breakers are used almost exclusively for medium voltage levels up to 36 kV. This restriction is due to the fact that the dielectric withstand performance of vacuum circuit breakers increases modestly with the contact gap. This implies that for voltages of 72 kV and above either a large contact gap must be used or a number of interrupters in series. The first solution is not applicable due to the difficult mechanical design, whilst the second results in an uneconomic cost increase. Vacuum circuit breakers are regularly used throughout the normal range of applications of the distribution switchgear for utility or industrial use. In addition, however, their specific properties of a high electrical and mechanical lifetime and inherent safety are the reasons why vacuum circuit breakers are also used in hardly accessible and hazardous applications. For example, an electric arc melting furnace with ratings up to 100 MVA makes a severe demand on the associated circuit breakers. Falling scrap in the melt causes frequently short circuits between the electrodes and the current to be switched can be up to 1.8 times the rated current of the arc furnace transformer. The frequency of switching might be about 50 to 80 times per day with currents up to 2 kA. The high electrical life and the general durability of vacuum circuit breakers make them particularly suitable for this application. Furthermore, they are used in AC traction systems where electric railway systems normally operate between 15 kV and 27.5 kV at frequencies of 50 Hz, 60 Hz or a $16\frac{2}{3}$ Hz. Here the circuit breaker must be capable of clearing frequently (often transient) short circuits extremely quickly. The rate of rise of the recovery voltage can be significantly steeper than that in most distribution circuits and the circuit breakers must also be able to clear out-of-phase fault conditions. For applications on a ship, the switching elements must be capable of operating at various horizontal positions and must also be resistant to vibrations. Sometimes, the requirements for switchgear involve not only the ability to withstand the frequency of operation, but also require safe manipulation of the equipment. The absence of flammable components and pressurised gas ensures that risk to personnel is minimal, and combined with the lack of fire or explosion risk makes the use of vacuum circuit breaker attractive.

1.2 Duties and concerns

The purpose of any circuit breaker is to open and close the circuit under fault conditions as well as to modify the configuration of the system under normal operating conditions.

During most of its life, the circuit breaker contacts are in closed position, so they must be able to carry currents under normal and under fault condition. The potential problem here is a thermal one and a circuit breaker can become thermally overloaded. Switching equipment experiences high currents under fault conditions, which they have to interrupt or not. In any case they must be able to withstand these currents.

A typical fault current is asymmetrical and consists of an exponentially decaying DC component and an AC component. The degree of asymmetry depends on the instant when the fault occurs. Under the most unfavourable condition the peak fault current can be nearly twice the symmetrical AC fault current peak. When we realise that the electromagnetic forces are proportional with the square of the current, the peak forces for a fully asymmetrical current are nearly four times as high as for a symmetrical single-phase current. If the fault occurs in a circuit with a very high time constant, the duration of these forces will be longer than usual. The task of a circuit breaker is to change rapidly from an ideal conductor to an ideal insulator. After a current interruption, the contact gap is subjected to an electrical stress called the transient recovery voltage (TRV). In medium and high voltage networks, the short-circuit currents are inductive in the majority of the cases and lag the voltage at nearly 90^0. Thus, when the current is interrupted, the supply voltage is at its peak. The TRV has a frequency in the range of kHz, and a rate of rise depending on the interrupted current and system configuration of a few tens of kV/μs. The circuit breaker must withstand this TRV, otherwise a reignition occurs. When the circuit breaker interrupts small inductive currents like in unloaded transformers, induction motors or reactors, the arc becomes unstable before the power frequency current zero, and the arc current can be forced to an early current zero. This means that the arc has no longer sufficient energy to create charge carriers and the arc extinguishes before the power frequency current zero. The current decays extremely fast, and we say that the current is 'chopped' because it declines toward zero with a slope of about 100 A/μs. Particularly for the vacuum circuit breakers, the chopping current typically has a value between 3 A and 8 A, and under specific switching conditions, it can lead to very severe switching overvoltages. The latest developments in vacuum technology succeeded to limit the chopping current to a value below 3 A. The value of the chopping current of vacuum switching devices depends mainly on the contact material and less on the circuit conditions. When the chopping current of the vacuum circuit breaker is so low that the overvoltages are minimal and less than the withstand voltage level, a successful interruption of the current is achieved. The switching of inductive loads like motor and unloaded transformer circuits can have three potential sources of overvoltage:

- chopping overvoltages,
- multiple reignition overvoltages and
- overvoltages caused by virtual current chopping.

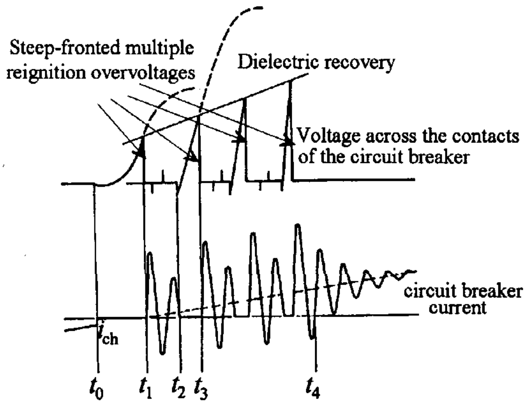
Steep-fronted multiple reignition overvoltages
Dielectric recovery
Voltage across the contacts of the circuit breaker
circuit breaker current
i_{ch}
t_0
t_1
t_2
t_3
t_4

Figure 1-1: Description of the process of multiple reignition in a vacuum circuit breaker

The chopping overvoltage results after a chopping current has cleared and is proportional to the value of the chopping current. This can be seen in Figure 1-1. The moment t_0 denotes the moment when the current chops. The rate of rise of TRV is higher than the recovery of the dielectric strength of the vacuum gap. When the contacts open near the power frequency current zero, even a low TRV can cause a reignition and a high frequency reignited current flows in the circuit breaker. These moments when a reignition occurs are denoted as t_1 and t_3. Due to the high clearing ability of the vacuum circuit breaker, the high frequency current is interrupted in one of the current zeros (moment t_2). When the high frequency current is cleared, the TRV starts building up again but now with a steep du/dt with a frequency in the range of the interrupted high frequency current.

Again a reignition occurs, and the TRV escalates. The final scenario can be successful or unsuccessful arc clearing. If the arc is not cleared, the 50 Hz current is re-established and the arc will be cleared in the next current zero. The moment of re-establishing the 50 Hz current in the circuit breaker is represented by the moment t_4.

When stalled motors are switched, the source of steep overvoltage are *multiple reignitions.* For a running induction motor, when it is first disconnected from the source, the rotor remains running for a while and due to its inertia the speed gradually reduces to zero. In this interval, the stator conductors continue to cut the residual flux and a voltage is induced in the stator windings. The frequency of the induced voltage drops from the power frequency to zero. During the relatively short period when the contacts separate, the voltages on both sides of the breaker do not change significantly in magnitude and the TRV increases slowly. Other factors which reduce the TRV are the losses of the real power load of the motor. From the instant when the vacuum circuit breaker contacts begin to part, the withstand voltage of the gap increases as the gap widens. If the recovery speed of the gap insulation is greater than the rate of rise of the TRV, there is no chance of reignition during opening. In general, the possibility of a high TRV while interrupting a running motor is rather small.

But, in the case of abnormal switching such as interrupting a motor at start-up, that is at the time when the rotor is just barely moving, high overvoltages can occur. This case is rather unusual but it does occur. It can happen due to an improper relay tripping or when a motor fault occurs during operation of the vacuum circuit breaker. The interruption of the inrush currents means that the vacuum circuit breaker faces a current 5 to 7 times the rated current of the motor. This is an almost pure inductive current and at the instant of interruption, when the power frequency current goes to zero, the source voltage is almost at its peak value. Immediately following the extinction of the arc, the voltages on both sides of the circuit breaker begin to oscillate. At the source side, the situation is similar to that occurring after interruption of a running motor, except that the voltage oscillation is around the full peak value instead of a part of it. At the motor side, the voltage oscillation is significantly different from that during interruption of a running motor. Because of the nearly stationary rotor, there is little induced voltage in the stator windings. The voltage at the motor terminals is caused by energy exchanges in the circuit between the motor and the circuit breaker, and can become twice the peak value of the nominal voltage. It contains different frequencies depending on the circuit components. In many cases the dominant frequency is considerably higher than the power frequency. Such a high frequency voltage component causes a rapid change of the TRV at the vacuum circuit breaker contacts. Often the gap fails to withstand this rapidly increasing voltage and a reignition occurs. After the reignition, both the power frequency and the high frequency current flow through the plasma channel between the contacts. In three-phase circuits, where there exist a (strong) mutual inductive and capacitive coupling, under certain conditions, the reignition of the current that is cleared in one phase can cause forced current chopping in the other two phases. This phenomenon is known as *virtual current chopping* (VCC) and sometimes it is a huge problem in low inductive current circuits. The overvoltages due to VCC are theoretically 50 - 60 times the nominal voltage. Of course, the equipment cannot withstand such a voltage and the insulation will fail at values which are far below this value. In such cases, surge arresters are applied to limit overvoltages.

Overvoltages due to VCC are characterised by their amplitude. Overvoltages due to multiple reignitions are much lower but very steep. Transformer or motor insulation frequently exposed to multiple reignitions can deteriorate and even fail. The impulse voltage withstand characteristics of the insulation are defined as a function of the surge rise time. Thus, for example for 6.6 kV motors, the maximum allowable rise time of the surge is 0.2 μs at 10.8 kV (2 p.u.) and 5 μs at 25.1 kV (4.6 p.u.) [68]. This implies that even overvoltages with small magnitudes can be dangerous and therefore protective measures against these overvoltages should also be considered.

These phenomena also take place for three-phase loaded and unloaded transformers. The steady-state magnetising currents are normally less than the chopping level of the vacuum circuit breaker, so the chopping occurs instantaneously. Reignition is possible and is governed by similar conditions as for the motor circuit. However, the high transformer losses and non-linearity of the transformer core mitigates the oscillations to lower overvoltage magnitudes. The chance that overvoltages are generated due to VCC does not exist because the magnetising currents are chopped at once. That is the reason why switching of motors and transformers under normal operating conditions is less of a problem.

When energising a load, whether by a vacuum circuit breaker or another type of breaker, prestrikes occur. This means that the current in the circuit is established by an arc before the contacts physically touch each other. After a prestrike, especially when energising a capacitive load like a capacitor bank or an unloaded cable, currents of high frequency can flow and a multiple reignition can occur when they are interrupted.

The behaviour of the circuit breaker depends on the frequency of the studied transients. Also the behaviour of the circuit breaker depends on the amplitude of the current to be switched. For high current arcs, a significant parameter is the post-arc current, but for a low current interruption this parameter does not play a significant role. The relation between closing and opening operations of circuit breakers and disconnectors, and the frequency interval is shown in Table 1.1.

1.2.1 General network description

The supply network wherein the transients oscillate due to vacuum circuit breaker operations consists of busbars, feeder cables, circuit breakers, loads (like unloaded or loaded transformers and motors), protective devices and source. A general system structure can be found in the single-line diagram of Figure 1-2. The transformer supplies the substation with electric power by a cable. The system can have more connections via transmission lines and instrument transformers, and capacitive banks can also be connected. They are not represented in the circuit because these elements hardly influence the high frequency transients while they exist from local oscillations and are not affected by the travelling waves. In this research, the effects of the part of the network beyond the primary side of the transformer are neglected: The source is considered to be an ideal voltage source. This is justified since in practice the effective capacitance of the main bus is rather large compared to the capacitances of the other buses with cables, transformers, motors etc. Another fact is that in practice, the length of the supply cable is greater than the length of the cable that is switched so that for the first few cycles of high frequency current, the effect of the main bus does not play a significant role. The configuration of the system differs depending on the layout of the substation or the industrial object which consists

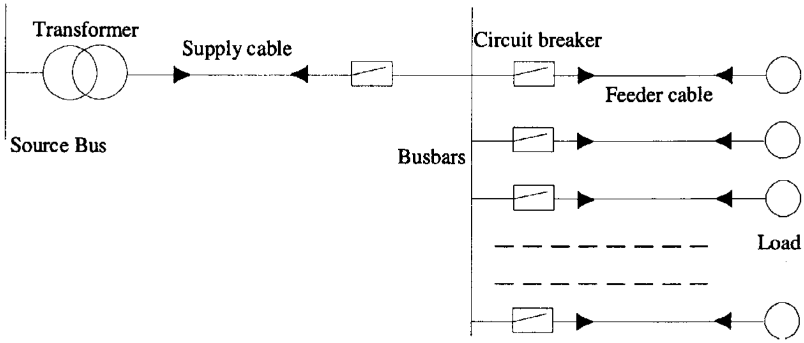

Figure 1-2: Single-line diagram of a load supply network

of different types of loads. In practice, the length of the substation busbars are between several meters and a few tens of meters. The length of the main busbars between two adjacent feeder connections is one or two meters. The load can, however, differ, take for example AC induction motors, which are mostly used as primary drives in many applications (water pumps, fans, compressors and so forth). Their power rating varies from a few hundreds of kVA up to a few MVA. The characteristic impedance of motors is determined by their geometrical dimensions, coil structure and winding connections [89]. These parameters determine the load inductances and capacitances. Transformers are loads with a rather complex structure because they can operate under different conditions: steady-state and transient condition, loaded an unloaded. In all these different types of operation, the transformer behaves differently when the load is switched by a circuit breaker. The transformers cover a large range in power rating. For instance, for feeding an arc furnace, the transformers have a power rating of several tens of MVA and are subjected to many switching operations per day.

Table 1.1: Relation between circuit breaker and disconnector performance and frequency interval

Circuit breakers and disconnectors	*Interval 1:* 0.1 Hz÷3 kHz	*Interval 2:* 50/60 Hz÷20 kHz	*Interval 3:* 10 kHz÷3 MHz	*Interval 4:* 100 kHz÷50 MHz
		Closing		
Mechanical pole spread	Important	Very important	Negligible	Negligible
Prestrike effect	Negligible	Important	Important	Very important
		Opening		
High current interruption (arc equation)	Important for interruption capability studies	Important for interruption capability studies	Negligible	Negligible
Current chopping (arc instability)	Negligible	Important for the interruption of small inductive currents	Important for the interruption of small inductive currents	Negligible
Reignition effect	Negligible	Important for the interruption of small inductive and capacitive currents	Very important	Very important
HF current interruption	Negligible	Important for the interruption of small inductive and capacitive currents	Very important	Very important
NSDD	Negligible	Negligible	Negligible	Important

1.3 Overview of earlier research work

A considerable amount of work has been done on the investigation of physical phenomena regarding the vacuum current interruption and vacuum arc circuit interaction. The large-scale application of vacuum circuit breakers, and the effect that the vacuum circuit breaker has when switching special network configurations boosted research in the past decades. In the early 1960s, when the first generation of vacuum circuit breakers was in use, the research was mainly focussed on the high chopping current level of the circuit breakers. The research work performed by *Greenwood* [34] explains how this chopping current reacts with transformer and motor circuits. Research on chopping current behaviour was performed in the late 1980s when *Czarnecki* and *Lindmayer* [14, 15, 16] made a study on the influence of contact material on the interrupting performance of the breaker around current zero. A very important result was an expression for the value of the chopping current. This was not easy at all, especially because of the statistical performance of the chopping current in vacuum. Research performed by *Gibbs* et al. [28, 29] and *van den Heuvel* and *Damstra* [88] compares the chopping currents of different SF6 circuit breakers with those of vacuum breakers. Measurements revealed that despite for SF6, the chopping current of the vacuum circuit breakers is randomly distributed with a value from a wide range that depends on the type of the contact material. The expression used by *Reininghaus* [72] for determining the chopping current level had a rather limited application for a small range of values of the load current. Later *Smeets* [75] carried out extensive research on the low current arc behaviour and found a more generally applicable expression for calculating the chopping current.

The problems that can arise from vacuum circuit breaker switching have been a (main) subject of research for more than 20 years. In particular the switching of small inductive currents has been a subject of study at various CIGRE conferences, especially the interruption of transformer magnetising currents [5, 6, 7, 9] and reactor switching [8, 10, 85, 86]. Also the interruption of transformers under load [55], and switching off induction motors [26, 44, 58, 69, 90] was extensively researched, and many measurements were carried out in order to provide enough information for determining the overvoltage level and the insulation coordination. Leading work was done by *Itoh* et al. [44] and

Murano et al. [50], who used equivalent single-phase test circuits for this purpose. Test circuits that can simulate reignition and restrike phenomena in vacuum were used by *Greenwood* and *Glinkowski* [33]. The majority of the work on current chopping done in the 1970s dealt with single-phase circuits. The capacitance, resistance and circuit inductance do have an influence on the level of chopping however, and in practical three-phase inductive circuits higher chopping levels are found that result in higher overvoltages because of the additional effect of VCC. *Panek* and *Ferhle* [60] gave an explanation for the overvoltage phenomena that appear as a result of VCC, and their theory can be generally applied to other low inductive current circuits as well. *Damstra* [21, 23] did extensive research on this topic and investigated in particular the occurrence of VCC while switching loaded transformers. It was made clear that in such circuits, phase-to-phase and phase-to-earth voltages can approach the basic insulation level (BIL) of the circuit components and adequate protection is necessary. The study of voltage transients in three-phase circuits is a rather laborious job. A major problem is the frequency dependency of the circuit components, which requires large computational effort. Bigger problem is, it is hard to collect the data of the system elements for a wide frequency range. As a result in many engineering studies only single-phase circuits with a limited level of complexity are used to calculate the voltage transients. In modelling the circuit components attention was given to specific physical effects that were considered in particular responsible for the generation of overvoltages. It were *Ihara* and *Panek* et al. [43, 82] who showed that under specific circumstances, the results obtained for single-phase transformers can also be applied to delta-star transformer connections despite the fact that for circuits with delta connected transformers the phenomena are generally more complicated as a result of the mutual couplings. The transformer model that they used is basically a parallel connection of a non-linear inductance representing the hysteresis effect, and a lumped capacitor representing the transformer capacitance.

Motors switched by a vacuum circuit breaker attracted great interest because of the wide application of vacuum contactors in motor circuits. Depending on the conditions of the motor when it is switched (normal load, unloaded motor, or motor at start up), the generated overvoltages which result from current chopping, multiple reignitions or VCC, and the probability of their occurrence can vary significantly. Because of the practical interest of the topic, an IEC motor testing circuit is used for this purpose. By varying different parameters of the circuit such as the length of the busbars and cable, with fixed values for the motor parameters, the most severe switching condition can be determined. Such a study based on experimental evidence was published by *Smeets* [74, 76] and *Smeets* et al. [73]. In this work especially the calculation of the probability of the occurrence of the voltage escalation and the VCC is carried out.

Not only de-energisation and energisation of motors [13, 17] but also capacitive loads [56] can lead to steep-fronted overvoltages, which can be caused by prestrike in the vacuum circuit breaker. When a prestrike occurs while a capacitive load is being energised, a high capacitive current flows through the contact gap. If this happens for a wide contact gap, it is very likely that this high frequency prestrike current is interrupted at the first high frequency current zero due to the high clearing ability of the circuit breaker. This will lead to voltage escalation. *Fu* and *Damstra* [27] combined experiments and computer simulation on energising a capacitive load and came to the conclusion that the actual phenomenon is not only influenced by the circuit breaker parameters but also by the network.

1.4 Aim of this work

The application of vacuum switchgear relates to the need for protecting the equipment and devices. In general, the vacuum circuit breaker has no difficulty with clearing currents, but under specific circumstances, unwanted overvoltages can occur across the transformer and motor terminals. In most of the cases these transients are not very high in amplitude and reach a value lower than the BIL of the device itself, but the amplitude and rate of rise do contribute to the deterioration of the insulation and shorten the equipment life. Under special switching conditions and a specific network configuration they can, however rise enough to cause a flashover from the transformer or motor windings to the core. Overvoltages resulting from fast surges can only be calculated if accurate system parameters and adequate characteristics of the circuit breaker are known. A similar system configuration but different component parameters, will give different overvoltages.

The goal of this research work is to study the overvoltages which are generated at the transformer primary terminals under steady-state and inrush current condition. By means of computer simulations, it is shown how different circuit breaker and network parameters influence the overvoltage level. In this work the circuit breaker is modelled in more detail in order to take into account the occurrence of reignitions. The cable is modelled by means of Π-sections in a way to take into account the frequency dependency. The new transformer model in a wide frequency range is also proposed and the overvoltages under different switching conditions are observed. Our analysis is done for a simplified circuit shown in Figure 1-2. There is *only one* feeder cable that is connected to the circuit breaker over busbars. The source side takes into account the source side capacitance which is the total capacitance of all possible elements (transformers and cables) connected to the studied circuit breaker. The protection of the transformer against fast transients should therefore be optimised, and different types of protection equipment each with its own protection characteristic for fast transients must be considered. The statistical analysis is done to investigate how frequent is the occurrence of high overvoltages and different protection solutions are observed. The effect of surge arresters and R-C branches is studied in detail.

For those who use vacuum circuit breakers in practice, it is useful to know how the probability of reignition varies with the possible overvoltage level for different power of the load and different cable lengths. This can assist the users of vacuum circuit breakers in estimating the overvoltages and reignition probability and to decide whether or not it is necessary to apply a protection.

1.5 Alternative Transient Program (ATP)

Due to the transient phenomena which occur when a circuit is switched by a vacuum circuit breaker, small differences in the values of the circuit parameters can result in large differences in the severity of duty. The switching overvoltages resulting from the change of network configuration are randomly distributed and depend on the actual system configuration, the conditions of the breaker and its parameters. In general, three different methods can be employed for investigating the overvoltage levels and the voltage oscillation that can be generated during vacuum circuit breaker switching:

- laboratory and field testing,
- theoretical quantitative analysis, and
- computer simulation.

A prominent problem for laboratory testing is the difficulty to obtain a realistic model for the load and the difficulty to make the test circuits match the practical service conditions. Field tests are expensive and difficult to perform. They bring the possible risk of circuit breaker failure and component damage. A simple straightforward theoretical analysis [84], however, can be very useful to obtaining insight in the problems related to vacuum circuit breaker switching and to perform a first order calculation, but it does not model the system and circuit breaker in detail. The models of the cables, transformers and motors, for example, should be frequency dependent and therefore computer simulation methods are necessary for the correct modelling of the system itself and the circuit breaker. Complex network configurations can be studied in a reasonable amount of time.

Computer simulations and calculations are in the majority of the cases done with the Alternative Transient Program (ATP) [53] which is a publicly available version of the Electromagnetic Transient Program (EMTP). The EMTP is a software for calculating electrical transients in power systems. It can compute currents and voltages in the system as a function of time after a disturbance like switching of a circuit breaker, the occurrence of a fault or changes in the network topology. The ATP is a large self-contained program written in FORTRAN code which originates from the Bonneville Power Administrations (BPA) EMTP but has been improved and extended by Dr. *W. S. Meyer* and others. With ATP, one can study single- and three-phase networks in the time domain and frequency domain. Steady-state analysis and transient studies can be done over a time interval ranging from microseconds to seconds.

Network studies can be done by means of a user-defined network of single-phase or three-phase cables and overhead lines with constant or frequency-dependent models, synchronous machines, transformers, motors, non-linear elements (like ZnO surge arresters, switching elements, saturation curves, arc resistances and hysteresis) and so forth. Apart from the electrical systems for which the program is designed, control networks can be implemented either operating stand alone or in interaction with a separately defined electrical network. ATP supports two control systems named TACS (Transient-Analysis-Control-System) and MODELS (a recent simulation tool) [18, 19]. The mode of representation offered by TACS is that of a user-defined block diagram arrangement of simple input-output components. A set of pre-defined types of building components is available; the parameters of their operation can be specified by the user while configuring the system. TACS is designed to represent systems which are mainly linear and tightly coupled with a fixed topology. Non-linear elements have to be considered to be integral part of the all system and can be solved separately from the overall set of equations.

MODELS, the more recent feature of the ATP, is an autonomous general-purpose simulation routine which is interfaced to the ATP. In MODELS, all aspects of the representation, the initialisation and the solution of the modelled components and control systems can be controlled by the user, who can represent the system by explicitly specifying the procedural algorithm describing its functionality. The operation is represented by a defined set of numerical or logical variables and by formulated expressions, functions, sub-models and characteristics which define their values during the simulation of the system's operation. This addition of dynamic control to the ATP gives a user the possibility to specify dynamic variations in the operation of the electrical components of the system according to arbitrary rules. So, MODELS is used to control the opening and closing of the switch as well as other dynamic operations which are important for representing the dynamic behaviour of the system components.

ATP-EMTP performs a digital computation by solving the equations at discrete intervals of time Δt. The basic idea is that each kind of circuit element is represented by an equivalent network and transforms an original set of continuous differential-integral equations into an equivalent set of linear algebraic equations at discrete time intervals. It can be proven that a lumped inductance branch can be described by a resistance and an equivalent current source paralleled with it. The voltage across the inductance can be expressed by:

$$e_{\mathrm{k}} - e_{\mathrm{m}} = L\frac{di_{\mathrm{k,m}}}{dt} \tag{1.1}$$

For the current in the inductance $i_{\mathrm{k,m}}$ holds:

$$i_{\mathrm{k,m}}(t) = i_{\mathrm{k,m}}(t-\Delta t) + \frac{1}{L}\int\limits_{t-\Delta t}^{t} (e_{\mathrm{k}} - e_{\mathrm{m}})\,dt \tag{1.2}$$

This integration is performed by the trapezoidal rule:

$$i_{\mathrm{k,m}}(t) = \frac{\Delta t}{2L}\left[e_{\mathrm{k}}(t) - e_{\mathrm{m}}(t)\right] + I_{\mathrm{k,m}}(t-\Delta t) \tag{1.3}$$

where the equivalent current $I_{\mathrm{k,m}}$ is known from the past history:

$$I_{\mathrm{k,m}}(t-\Delta t) = i_{\mathrm{k,m}}(t-\Delta t) + \frac{\Delta t}{2L}\left[e_{\mathrm{k}}(t-\Delta t) - e_{\mathrm{m}}(t-\Delta t)\right] \tag{1.4}$$

So according to the above expressions, an equivalent circuit for the inductance can be

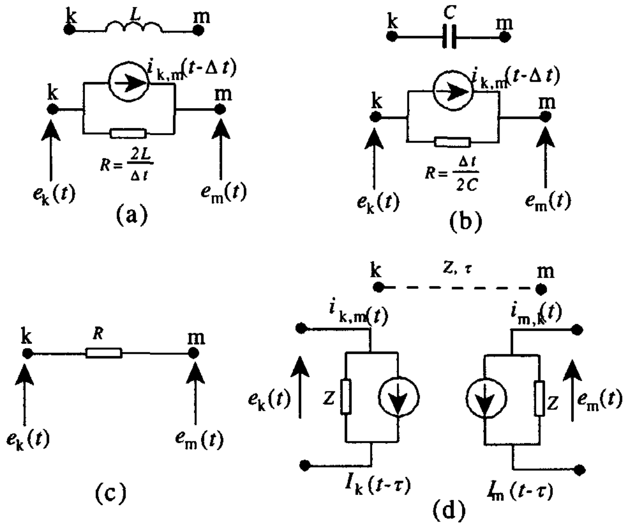
k
L
m
$i_{k,m}(t-\Delta t)$
k
m
$R=\frac{2L}{\Delta t}$
$e_k(t)$
$e_m(t)$
(a)
k
C
m
$i_{k,m}(t-\Delta t)$
k
m
$R=\frac{\Delta t}{2C}$
$e_k(t)$
$e_m(t)$
(b)
k
R
m
$e_k(t)$
$e_m(t)$
(c)
k
Z, τ
m
$i_{k,m}(t)$
$i_{m,k}(t)$
$e_k(t)$
Z
Z
$e_m(t)$
$I_k(t-\tau)$
$I_m(t-\tau)$
(d)

Figure 1-3: Equivalent networks for R, L, C and lossless line

constructed as shown in Figure 1-3a. The value of the resistance is twice the value of the inductance divided by the time interval Δt. The value of the equivalent current source at time t is found from the branch current and voltage at the previous time step.

The equivalent network for a capacitance is described in a similar manner as that for an inductance except for the equivalent resistance, which takes a value equal to the time interval Δt divided by twice the value of the capacitance. For the voltage of the capacitance between nodes k and m the following holds:

$$e_{\mathrm{k}}(t) - e_{\mathrm{m}}(t) = \frac{1}{C}\int\limits_{t-\Delta t}^{t} i_{\mathrm{k,m}}(t)dt + e_{\mathrm{k}}(t-\Delta t) - e_{\mathrm{m}}(t-\Delta t) \tag{1.5}$$

Applying the trapezoidal rule once more gives:

$$i_{\mathrm{k,m}}(t) = \frac{2C}{\Delta t}\left[e_{\mathrm{k}}(t) - e_{\mathrm{m}}(t)\right] + I_{\mathrm{k,m}}(t-\Delta t), \tag{1.6}$$

where

$$I_{\mathrm{k,m}}(t-\Delta t) = i_{\mathrm{k,m}}(t-\Delta t) - \frac{2C}{\Delta t}\left[e_{\mathrm{k}}(t-\Delta t) - e_{\mathrm{m}}(t-\Delta t)\right] \tag{1.7}$$

For a resistance branch, the equivalent circuit is simply the resistance itself. The relation between the current and the voltage is linear and has nothing to do with their historical values and it can be expressed by

$$i_{\mathrm{k,m}}(t) = \frac{1}{R}\left[e_{\mathrm{k}}(t) - e_{\mathrm{m}}(t)\right] \tag{1.8}$$

Also, for a lossless distributed line, the magnitude of the equivalent current source at time t is related to circuit quantities which appeared at time $t-\tau$ at the remote end where τ is a wave travel time of the line. So, at each end, an equivalent current source is introduced in parallel with the characteristic impedance Z of the line and the following equation must be true:

$$e_{\mathrm{m}}(t-\tau) + Z\ i_{\mathrm{m,k}}(t-\tau) = e_{\mathrm{k}}(t) - Z\ i_{\mathrm{k,m}}(t) \tag{1.9}$$

From equation (1.9) the following two-port equations can be deduced:

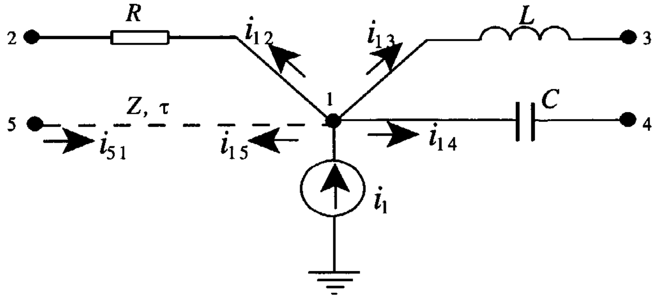

Figure 1-4: Description of the network connection

$$\begin{aligned}
i_{\mathrm{k,m}}(t) &= \frac{e_{\mathrm{k}}(t)}{Z} + I_{\mathrm{k}}(t-\tau) \\
I_{\mathrm{k}}(t-\tau) &= -\frac{e_{\mathrm{m}}(t-\tau)}{Z} - i_{\mathrm{m,k}}(t-\tau) \\
i_{\mathrm{m,k}}(t) &= \frac{e_{\mathrm{m}}(t)}{Z} + I_{\mathrm{m}}(t-\tau) \\
I_{\mathrm{m}}(t-\tau) &= -\frac{u_{\mathrm{k}}(t-\tau)}{Z} - i_{\mathrm{k,m}}(t-\tau)
\end{aligned} \tag{1.10}$$

where I_{k} and I_{m} are equivalent current sources which are known at state t from the past history at time $t - \tau$. The resulting models for the inductance, capacitance, resistance and a lossless line are shown in Figure 1-3.

Figure 1-4 shows the details for the region around node 1 of some system. When all circuit branches are replaced by their equivalents, the equation for the node 1 can be written as:

$$\left(\frac{1}{R} + \frac{\Delta t}{2L} + \frac{2C}{\Delta t} + \frac{1}{Z}\right) V_1 - \frac{1}{R}V_2 - \frac{\Delta t}{2L}V_3 - \frac{2C}{\Delta t}V_4 = i_1 - I_{13} - I_{14} - I_{15} \tag{1.11}$$

In this equation the unknown parameters are the voltages, while the currents are known from the values of preceding time steps. For a network containing n nodes, a set of n equations can be formed and can be expressed through a matrix expression:

$$[G]\,[V] = [i] - [I] \tag{1.12}$$

where

$[G]$ - is the nodal conductance matrix,

$[V]$ - vector of n node voltages,

$[i]$ - vector of applied current sources and

$[I]$ - vector of n known history terms.

Normally, some nodes have known voltages either because voltage sources are connected to them, or because the node is grounded. In this case the last equation can be partitioned into a set A of nodes with unknown voltages and a set B of nodes with known voltages. The unknown voltages are obtained by solving

$$[G_{\mathrm{AA}}]\,[V_{\mathrm{A}}] = [i_{\mathrm{A}}] - [I_{\mathrm{A}}] - [G_{\mathrm{AB}}]\,[V_{\mathrm{B}}] \tag{1.13}$$

where $[i_{\mathrm{A}}]$ and $[V_{\mathrm{B}}]$ are known from the boundary condition.

The program carries out a transient calculation by proceeding as follows: at each time step, circuit status is checked, matrices $[G_{\mathrm{AA}}]$ and $[G_{\mathrm{AB}}]$ are formed in correspondence to updated circuit conditions, and $[G_{\mathrm{AA}}]$ is triangularised by order elimination. The vectors on the right-hand side of equation (1.13) are prepared from past history terms, and current and voltage sources. Then the system of linear equations is solved for $[V_{\mathrm{A}}]$, using the information contained in the triangularised conductance matrix. Before proceeding to the next time step, the term $[I_{\mathrm{A}}]$ in equation is updated for use in future time steps. The weak point in ATP-EMTP is that there is no recalculation after a topography change. This can lead to numerical oscillations and therefore damping resistors for the inductive and capacitive elements should be applied in order to damp the numerical oscillations.

1.6 Outline of this Dissertation

Chapter 1 gives a general introduction which covers the application of vacuum switchgears today. Problems which can occur during the switching of the equipment (motors and transformers) with a vacuum circuit breaker are described. Also, this chapter gives an explanation of the source of switching overvoltages in specific circuits. An overview of the previous research work done by different researchers is given and the aim of the work is defined. The ATP-EMTP is introduced as a tool used for modelling the components and performing the computations.

Chapter 2 describes different methods for modelling reignitions which can occur during switching small inductive currents with a vacuum circuit breaker. A short description of the chopping current is given and simulations with different models are done in order to verify the validity of the models. The occurrence of reignitions after switching off the circuit breaker is shown on single-phase circuits while the Appendix shows results of the application of both models when used in a more detailed three-phase motor network.

Chapter 3 presents the models of the cable and busbars which are used in this study. The description of the busbar modelling is given and a comparison with the ATP's Line constants is done, from where it is concluded that the short busbars can be fully represented by an inductance. The frequency dependency of the cable is investigated and compared with the standard ATP routines.

Chapter 4 proposes a new transformer model for a wide range of frequencies which is upgraded from the currently known frequency-dependent transformer models. This chapter describes the effect of the transformer at high and low frequency transients.

Chapter 5 gives an overview of the currently known surge arrester models and also proposes a new simplified arrester model for application in circuits which are switched by a vacuum circuit breaker. The model is applied according to the ANSI/IEEE Std. C62.11-1993, and the residual voltages during applying impulses with different shape on the arrester are observed. Also, in this chapter the effect of applying a R-C suppression branch is discussed.

Chapter 6 deals with the study of overvoltages in three-phase transformers when switched by a vacuum circuit breaker. All previously defined models are installed and the overvoltages during switching magnetising and inrush currents are calculated. The probability of overvoltage occurrence is studied and the application of protection measures with surge arresters and R-C suppression branches are observed.

Chapter 7 presents the computation of the probability of reignition during switching circuits with a vacuum circuit breaker. The goal in this chapter is to develop a method for calculation of the reignition probability which can be used in a circuit with any type of load. Therefore, the standard IEC motor circuit is used. Also, in this chapter, the geometrical place of the combination between the cable length and the motor power where 3 per unit and 5 per unit overvoltages exist is calculated.

Chapter 8 gives the conclusions of the dissertation and suggestions for future possible work.

Chapter 2

Modelling reignitions in vacuum circuit breakers

2.1 Introduction

Vacuum circuit breakers are safe and quiet in operation, reliable, require low maintenance and are small in size and low in weight. The modern generation of vacuum circuit breakers have good performances and as we can see from Figure 2-1, the diameter of the vacuum circuit breaker has reduced from 18 cm in 1967 to 5 cm today [79]. This reduction in size is a result from major developments in vacuum technology, contact material development, manufacturing and so forth.

The application of vacuum circuit breakers at the distribution level has increased in this period. From Figure 2-2, it can be seen that in 1980 only 20 % of all installed circuit breakers were vacuum circuit breakers. In 1990 this number was 50 % and today almost 65 % of all circuit breakers for medium voltage level in the world are vacuum circuit breakers. Although the SF6 gas technology, first used for transmission voltages entered the distribution market, it is expected that the vacuum circuit breaker will dominate distribution switchgear market in the near future.

Vacuum technology has three major advantages of over SF6:

- Vacuum circuit breakers has an operational electrical lifetime that exceeds the mechanical lifetime of the equipment. This makes vacuum circuit breakers popular

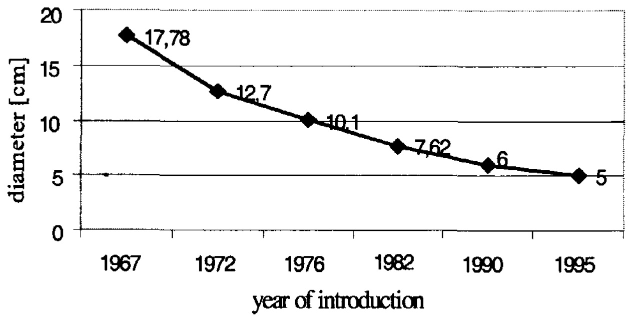

Figure 2-1: Size reduction of a 15 kV, 12 kA Vacuum Circuit Breaker between 1967 and 1995 [78]

for application in circuits where many operations per day are necessary,

- A vacuum circuit breaker does not cause toxic byproducts after current switching, and they do not need the special gas handling that SF6 circuit breakers require when routine maintenance is performed or when the SF6 circuit breaker is dismantled at the end of its electrical lifetime.
- Maintenance of vacuum circuit breakers is easier than that of the other circuit breakers.

But problems can arise in the case of switching small inductive and capacitive currents. This has been the subject of many research efforts. High overvoltages can be generated when the current is interrupted before the power frequency current zero. In this case the arc becomes unstable and the current declines toward zero with a very high di/dt. This is called current chopping, a phenomenon related to the interruption of small inductive currents. The point at which the current begins to decline is the *chopping level* and the value of the current at this point is called the *chopping current.* The arc instability and the resulting current chopping is mainly caused by the choice of contact material. Other parameters that influence current chopping are the amplitude of the power frequency load current and the type of the load that is switched. When the load current is high, at current zero, the arc has less instability than if the load current has a small rms value.

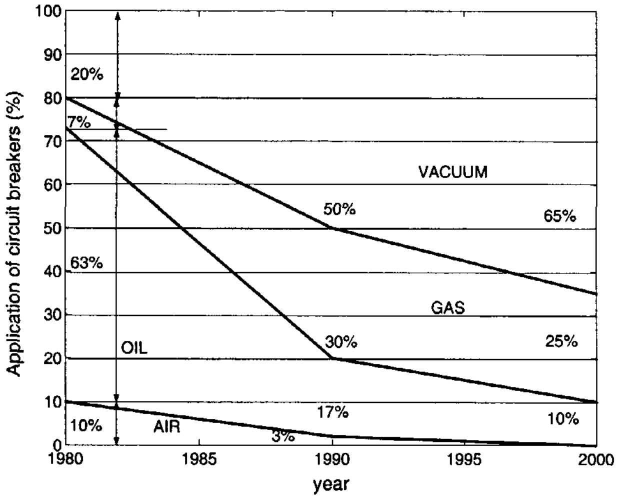

Figure 2-2: Total number of medium voltage circuit breakers in operation in the world between 1980 and 2000

Thus, for high current vacuum arcs the chopping current practically does not exist. The chopping current is also influenced by the type of load and this will be explained in section 2.3.1. The higher the chopping current level, the higher the generated overvoltage. The value of the peak of the TRV is important with respect to the dielectric breakdown and it is related to the magnitude of the chopping current. This means that the chopping current level is a parameter for the first reignition. The instant of contact separation is also a significant parameter that determines whether the reignition will occur or not. The dielectric recovery of the vacuum gap depends mainly on the contact separation velocity. When the contacts open at some instant of the power frequency current, the arc will exist while the current zero is reached. The time interval between the instant of opening of the circuit breaker and the natural current zero is called an *arcing time.* At short arcing times, after the arc is extinguished, the contact gap will be small and only a small TRV is needed for a reignition to occur. The reignition will occur when the TRV exceeds the dielectric characteristic of the actual gap. So, on the one hand the first reignition depends on the chopping current because the TRV is proportional to the chopping current level, and on the other it depends on the ability of the circuit breaker to withstand the TRV. The dielectric recovery of the gap should be steeper and the parameter that influences the steepness is the speed of contact opening. For the next scenario, whether or not the reignition will occur depends no longer on the chopping current but on the TRV and dielectric recovery of the gap.

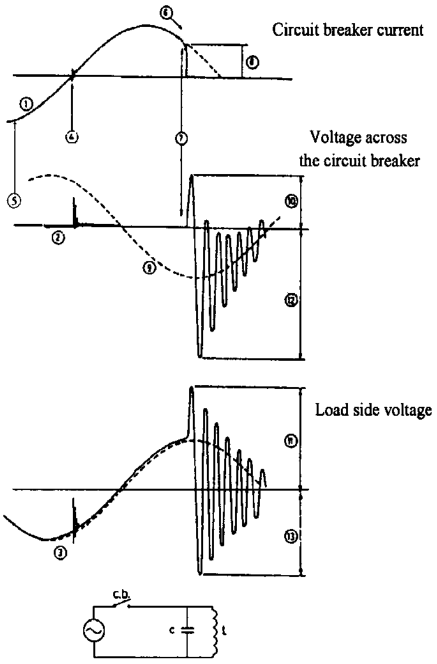

Figure 2-3: Survey of the chopping phenomena in a single-phase circuit
1. Current to interrupt, 2. Voltage across circuit breaker,
3. Voltage across inductive load, 4. Failed interruption,
5. Opening time of the circuit breaker, 6,7. Instant when the current is chopped,
8. Chopping current level, 9. Main voltage,
10,11. First voltage maximum across breaker and load (suppression peak),
12,13. Second voltage maximum across breaker and load

During the interruption of the transformer magnetising currents because of the chopping, the magnetic energy stored in the inductance is transferred in the circuit capacitances and vice versa. The result is a damped oscillation of the TRV in the switched-off circuit. To explain the events after switching we will use Figure 2-3. It represents the variation of the current in the circuit breaker, the voltage across the circuit breaker and the voltage at the load side. The transformer is represented by its primary inductance and parallel capacitance. After the current is switched due to the small contact distance, the arc is re-established after a few reignitions at current zero. This is represented by point 4 in Figure 2-3. Therefore the 50 Hz current continues to flow until the next current zero. Before next current zero, the arc becomes unstable and the current is chopped (see point 6). The maximum energy that can charge the transformer capacitance after chopping is:

$$\frac{1}{2}CU_{\mathrm{m}}^2 = \frac{1}{2}Li_{\mathrm{ch}}^2 + \frac{1}{2}CU_0^2 \qquad (2.1)$$

where:

L - inductive load to be switched,

C - capacitance in parallel with L,

i_{ch} - chopping current,

U_0 - voltage across C at the moment of current chopping,

U_{m} - maximal voltage across C.

Before chopping, most of the total current flows through the inductance and only a small part of current flows in the transformer capacitance. The first element on the right side of equation (2.1) represents the magnetic energy that is stored in the primary inductance, and the second element represents the electric energy in the capacitor at the moment when the chopping occurs. So, the total energy oscillates between the inductance L and capacitance C with a frequency determined by the values L and C. This causes the voltage at the transformer terminal to rise and so the TRV across the circuit breaker increases.

A large inductance L, a small capacitance C and a high chopping current i_{ch} may result in unacceptably high overvoltages. The highest overvoltage across the inductive load is a peak voltage arising directly after the chopping current (point 11). The highest voltage across the breaker contacts is the recovery peak after polarity change of the TRV (point 12). At that moment of chopping, the contacts of the breaker have reached full distance and the dielectric ability of the gap has its maximum value. Therefore the dielectric characteristic of the circuit breaker exceeds the TRV, so a reignition does not occur. In practical power system networks, the process is usually more complicated than that described above because of the following reasons:

- the capacitance and inductances involved are distributed elements of the transformer and motor windings,
- damping elements are involved such as stray resistance of transformer windings, hysteresis and eddy current losses and they have a significant influence when the transformer is switched under no load,
- the elements are frequency dependent,
- the circuits are three-phase networks and inductively and capacitively coupled which result in penetration of the transients from one circuit to another causing multi-frequency oscillations.

The reasons mentioned above make the computation and analysis very complicated. The transformer windings are actually distributed elements and their representation by concentrated capacitances and inductances does not reflect the real response in the transformer, especially when voltage transients with different frequencies are involved. In this case, the transmission line theory for the windings holds, and the modelling of the winding is necessary if propagation of the transient oscillations along the winding is observed. The transformer losses must be taken into account because they damp the voltage transients and contribute to lower overvoltages in the transformer. The transformer losses are frequency dependent and their values can significantly vary from those which are normally measured by the manufacturer at 50 Hz.

Multiple reignition in vacuum involves many high frequency components that force the load side to show different behaviour at different frequencies. Therefore, when modelling the vacuum circuit breaker reignition and calculating the TRV, one should pay attention not only to the circuit breaker model but also to how the load side, for example cables, motors and transformers is modelled.

From a practical point of view, the interruption of a large non-linear inductance like a transformer under no load usually causes less concern but will be studied in chapter 6. The amplitude for the steady-state no-load current (magnetising current) is much lower than the chopping level of the vacuum circuit breaker and in the expression (2.1) the value of i_{ch} is not determined by the chopping tendency of the circuit breaker. For switching unloaded transformers, the only load that is seen from the transformer terminals is the transformer core, which consists of the primary inductance, the hysteresis and eddy current losses. While transformer losses represent a large damping of the theoretical maximum, the mangetising inductance, due to its non-linear behaviour and residual magnetic flux, does not release all magnetic energy into transformer capacitance, but only part of it. Therefore, only a small part of the released energy contributes to the overvoltage rise and the rest of the energy is wasted by the hysteresis losses and used to magnetise the transformer core.

But not all interruptions of the transformer current are without risk. Some combinations of vacuum circuit breaker and transformers, and a specific state of work can lead to very severe overvoltages. Thus, when the magnetising currents are being switched, overvoltages of up to 4 per unit can occur. More serious is the case of inrush current switching. These currents can occur when the transformer is energised under no load. The inrush currents consist of many local maxima, which aperiodically decay over time. The damping effect is slow and may take many seconds. The maximum value of the inrush currents could be as high as 8 per unit. When this current is interrupted, the chopping current is determined by the vacuum circuit breaker.

In three-phase circuits the determination of the TRV is much more complicated because of the greater number of circuit elements, the capacitive and inductive inter-phase couplings and the different initial conditions. There are some additional phenomena which are not observed in single-phase networks. A current chopping in the first phase to interrupt, followed by a reignition at a high value of the TRV, introduces a high frequency oscillation current, like in the single-phase case. All capacitive and inductive elements in the circuit in the direct vicinity of the circuit breaker are involved in the energy exchange of this oscillation. So in the three-phase case, part of the current may flow through the other breaker poles, causing a high frequency oscillation superimposed on the momentary main frequency current through these poles. The resulting current may pass zero and consequently be interrupted, even though a relatively high current is flowing through the inductive load causing virtual current chopping. The high frequency oscillation after a reignition in the last phase to interrupt is also fed from the capacitances of the three phases. Therefore, high frequency voltages can be generated in the other phases and be superimposed on the momentary value of the TRV in these phases.

2.2 Modelling circuit breaker reignitions

2.2.1 Description of the vacuum arc

In a vacuum circuit breaker in a closed position, the current at the contact surface of two electrodes passes through a number of small areas. The number and size of these areas depend on contact pressure, roughness and hardness of the electrode surface. When the contacts begin to separate, the number of these areas decreases and eventually all current has to pass through only one spot. At this spot due to ohmic losses, the dissipated heat will be sufficient to bring the metal to its boiling point. The metal evaporates and the arc will start to burn in the metal vapour.

Vacuum arcs have more than one physical state. The state of the arc depends on the current level and to a significant extent on the size of the contacts. The vacuum arc can be diffuse or constricted. At lower currents the arc assumes the diffuse mode. This is characterised by one or more exceedingly bright spots on the cathode electrode. These cathode spots are in constant motion over the contact surface, and appear to repel each other, even to the extent of sometimes moving down the side of the contact. They have a finite, though variable lifetime and new spots are created often by the splitting of existing spots, as other spots extinguish. The number of spots are determined by the magnitude of the current, and this number increases to the peak of the current and decreases near current zero. Cathode spots feed the arc with metal vapour plasma, so that the region in between the electrodes becomes filled with a diffuse homogeneous plasma. The anode acts as a passive collector of plasma. By an increase of the current, the small cathode spots are grouped together and the arc current is concentrated in narrow channels. The current channels contrast visibly with their surroundings results in an optical image of multiple arcs. This state is known as the constricted mode. The current at which the transition from diffuse to constricted mode takes place depends on the contact material and the magnetic field in the chamber. Despite the high voltage that exists across the gaseous arcs, the voltage of the vacuum arc is surprisingly low. For a 200 A copper arc, for example, the arc voltage is about 20 V. For some other metals even lower arc voltages have been measured and somewhat higher voltages for refractories. As the current increases, the voltage increases slowly as well. This is in contrast to the gaseous arc, which has a negative resistance characteristic; the voltage decreases as the current increases. The further increase of the current causes greater increase of the voltage, of 100 V or more in copper arcs. This activity is a transition from the diffuse to the constricted state of the discharge. The higher voltage in the constricted mode is caused by extra ion collisions in the neutral plasma. Since the vacuum arc consists of a vapour metal from the contacts, it is the contact material that determines the withstand capabilities of the vacuum circuit breaker. The choice of the contact material is a compromise and today mainly contact materials of Cu/Cr are used.

After interruption, the arc column returns to its original cold state within a few microseconds but the fast recovery withstand capability is extended into the millisecond region when the arc is in constricted mode. This is due to the higher concentration of ions and it is a reason for reignitions. However, the withstand capability can be improved by a better choice of contact geometry. Thus, a radial magnetic geometry forces the arc to rotate and an axial magnetic geometry prevents the arc from changing from the diffuse mode to the constricted state.

2.2.2 Reignition in vacuum

In section (2.1) a survey of the phenomena due to current chopping based on the stored energy in the load was explained. The section also explained that because of the opening at the contacts close to current zero, the breaker fails to interrupt the current at the first current zero. To explain this in more detail we have to simulate the reignition current and therefore, it is necessary to have a model that is capable of simulating the high frequency reignitions. For practical purposes we need to know roughly under which circumstances the reignitions occur. *Lindmayer* and *Czarnecki* [15] used the induction motor shown in Figure 2-4 to describe different types of reignition at current zero, and *Kosmač* and *Žunko* [46] used the same circuit to verify their statistical vacuum circuit breaker model.

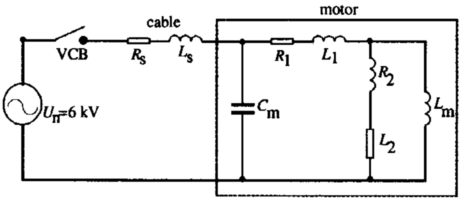

Figure 2-4: An induction motor for studying reignitions [15, 46]

The motors as highly inductive loads can be exposed to reignition overvoltages and therefore these authors observed the switching of an induction motor at its start up with respect to the instant of contact opening. If circuit breaker contacts open after the approximately 150 μs before current zero, an arc is drawn between the contacts that helps the current to flow until the first current zero. The arc voltage drop for a vacuum circuit breaker does not vary in a wide range of the current change, and its value is a few tens of volts. The simulated current through the circuit breaker is shown in Figure 2-5. The current and the voltages are observed within 1 ms time. From Figure 2-5 it follows that the arc is unsuccessfully cleared at first current zero. The reason for this is that due to the short arcing time, the gap is short when the TRV begins to rise, so the dielectric characteristic of the vacuum rises slower than the TRV. The TRV across the circuit breaker and the voltage at the motor terminal are shown in Figure 2-6. It can be seen that the reignition does not occur at the first local maximum of the TRV, but at the second maximum, which is in fact the recovery peak. The first maximum, as it was also explained in Figure 2-3, is the suppression peak. It is also called the chopping overvoltage because its value is proportional to the chopping current.

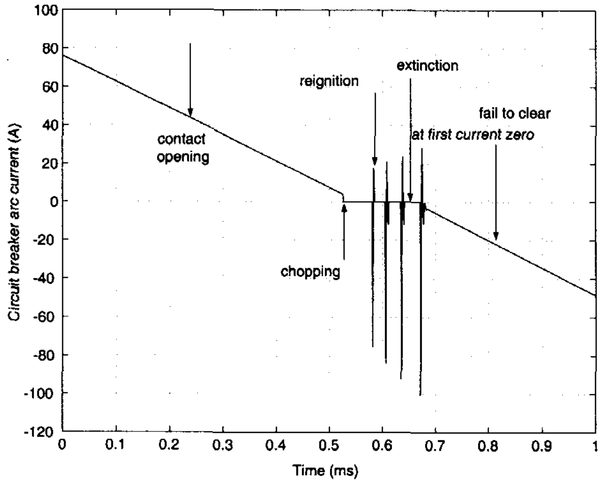

Figure 2-5: Circuit breaker current when contacts open at 150 μs before current zero for the circuit in Figure 2-4

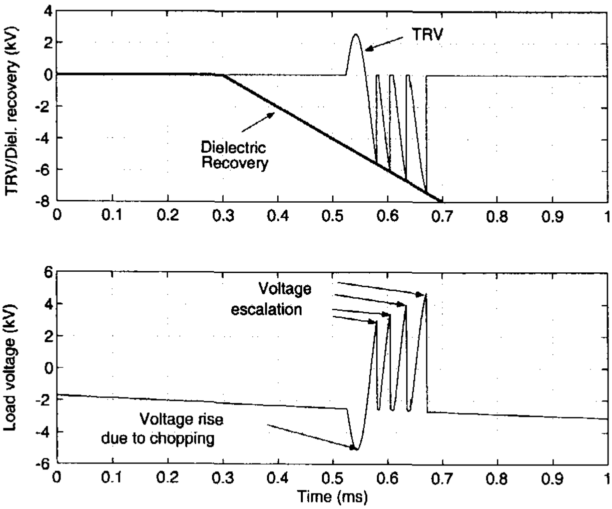

Figure 2-6: Reignition voltage when contacts open 150 μs for the circuit in Figure 2-4; upper trace: TRV; lower trace: load side voltage

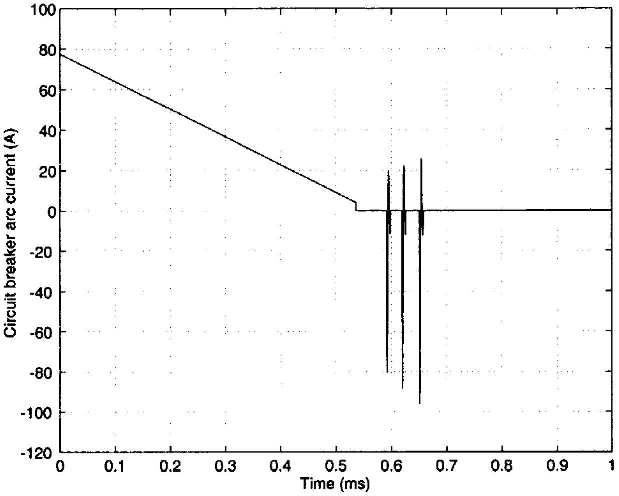

Figure 2-7: Circuit breaker current when contacts open 250 μs before current zero for the circuit in Figure 2-4

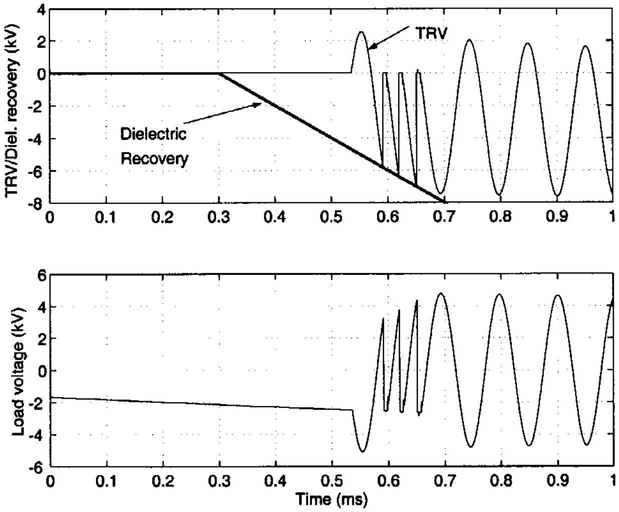

Figure 2-8: Reignition voltage when contacts open 250 μs before current zero for the circuit in Figure 2-4; upper trace: TRV; lower trace: load side voltage

The voltage escalates with the same frequency as the reignited current, and both the current and the voltage will contain high frequency components the values of which depend on the type of the load, length of the cable, and the length of the busbars that connect the vacuum circuit breaker to the load. Figure 2-7 and Figure 2-8 present the variation of the current through the breaker, the TRV and load side voltage respectively when the contacts begin to separate about 250 μs before current zero. In this case the arc is successfully cleared with three reignitions and the voltage after the escalation results in a damped oscillation with a frequency determined by the motor inductance and capacitance. In practice, the same effect can be achieved by decreasing the total inductance between the circuit breaker and the load. This inductance is mainly from the busbars and the cable inductance, and the investigations show that the length of the busbars can control the amount of reignitions in the circuit breaker.

When the contacts open far enough from the current zero, until the current reaches the natural current zero, the gap will be large enough to withstand the TRV and the arc is cleared with chopping without reignition.

The vacuum circuit breaker has a probability of reignition only when certain operating and circuit parameters are met. These parameters are the following [79]:

- it occurs when the circuit breaker interrupts currents of less than 500 to 600 A,
- the breaker contacts must part 0.5 ms to 1 ms before current zero with a speed of 1 m/s,
- the TRV must rise faster than the breakdown strength of the vacuum gap.

If the load exceeds 600 A, the vacuum arc will not extinguish at the first current zero with closely spaced contacts. Because the contacts continue to open during the ensuing half cycle of arcing, the dielectric strength of the contact gap in the next current zero is high enough to prevent a voltage breakdown. The breakdown strength of the vacuum gap depends almost entirely upon the contact gap.

When a breaker operates with an opening speed of about 1 m/s and the contacts part at a time of about 0.5 ms before current zero, then the gap will recover from 10 to 20 kV in the first a few microseconds. If it operates at 2 m/s, then the recovery will be between 20 to 30 kV. Most vacuum circuit breakers operate at this range. When the rate of rise of the recovery voltage is less than the rate of increase of the dielectric strength of the contact gap, no reignitions will occur. If the currents are lower than 20 A, for example transformer magnetising currents, reignitions are possible and these overvoltages are mainly damped by the transformer losses. But more extreme situations are possible in some specific cases where for a short time more frequent switching takes place, for example the switching of arc furnace transformers or inductively loaded transformer.

2.3 Circuit breaker model

The model that will represent the reignition phenomenon must take into account all matters that contribute to reignition during the switching: the chopping current, the dielectric characteristics and the ability of the circuit breaker to clear high frequency currents.

2.3.1 Chopping current

The chopping current is a parameter that causes the sequence of events which occur after the switching of small inductive currents. This parameter is a subject that has been studied since the early 1960s, and because of its ability to produce high chopping overvoltages, it was often regarded as a major disadvantage of vacuum circuit breakers by the competing technologies. According to the latest developments in contact material, the chopping current is no longer a concern and today, its value is the same as that of the chopping currents in other types of circuit breakers.

The chopping current depends mainly on the contact material, but its value also differs for different instants of contact opening. When the contacts open close to current zero, the chopping level is lower [77]. Another factor that influences the chopping current is the type of load and the characteristic impedance of the circuit that is switched. It is difficult to make an exact numerical description of the phenomena involved because of the chopping current. Especially for the vacuum circuit breaker, measurements [88] have shown that this parameter varies with a higher standard deviation than for the other

Table 2.1: Chopping current constants

Type of contact	a	b	c
Cu/Cr 75/25 (most frequently used).	14.0	0.014	2.3
Cu/Cr 62/38	12.2	0.011	2.1
Cu/Cr 51/49	11.6	0.019	1.8
Cu/Cr 44/56	12.0	0.015	1.8
Cu/Cr 42/58	11.8	0.021	1.8
Cu/Cr 33/67	11.3	0.011	1.8
Cu/Bi 99.7/0.3	34.8	0.049	5.8
Cu/Bi 99.5/0.5	30.0	0.022	5.5
W/Cu 70/30	11.2	0.016	1.6
W/Cu 90/10	7.00	0.006	1.2
Mo/Cu 80/20	10.4	0.009	1.6

circuit breakers.

So far a few formulas have been determined that can approximately represent the value of the chopping current for different contact materials. According to [72], the chopping current can be calculated by the expression:

$$i_{\mathrm{ch}} = a - b\,\hat{I} - c\log Z_{\mathrm{N}} \qquad (2.2)$$

where a, b and c are constants that depend on the contact material, Z_{N} is the characteristic impedance of the circuit that is switched and $\hat{I}$ is the amplitude of the load current. For different types of contact material, the constants a, b and c are summarised in Table 2.1. This implies that independently of the contact material, an increase of the load current and the characteristic impedance results in a decrease of the chopping level of the current.

This relationship was experimentally verified for load currents between 45 A and 170 A. The influence of circuit parameters on current chopping behaviour was also studied by *Damstra* [22, 23]. *Smeets* [75] used another relationship for the chopping current. He expressed the mean chopping level as:

$$\hat{i}_{\mathrm{ch}} = \left(2\pi f\,\hat{I}\,\alpha\beta\right)^{q} \qquad (2.3)$$

f - power frequency (50/60 Hz),

For commercially available vacuum tubes he found the following values for the constants:

α = 6.2 10-16 s, β = 14.3, q = -0.07512

The values of the chopping current calculated by equation (2.3) are between 3 A and 8 A. However, the expression is not valid for load currents less than the chopping current level. These currents are chopped instantaneously. This is for instance the case for transformer magnetising currents, which often have values lower than the chopping current level. The value of the chopping current appears to be randomly distributed in a particular interval and therefore the calculated values can be varied randomly with a specific standard deviation. Normally this standard deviation is taken as 15%.

2.3.2 Dielectric and quenching capability

After the vacuum circuit breaker has interrupted the current, the dielectric withstand capability of the contact gap tries to withstand the voltage stress. The modelling of the withstand capability is of great importance for the study of reignition overvoltage. If the TRV is greater than the withstand voltage, the arc will be reignited. The withstand voltage is a function of the contact distance, and it is proportional to the square root of the gap distance. It can be considered as linearly dependent for the first millimeter after contact opening. This implies that the withstand capability is also a function of the speed of contact opening. The parameters determining the dielectric strength vary for different vacuum circuit breakers. Measurements reveal, however, that even for the same vacuum circuit breaker, the withstand voltage can show different behaviour. This means that the dielectric withstand capability can also vary with a normal distribution and a particular standard deviation.

When reignition occurs, a high frequency reignition current flows through the vacuum circuit breaker. The high frequency current is superimposed on the power frequency current and may be interrupted in one of the high frequency current zero crossings. An interruption is followed by a TRV of which the frequency is determined by the local inductance and capacitance.

The arc extinguishes at the instant of a high frequency current zero, when the slope of the current is lower than the so called critical current slope, a parameter that is hard

Table 2.2: Characteristics parameters according to equation (2.5)

$\overline{U_\mathrm{b}}/\overline{di/dt}$	A_A[V/s]	B_B[V]	C_C[A/s^2]	D_D[A/s]
High	1.70E7	3.40E3	-3.40E11	255.0E6
Medium	1.30E7	0.69E3	0.32E12	155.0E6
Low	0.47E6	0.69E3	1.00E12	190.0E6

to determine. Therefore, several researchers rather represent the interrupting capability with a fixed value and introduce the probability of arc. If the critical current slope is B for instance, then the probability p of arc quenching can be calculated by the following equations:

$$\begin{gathered} p = 1, \left|\frac{di}{dt}\right| < B \\ p = 2 - \frac{\left|\frac{di}{dt}\right|}{B}, B < \left|\frac{di}{dt}\right| < 2B \\ p = 0, \left|\frac{di}{dt}\right| > 2B \end{gathered} \tag{2.4}$$

Recent research shows that the quenching capability is not constant, but depends on the reignition voltage.

The vacuum circuit breaker characteristics have been experimentally investigated by several researchers [30, 37, 52, 71]. These characteristics have in general a statistical nature and their functions that closely match the characteristics are statistically distributed with a normal distribution. In this thesis, the characteristics of the dielectric and arc quenching capability as measured by *Glinkowski* [30] are used. These characteristics can fully represent the dielectric characteristic and the critical current slope during the first millimeter of contact separation.

$$\begin{aligned} \overline{U_\mathrm{b}} &= A_\mathrm{A}\,(t - t_0) + B_\mathrm{B} \\ \overline{di/dt} &= C_\mathrm{C}\,(t - t_0) + D_\mathrm{D} \end{aligned} \tag{2.5}$$

Equation (2.5) characterises the withstand voltage and critical slope of the high frequency current as a function of time. They are denoted by $\overline{U_\mathrm{b}}$ and $\overline{di/dt}$, representing the mean values of these characteristics. Because of their statistical variation, the applied characteristics for the vacuum circuit breaker are randomly varied with a 10 %

normal distribution. How this is done is explained in Appendix A. The time instant t_0 corresponds to the instant of contact separation. Table 2.2 shows the parameters A_A, B_B, C_C and D_D for nine vacuum circuit breakers measured by *Glinkowski* [30], which are classified in three groups: Characteristics with high, medium and low ability, both for the dielectric and the quenching ability of the circuit breaker.

2.3.3 Modelling reignitions by taking into account the arc resistance

The model of the vacuum circuit breaker discussed in the previous section is able to simulate the reignited currents and voltage escalation. The ideal switch that represents a reignition by closing and opening under specific conditions does not take into account the presence of the arc because the voltage drop across the arc is small and does not have a noticeable influence on the voltage transients. The arc extinction is represented by an open position of the ideal switch, assuming that the resistance between the vacuum circuit breaker contacts has an infinite value.

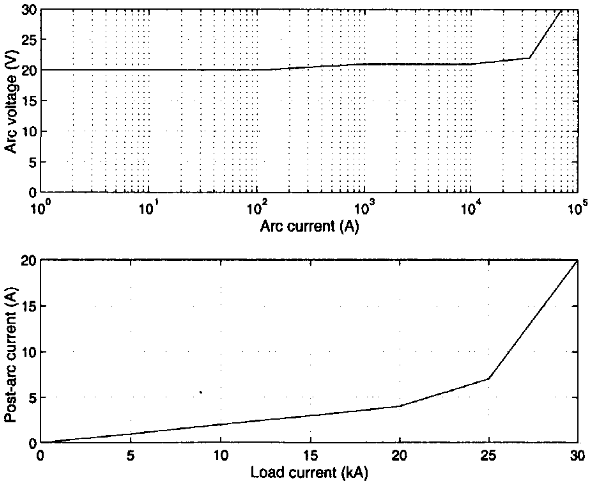

Figure 2-9: Arc voltage and post-arc current for different arc and load current

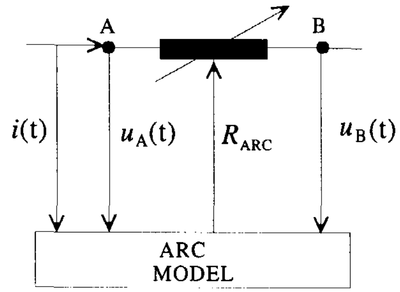

Figure 2-10: Arc resistance calculated by the breaker's voltage and current

In practice, during the arcing period, the arc voltage is not zero, and during the arc extinguishing period, a small current results due to the remanent ions between the contacts and due to the parasitic capacitance of the gap. So, in neither case, the period of the arcing and extinguishing can have zero and infinite resistance, respectively. Therefore, the model of the arc can incorporate the arc resistance at every instant from contact opening. Such a model was first developed by *Kosmač* [46]. From a measured volt-ampere characteristic he determined the arc resistance for the time period when the arc burns. When the arc extinguishes the arc resistance is calculated from the post-arc current, which depends on the amplitude of the load current. These characteristics are shown in Figure 2-9. Thus,

$$R_{\mathrm{arc}} = \frac{u_{\mathrm{arc}}}{i_{\mathrm{arc}}} \tag{2.6}$$

$$R_{\mathrm{arc}} = \frac{u_{\mathrm{TRV}}}{I_{\mathrm{pa}}} \tag{2.7}$$

From the arc characteristics we can calculate the arc resistance at every instant during the simulation. The current and voltages, which are network variables, are input parameters for the model. In the model, by observing the current and voltage of the breaker at every instant, the arc resistance is calculated. Also, the model should be able to detect when the arc burns and when it extinguishes. This is controlled by the dielectric characteristic and critical current slope mentioned in the previous section. So for each of the two possible regimes of the vacuum circuit breaker, the correct arc resistance calculated by (2.6) and (2.7) is inserted into the circuit. Unlike the model discussed earlier that uses a time-dependent dielectric characteristic, this particular model takes into account the speed of contact opening and this is close to the results and shows how different characteristics influence the overvoltage level. The modelling of the arc resistances is shown in Figure 2-10.

2.3.4 An algorithm for the vacuum circuit breaker

With the help of the circuit breaker voltage and current, it is possible to simulate the reignitions in the circuit breaker. The ideal switch option in ATP can open and close only at a specific time. This is not enough for simulating of reignitions in a vacuum circuit breaker because we noticed that they occur under special conditions. The circuit breaker is therefore modelled by an ATP type-13 switch [45, 58-63] that is controlled by a MODELS variable called STATE. This variable can have a value of either one or zero. If the STATE variable is equal to zero, the switch opens; otherwise it remains closed. The MODELS variable STATE is controlled by the voltage across the switch and the current through the switch.

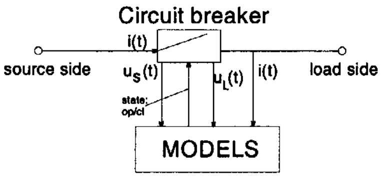

Figure 2-11: The ATP-EMTP circuit breaker model

The conditions for opening the switch are [30]:

- the instant of opening should be greater than a pre-set value t_0,
- the switch is closed,
- the actual current is less than the chopping current and
- the derivative of the high frequency current at current zero is not higher than the calculated quenching capability according to (2.5).

The condition for closing the switch (reignition) are:

- the switch is open,
- the voltage across the vacuum circuit breaker exceeds the dielectric ability of the breaker.

Figure 2-11 shows the ATP-EMTP model of a vacuum circuit breaker to be used for reignition studies.

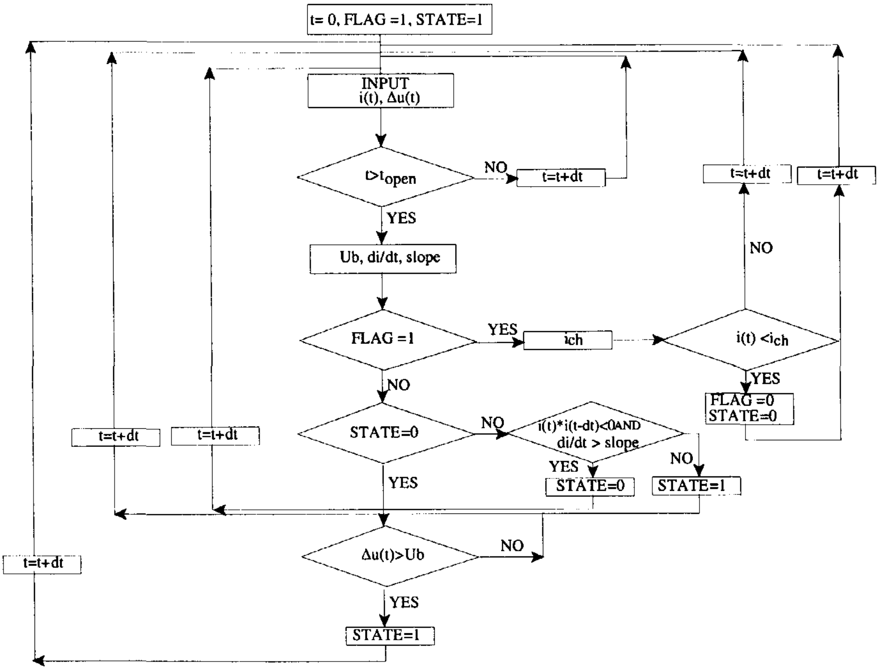
t= 0, FLAG =1, STATE=1
INPUT
i(t), Δu(t)
t>t_open
NO
t=t+dt
YES
Ub, di/dt, slope
FLAG =1
YES
ich
i(t) <ich
NO
t=t+dt
t=t+dt
YES
FLAG =0
STATE=0
NO
STATE=0
NO
i(t)*i(t-dt)<0AND
di/dt > slope
YES
STATE=0
NO
STATE=1
t=t+dt
t=t+dt
YES
Δu(t)>Ub
NO
t=t+dt
YES
STATE=1

Figure 2-12: Flow chart of the circuit breaker's reignition modelling

The flow chart of the model of the breaker is shown in Figure 2-12. The input values which are important for determining the state of the switch are the current through the breaker denoted as i(t) and the voltage across the switch Δu which is in fact the difference between the voltages $u_s(t)$ and $u_L(t)$, as shown in Figure 2-11. The t_{open} is a parameter that is determined by the user and denotes the instant when the contacts begin to open. $U_b(t)$ and di/dt are the characteristics of the breaker determined by equation (2.5) and the variable 'slope' denotes the actual slope of the circuit breaker current computed at every instant of the simulation. The output from the MODELS routine is the parameter STATE that gives an order to ATP to open or close the switch. In the second model the output is the value of the non-linear arc resistance computed from the arc voltage and arc current. This value can be exported into the ATP network by means of a TYPE-91 routine. The algorithm of programming and the control operation of the circuit breaker consists of four steps:

1. *Check if the chopping current level of the vacuum circuit breaker is reached.*
2. *Check if the criteria for reignition are fulfilled.*
3. *If reignition has occurred, check if the criteria for arc extinction are fulfilled.*
4. *Determine the actual value of the state variable.*
   (calculate the actual value of the arc resistance)

The comparison between the two ways of modelling a system in detail is given in the Appendix B. In the further application of these models we will denote the vacuum circuit breaker represented by a controlled switch type-13 as model A and the model represented by a variable arc resistance type-91 as model B.

2.4 Simulation in a single-phase circuit

In order to simulate the phenomena which occur when a transformer is switched off at no load, we first examine what happens when we disconnect a simple single-phase circuit with a vacuum circuit breaker. This circuit is shown in Figure 2-13. The supply is connected by a vacuum circuit breaker with L_n and C_n representing the supply side, busbars and the cable connection to the vacuum circuit breaker. R_σ and L_σ represent the cable connection to the load. Capacitance C_L is the total capacitance, which is the sum of the cable capacitance and load capacitance, and R_s, L_s and C_s are parasitic parameters of the gap. The cable capacitance normally should be added with a half value at the beginning and the end of the cable, but because of simplicity in this circuit it is treated as one capacitance together with the load. The values for these parameters are shown in Table 2.3. The system voltage is 6 kV.

The results of a simulation are shown in Figure 2-14 and Figure 2-15. Figure 2-14

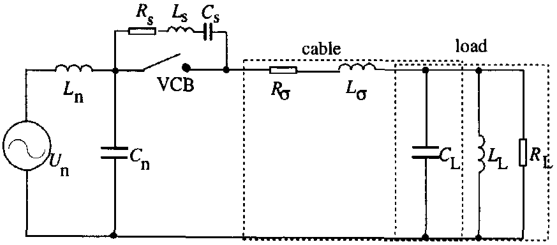

Figure 2-13: Single-phase circuit for reignition study

Table 2.3: Circuit data

	$R[\Omega]$	L[mH]	C[nF]
L_n,C_n		5	100
R_s,L_s,C_s	100	5.e-5	0.1
R_σ,L_σ	2	4e-2	
R_L,L_L,C_L	1.e4	120	0.1

shows the variation of circuit breaker current and voltage across the breaker's contacts, whilst Figure 2-15 displays the current and voltage at the load side. The first reignition after chopping is depicted in Figure 2-16. After the vacuum circuit breaker contacts have opened, the current flows until it reaches a value where it chops. After chopping, a TRV occurs and depending on the circuit topology, voltage oscillations with two different frequencies can exist. One frequency is in the range of a few MHz. When a reignition occurs, the load inductance slightly influence the high frequency component after the chopping, that is determined by the capacitance of the cable and load, the source side capacitance, the parasitic capacitance of the vacuum circuit breaker across the contact gap, the supply side inductance of the busbars and the cable. If we take into account that $C_n >> C_L$ and $L_s << L_\sigma$ then this frequency can be calculated with:

$$f_1 \approx \left(2\pi\sqrt{L_\sigma \frac{C_s C_L}{C_s + C_L}}\right)^{-1} \tag{2.8}$$

The other frequency component of the voltage oscillation is considerably lower and depends on the load parameters. It is the natural frequency of the load and its value is

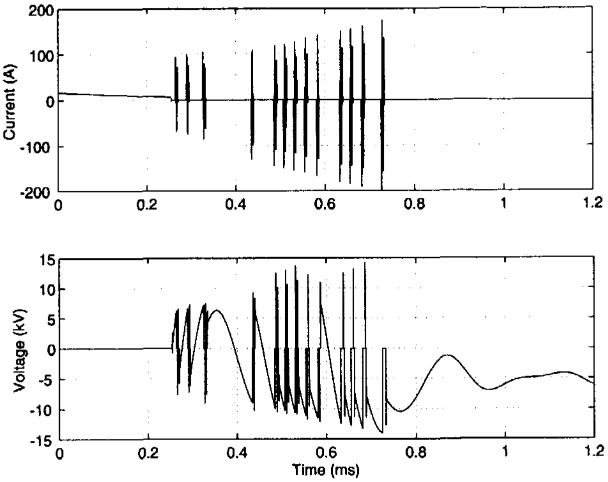

Figure 2-14: Simulated reignited current (upper trace) and voltage across the breaker contacts (lower trace) for the circuit in Figure 2-13

in the range of kHz. This frequency can be calculated by:

$$f_2 \approx \left(2\pi\sqrt{L_{\mathrm{L}}C_{\mathrm{L}}}\right)^{-1} \tag{2.9}$$

When the TRV surpasses the withstand voltage level of the vacuum gap, the breaker reignites and a high frequency current flows through a part of the network. The reignited current has two high frequency components superimposed on the power frequency current. One has a value of approximately 250 kHz and is calculated by:

$$f_3 \approx \left(2\pi\sqrt{L_{\sigma}C_{\mathrm{L}}}\right)^{-1} \tag{2.10}$$

and is the dominant frequency. The other oscillation is very high frequent and is superposed on the current oscillations with frequency f_3. This high frequency oscillation finds its origin in the parasitic capacitance and inductance of the gap and can be calculated by:

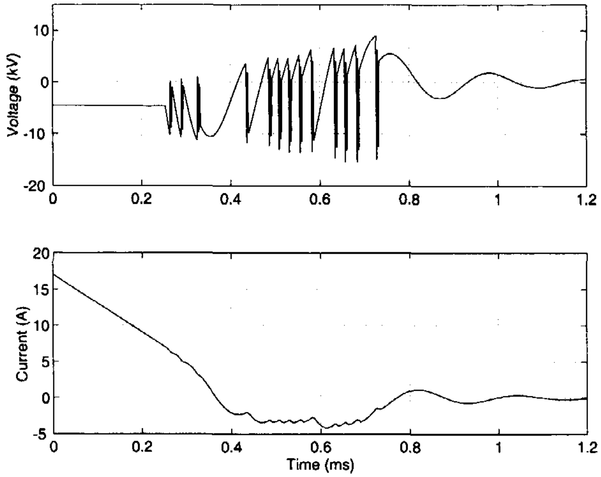

Figure 2-15: Simulated voltage (upper trace) and current (lower trace) at the load side for the circuit in Figure 2-13

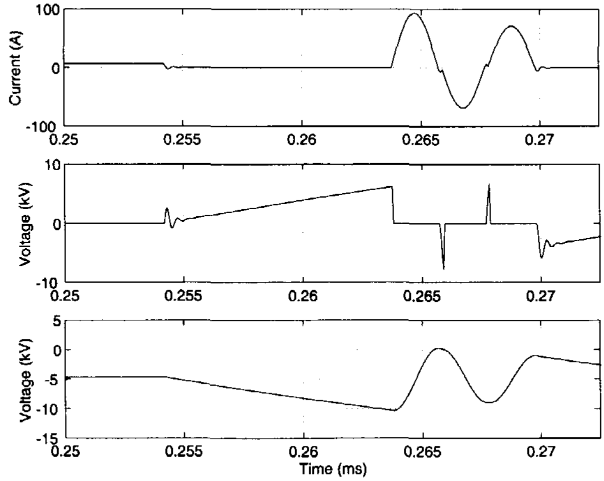

Figure 2-16: Simulated reignited current (upper trace), voltage across the breaker contacts (middle trace) and load side voltage (lower trace) for the circuit in Figure 2-13 during the first reignition

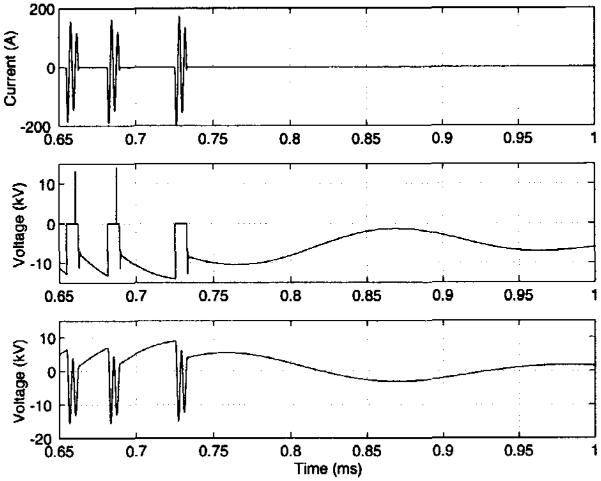

Figure 2-17: Zoomed values of the last three current reignitions, circuit breaker voltage and load side voltage from Figure 2-14

$$f_4 \approx \left(2\pi\sqrt{L_s C_s}\right)^{-1} \tag{2.11}$$

This frequency is in the range of a few tens of MHz. This corresponds to a high frequency peak voltage as shown in Figure 2-16. Measurements [37, 52, 73] confirm that it is likely that additional high frequency reignition components originate at the high frequency current zero followed by voltage spikes. These current waves last nanoseconds and could only be calculated if a very small time step is used. After the first reignition has damped out, the TRV rises again and this scenario is repeated until the arc completely extinguishes or is re-established. The last three current reignitions and the voltage across the vacuum circuit breaker and source side are shown in Figure 2-17.

2.5 Analytical analysis of the reignition overvoltages

In order to investigate the validity of the approach used for modelling reignitions in vacuum, an analytical analysis based on the simultaneous solution of circuit differential equations is carried out. For the period of reignition and that of extinction of the vacuum circuit breaker, two different circuits can be drawn, each described by different sets of equations.

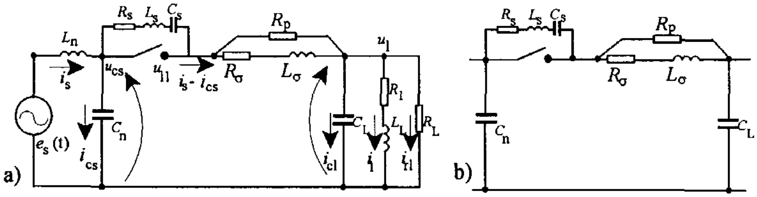

Figure 2-18: An analytical calculation of reignitions a) Sample circuit for computation reignitions; b) Part of the circuit that determines the high frequency component

During the reignition period, the switch is in closed position; when the arc extincts, the switch opens and the branch R_s - L_s - C_s forms part of the circuit. The studied circuit is displayed in Figure 2-18a. The set of equations for the period of reignition is:

$$\frac{di_s}{dt} = \frac{e_s(t)}{L_n} - \frac{u_{cs}(t)}{L_n} \tag{2.12}$$

$$\frac{du_{cs}}{dt} = \frac{i_{cs}}{C_n} \tag{2.13}$$

$$\frac{du_l}{dt} = \frac{1}{C_L}\left(i_s - i_{cs} - i_l - \frac{u_l}{R_L}\right) \tag{2.14}$$

$$\frac{di_l}{dt} = \frac{u_l}{L_L} - \frac{R_l}{L_L} i_l \tag{2.15}$$

$$\begin{aligned}\frac{di_{cs}}{dt} &= \frac{1}{L_\sigma}\left[u_l - u_{cs} + R_\sigma (i_s - i_{cs}) - \frac{R_\sigma}{R_p}(u_{cs} - u_l)\right] \\ &\quad + \frac{di_s}{dt} - \frac{1}{R_p}\left(\frac{du_{cs}}{dt} - \frac{du_l}{dt}\right)\end{aligned} \tag{2.16}$$

The high frequency component in this period depends mainly on the capacitances

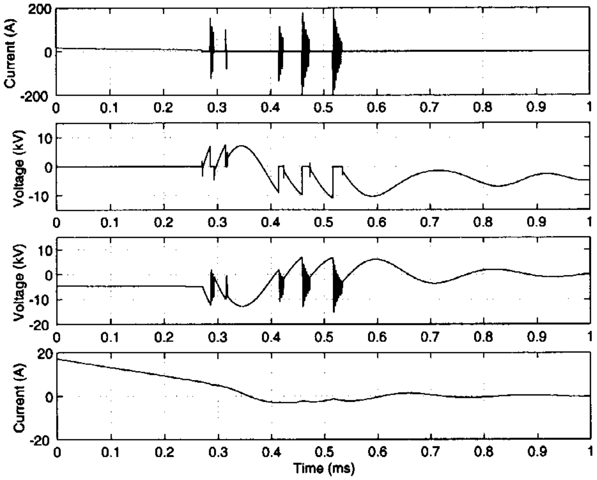

Figure 2-19: Calculated circuit breaker current (upper trace), circuit breaker voltage (upper middle trace), load side voltage (lower middle trace) and load side current (lower trace) from Figure 2-18a

and connected inductances, as shown in Figure 2-18b.

The period of arc extinction is described with another set of equations. It consists of seven equations; the equations (2.12) through (2.16) and two other equations which take into account the R_s - L_s - C_s branch:

$$\begin{aligned}(L_\sigma + L_s)\frac{d^2 i_{cs}}{dt^2} &= -\frac{du_{cs}}{dt} + (R_\sigma + R_s)\left(\frac{di_s}{dt} - \frac{di_{cs}}{dt}\right) + (L_\sigma + L_s)\frac{d^2 i_s}{dt^2} - \frac{R_\sigma}{R_p}\frac{du_{l1}}{dt} \\ &\quad + \left(\frac{R_\sigma}{R_p} + 1\right)\frac{du_l}{dt} + \frac{L_\sigma}{R_p}\left(\frac{d^2 u_l}{dt^2} - \frac{d^2 u_{l1}}{dt^2}\right) + \frac{1}{C_s}(i_s - i_{cs}) \qquad (2.17)\end{aligned}$$

$$\frac{du_{l1}}{dt} = \frac{du_{cs}}{dt} - R_s\left(\frac{di_s}{dt} - \frac{di_{cs}}{dt}\right) - L_s\left(\frac{d^2 i_s}{dt^2} - \frac{d^2 i_{cs}}{dt^2}\right) - \frac{1}{C_s}(i_s - i_{cs}) \qquad (2.18)$$

In (2.17) and (2.18), u_{l1} is the voltage of the vacuum circuit breaker's source side when the vacuum circuit breaker is open.

When the switch is closed, this voltage is equal to the source side voltage u_{cs}. These

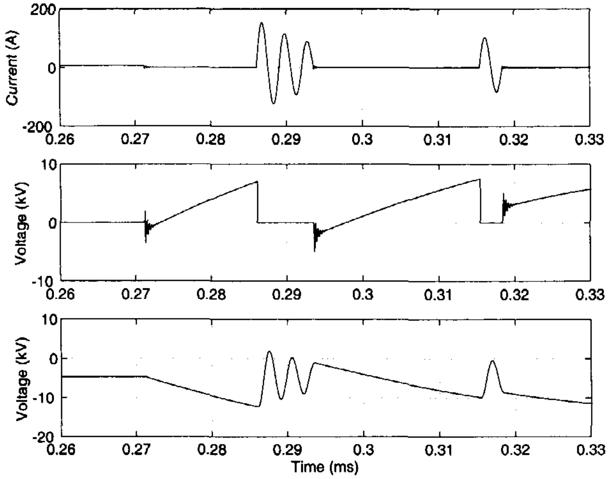

Figure 2-20: Description of the first two reignitions from Figure 2-19; circuit breaker current (upper trace); circuit breaker voltage (middle trace); load side voltage (lower trace)

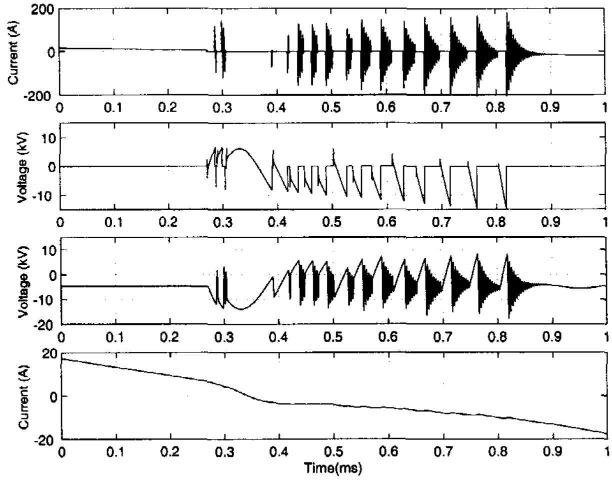

Figure 2-21: Calculated circuit breaker current (upper trace), circuit breaker voltage (upper middle trace), load side voltage (lower middle trace) and load side current (lower trace) from Figure 2-18a

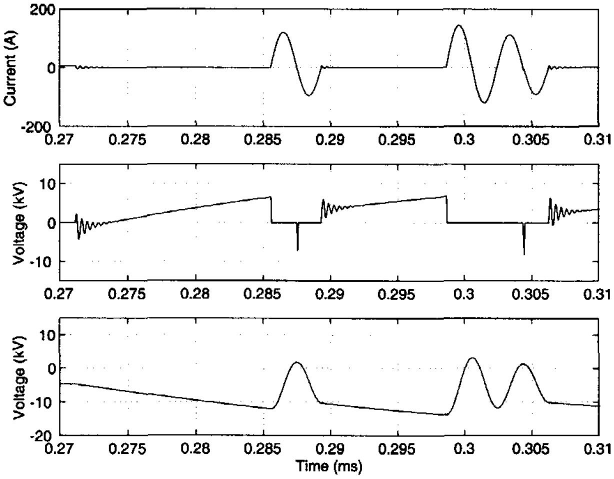

Figure 2-22: Description of the first two reignitions from Figure 2-21; circuit breaker current (upper trace); circuit breaker voltage (middle trace); load side voltage (lower trace)

equations can be simplified if the frequency of restrikes is much higher than the source frequency. In this case, the source can be regarded as having a constant amplitude. This assumption significantly simplifies the solution of equations (2.17) and (2.18). The equations can be solved accurately enough by means of a fourth order Runge-Kutta method. The withstand voltage characteristic and the arc quenching characteristic of the high frequency current are used to determine the instant of arc reignition and the instant of extinction, respectively. Thus, this instant is used as a parameter that shows which set of equation must be solved with respect to the state of extinction or state of reignition of the arc. The solutions of the one set of equations at that instant are initial conditions for the solutions of the next set of equations. During the period of reignition, whenever the high frequency current passes through current zero, the arc temporarily extinguishes. At this instant a very high frequency current flows. This current part is determined by the R_s-L_s-C_s branch and the voltage equation is:

$$L_s \frac{di_b}{dt} + R_s i_b + \frac{1}{C_s} \int_{t_{off}}^{t} i_b dt = U_b(t_{off}) \tag{2.19}$$

where t_{off} is the instant when the high frequency current zero is reached and $U_{\mathrm{b}}(t_{\mathrm{off}})$ is the recovery voltage at this time instant. In equation (2.19) it is assumed that L_{s} and C_{s} are constant and linear. According to the last equation, the current is:

$$i_{\mathrm{b}} = \frac{2U_{\mathrm{b}}(t_{\mathrm{off}})}{dL_{\mathrm{s}}} e^{(-\frac{\delta}{2}(t-t_{\mathrm{off}}))} \sin(\frac{d}{2}(t-t_{\mathrm{off}})) \tag{2.20}$$

where $\delta = \frac{R_{\mathrm{s}}}{L_{\mathrm{s}}}$ and $d = \sqrt{4\omega_{\mathrm{s}}^2 - \delta^2}$, $\omega_{\mathrm{s}}^2 = \frac{1}{L_{\mathrm{s}}C_{\mathrm{s}}}$ and $t > t_{\mathrm{off}}$. At each next current zero this component is superposed on the high frequency current and subsequently the voltage is calculated. This results in voltage spikes as can be seen from the computation. The voltage spikes, the high frequency components and therefore the number of current zero crossings during reignition occur randomly, because of the stochastic nature of the critical current slope and the resulting withstand voltage. The amplitudes and frequencies depend on the values of the circuit parameters.

Figure 2-19 through Figure 2-22 show the results of the numerical calculation of the reignition for the given test circuit. Figure 2-19 and Figure 2-20 depict the *successful* arc clearing. The contacts separate approximately 200 μs before current zero. The busbar inductance between the load and the vacuum circuit breaker is approximately $L_\sigma = 25$ μH. Figure 2-21 and Figure 2-22 show the results of an *unsuccessful* arc clearing. The arcing time is in this particular case 150 μs and the bus connection $L_\sigma = 40$ μH. As can be seen voltage spikes are visible in this case. The very high frequency of voltage spikes requires a very small time step and that makes the calculation time rather long.

2.6 Conclusion

A vacuum circuit breaker model that takes into account the reignition phenomena has been introduced. A study of reactor switching based on a simplified single-phase circuit has been performed. The mechanisms for overvoltage generation are: current chopping, reignition and multiple reignitions. The instant of contact opening and the mean chopping level of the vacuum circuit breaker play a significant role in the interruption process. The shorter the arc angle, the higher the probability of multiple reignitions. The amplitude of the chopping current is the parameter that determines the likelihood of the first reignition. Due to reignitions, voltage oscillations with very high frequencies are generated. These voltage transients can be a few times higher in amplitude than the rated voltage of the network and they have a very short rise time. Whether or not a reignition will occur depends on the value of the chopping current *and* the ability of the vacuum circuit breaker to withstand the TRV. The parameters determining whether or not the reignitions occur are the dielectric withstand capability of the gap and the values of the circuit components. When a vacuum circuit breaker operates in a three-phase network, it is not only important to model the vacuum circuit breaker but also the surrounding network. The inductance of the busbar from the vacuum circuit breaker to the load controls the number of reignitions. The circuit parameters also determine the reignition frequency and the amplitude of the reignited current. The higher slope of the reignited current leads to more severe reignitions. The load side inductance influences the value of the TRV peak. For a particular value of the chopping current, a larger load inductance can store more magnetic energy and that generates a higher overvoltage. For unloaded transformers, this inductance is non-linear and the iron losses play an important role. Even though no reignition may take place, it is important to model this inductance accurately to calculate the TRV.

Chapter 3

Modelling of the Supply Network

3.1 Introduction

In this chapter the representations of cables and busbars are analysed. The comparison between the frequency characteristic of the modelled cable with the standard ATP models is shown. The busbars are modelled only with an inductance and the results are compared by some ATP models when busbars are represented by transmission lines. The modelling of transformer and surge arresters used for equipment protection is treated in the next chapters.

3.2 Busbars

Busbars play an important role in the switching studies especially when short cable connections are used between the interrupting device and the load. In that particular case, the busbar reactance is the dominant element and the length of the busbars influences the number of reignitions in the vacuum circuit breaker. The transient response of a substation busbar is similar to that of short length of overhead transmission line. Because of the construction of the conductors and its installation environment, for example for gas insulated substations, the characteristic impedance of the busbar can be lower than that of a transmission line. The ohmic losses for short busbars can be neglected. Therefore, in the switching surge studies, a busbar can be described by an ideal transmission line having a specific characteristic impedance and a certain wave speed. In our calculations the busbars are represented by an inductance determined from the wave travel time τ and the characteristic impedance. For instance, if a given busbar with length l has a characteristic impedance $Z_C = \sqrt{\frac{L_0}{C_0}}$ and a traveling wave speed $v = \frac{1}{\sqrt{L_0 C_0}}$, then the equivalent inductance can be calculated as:

$$L_{\text{eq}} = Z_C \tau$$

where L_0 and C_0 are the inductance and the capacitance per unit length. The stray capacitance of a busbar is much less than the effective capacitance of the cables and the capacitance of the components that are connected to the bus. Figure 3-1 shows a simple network with two cables. The cables are connected through a busbar of 5 m length of which the equivalent inductance of the busbar is 1 μH/m. The characteristic impedance of the cables is 30 Ω and they are 100 m and 50 m long. The resistive load of 500 Ω is connected to the second cable. The system is energised and the current through the switch and voltage of the load is calculated for two cases. In the first case, the busbar is simply represented by its equivalent inductance. In the second case, the busbar is modelled accurately by a *JMarti* [53, 54] frequency-dependent model. The results of these calculations are presented in Figure 3-2 and Figure 3-3 respectively. These results show that we can use a lumped inductance representation without a big error. For cases where the length of the busbar is comparable to that of the cable, the stray capacitance of a busbar has a value that cannot be neglected. In this case, the capacitance should be divided into two parts and added at each side of the equivalent inductance as a lumped capacitor.

3.3 Cable Modelling

Cables can be divided in shielded cables and unshielded cables. The purpose of the shield is to confine the electric field between the screen and the conductor. The magnetic field is not treated in the same way and it is influenced by the presence of the shield (and

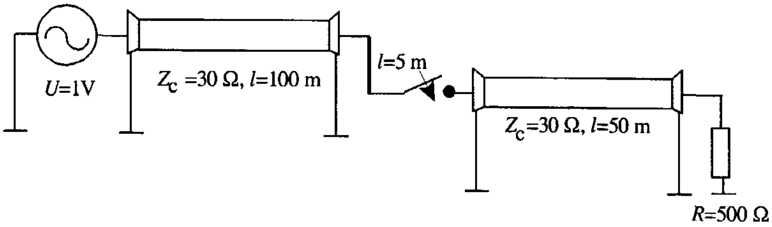

U=1V
Z_c =30 Ω, l=100 m
l=5 m
Z_c=30 Ω, l=50 m
R=500 Ω

Figure 3-1: Cable system for busbar response testing

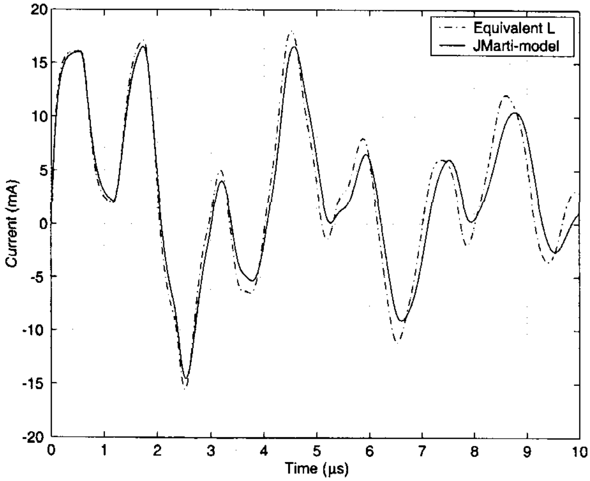

Figure 3-2: Switch current at the busbar from Figure 3-1

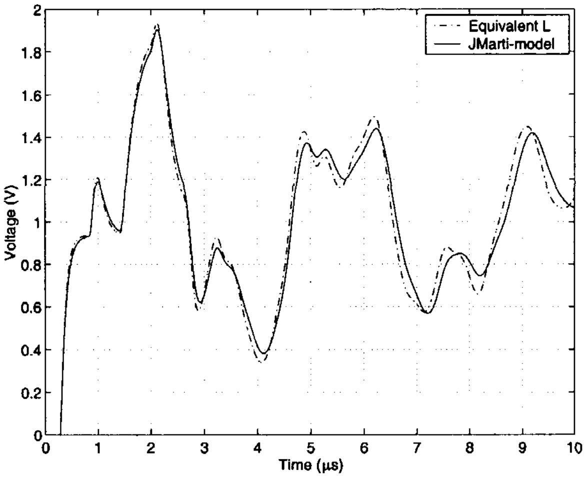

Figure 3-3: Voltage response at the load from Figure 3-1

other metal armours if present) because of the induced eddy currents and the magnetic permeability.

Power cables are frequently laid in metal conduits. The conduit is generally grounded and like the screen of a shielded cable, the conduits acts as an equipotential surface for the electric field of the conductor. Similar to overhead lines, there are cases where a cable can be represented by an impedance equal to its characteristic impedance. The cable characteristic impedance is in general lower than the characteristic impedance of an overhead line. The distance between the cable conductors is less than the distance between overhead line conductors. This results in an increased capacitance and a reduced inductance of the cable. The values of the cable characteristic impedance varies between 20 Ω and 50 Ω. The cable capacitance is also influenced by the dielectric permittivity, which also reduces the speed of wave propagation along the cable up to typically one half to two thirds of the speed of light.

For low frequency transients, the dominant parameter of a cable is its capacitance. A cable can therefore be modelled by its capacitance. In general, for a wide range of frequency transients, like switching surges produced by a reactor switching with a vacuum circuit breaker or lightning impulses, a frequency-dependent cable model is required.

ATP-EMTP has cable models for shielded and for unshielded cables. A cable with Π-sections is modelled by means of the Cable Constants routine, where each Π-section consists of a resistance, an inductance and a phase-to-ground capacitance per unit length. The frequency-dependent ATP cable model can lead to possible instabilities in the calculation. Therefore, the cable is often modelled by making use of Π-sections with capacitive and inductive mutual coupling between the phases. This chapter introduces a simplified cable model that makes use of Π-sections. The frequency characteristic is calculated and compared to that of the JMarti frequency-dependent cable model.

3.4 Single-phase cable model

When treated as a two-port network, cables and overhead lines satisfy the following equations:

$$\begin{aligned} V_{\mathrm{S}} &= V_{\mathrm{R}} \cosh(\gamma l) + Z_{\mathrm{C}} I_{\mathrm{R}} \sinh(\gamma l) \\ I_{\mathrm{S}} &= I_{\mathrm{R}} \cosh(\gamma l) + \tfrac{V_{\mathrm{R}}}{Z_{\mathrm{C}}} \sinh(\gamma l) \end{aligned} \tag{3.1}$$

where V_{S} , I_{S} and V_{R} , I_{R} are the voltages and currents at the sending and receiving end, respectively, γ is the propagation constant, and l is the cable length. The propagation constant is:

$$\gamma = \sqrt{zy} \tag{3.2}$$

where z and y are the cable impedance and admittance per unit length. The characteristic impedance depends on the frequency:

$$Z_{\mathrm{C}}(\omega) = \sqrt{\frac{z}{y}} = \sqrt{\frac{R + j\omega L}{G + j\omega C}} \tag{3.3}$$

For very high frequencies, the characteristic impedance becomes:

$$Z_{\mathrm{C}}(\omega) = \lim_{\omega \to \infty} \sqrt{\frac{R + j\omega L}{G + j\omega C}} = \sqrt{\frac{L}{C}} \tag{3.4}$$

If the receiving end of the cable is open, the current at the end of the cable is zero. The equation 3.1 becomes:

$$\begin{aligned} V_S &= V_R \cosh(\gamma l) \\ I_S &= \tfrac{V_R}{Z_C} \sinh(\gamma l) \end{aligned} \tag{3.5}$$

The driving impedance function is in that case

$$Z_{\text{in}} = \frac{V_S}{I_S} = Z_C \frac{\cosh(\gamma l)}{\sinh(\gamma l)} \tag{3.6}$$

For a lossless cable $\gamma = \sqrt{LC}s$ and (3.6) becomes:

$$Z_{\text{in}} = Z_C \frac{\cosh(\tau s)}{\sinh(\tau s)} = -jZ_C \frac{\cos(\omega\tau)}{\sin(\omega\tau)} \tag{3.7}$$

where $s = j\omega$ and τ is the travel time of the wave along the cable. One can see that the zeros appear at angular frequencies

$$\omega\tau = \frac{k\pi}{2}, \ (k = 1, 3, 5, ...)$$

and poles appear at

$$\omega\tau = k\pi, \ (k = 0, 1, 2, 3, 4, ...).$$

So, there is an infinitely large number of poles and zeros which are spaced with a separation distance of $\pi/2$. The resonant frequencies of the impedance are related to the cable transit time. The first natural frequency corresponds to a period that is four times the travel time of a cable. For steady-state analysis, the length of a Π-section can be adjusted such that they precisely represent a piece of cable at power frequency. For transient analysis an infinite number of frequencies exists, and to acquire an accurate representation we need to increase the number of Π-sections. When the number of sections for a typical cable length is increased, each section becomes smaller and smaller and the approximation leads to a distributed cable model.

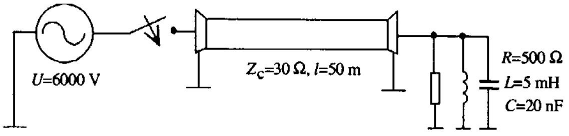

Figure 3-4: Cable with a *RLC* load

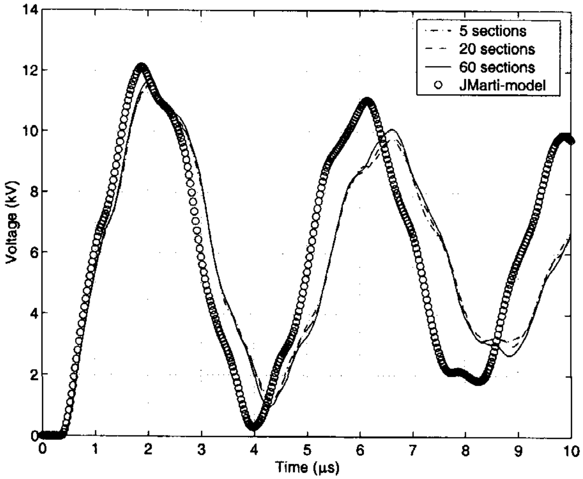

Figure 3-5: Voltage at the receiving end of the cable from Figure 3-4

The parameters for the cable resistance R, cable inductance L and cable capacitance C can be accurately calculated for a constant frequency at 50 Hz by ATP's Cable Constants. Thus, a Π-section can also account for the losses and this leads to a more realistic cable model. Figure 3-4 shows a cable supplying a load. We compare the current at the sending end of the cable and the voltage response at the receiving end of the cable for the frequency-dependent cable model and a cable representation with lumped Π-sections. These results are presented in Figure 3-5 and Figure 3-6.

The ATP cable constants routine does not take into account the cable dielectric losses and the lumped parameters are only calculated for power frequency. For fast switching surge calculations, the model should represent the terminal impedance at different fre-

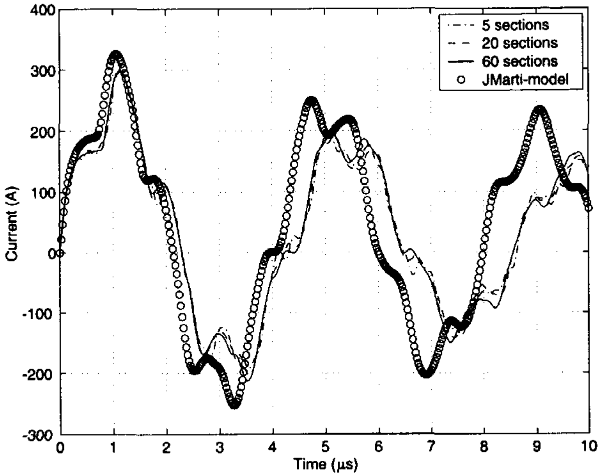

Figure 3-6: Current at the sending end of the cable from Figure 3-4

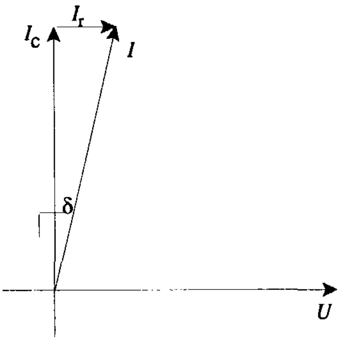

Figure 3-7: Phasor representation of the cable dielectric losses

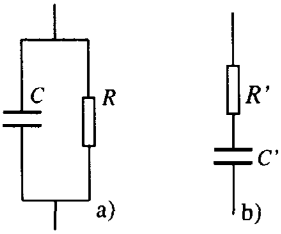

Figure 3-8: Equivalent circuits for lossy capacitors

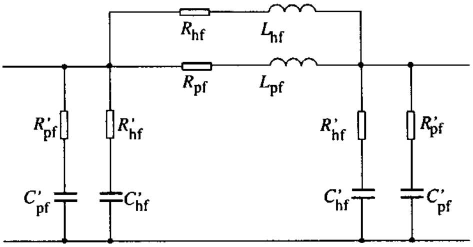

Figure 3-9: Lumped element representation of a single-phase cable Π-section

quencies, which is why it is necessary to find another representation of the cable. First, we have to account for the dielectric losses in the cable. In an insulation material these losses are small, but from the point of view of electromagnetic transients, they influence the cable characteristics significantly. Dielectric losses are expressed by loss component I_r, of the dielectric current as shown in Figure 3-7.

The relationship between the resistive loss component and the capacitive component is:

$$I_r = I_c \tan\delta \tag{3.8}$$

and the losses for a specific frequency are:

$$P_c = UI_c \tan\delta = U^2 \omega C \tan\delta \tag{3.9}$$

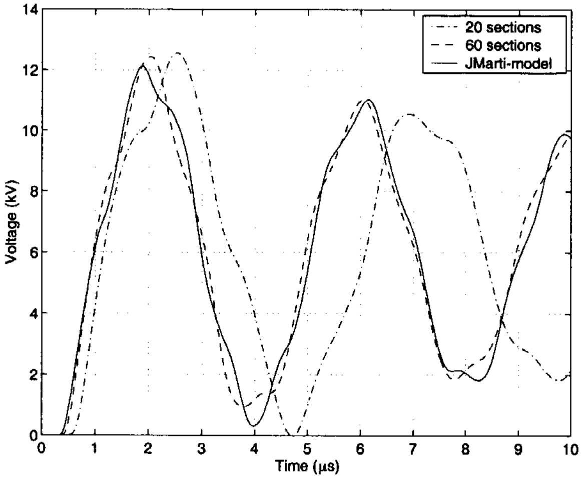

Figure 3-10: Comparison between voltage at the receiving end of the cable from Figure 3-4 with upgraded Π-section model

Expression (3.9) shows that the losses are directly proportional to $\tan\delta$. So the lossy capacitor can be represented by one of the equivalent circuits of Figure 3-8. The parallel circuit is more often used. We can see in Figure 3-8a that the parallel circuit of a lossy capacitor has two branches instead of one which are used to represent series circuit for a lossy capacitor. If we were to use a lot of Π-sections to represent the cable better, the parallel circuit would increase the total number of branches included in the ATP program. We have to avoid using a lot of branches in order to decrease the computation time. From Figure 3-8a it is clear that the smaller the hypothetical parallel resistance, the larger the loss tangent. For the series circuit the opposite is true: the $\tan\delta$ increases proportionally with the hypothetical series resistance. The relationship between the parameters in Figure 3-8a and Figure 3-8b is given by expressions (3.10) and (3.11):

$$R' = \frac{R\tan^2\delta}{1+\tan^2\delta} \approx R\tan^2\delta \tag{3.10}$$

$$C' = C\left(1+\tan^2\delta\right) \approx C \tag{3.11}$$

These parameters are calculated for one frequency only, but the tan δ is also considered for power frequency. Since the model must be valid for high frequencies, a Π-section with parameters calculated at high frequency is connected in parallel with the Π-section with parameters calculated at power frequency, because the values of parameters for high frequencies differ from the ones at power frequency. All the parameters of the Π-section are calculated by means of the Cable Constants routine, and a correction for the losses in the capacitance are included by taking into account the $\tan\delta$. The value of the tan δ also depends on the frequency: higher frequencies correspond to lower tan δ, because $\tan\delta = \omega R'C'$. Figure 3-9 shows a Π-section for representing a single-phase cable. Figure 3-10 compares the calculated voltage response of the JMarti-model and an upgraded Π-section.

3.5 Investigation of the cable's frequency dependency

In accordance with the cable model described in section 3.4, in this section the results of the frequency-dependent impedance response is presented and compared with the results of the frequency-dependent ATP routine. The cable under study has no external screen around the phase conductors. The cross section of one phase of the cable is shown in Figure 3-11.

The filled part with radius $r_2 - r_1$ represents the conductor of the phase and the ring with a width $r_4 - r_3$ is the cable's sheath. Phase conductors and sheath also have a specific resistance and a magnetic permeability ρ_c, μ_c and ρ_s, μ_s respectively. The insulation is determined by its magnetic permeability and dielectric permittivity μ_{i1}, ε_{i1} and μ_{i2}, ε_{i2} for the inner and outer insulator, respectively. The data used for a 20 kV cable are summarised in Table 3.1. With these parameter values, a Π-section cable model is defined and implemented in ATP-EMTP.

In order to verify the validity of the model, the frequency and amplitude characteristics are compared with those calculated with ATP's frequency-dependent model and with measurements [38]. A frequency scan of the cable is done for an unloaded cable with an open and shorted receiving end as shown in Figure 3-12. It can be seen that this

Table 3.1: Data for a 20 kV cable, NA2XS2Y

Inner radius of the phase conductor r_1	0 m
Outer radius of the phase conductor r_2	$0.495e-2$ m
Inner radius of the sheath r_3	$1.2e-2$ m
Outer radius of the sheath r_4	$1.22e-2$ m
Outer radius of the second insulator r_5	$1.6e-2$ m
Specific resistivity of the conductor ρ_c	$2.84e-8$ Ωm
Relative magnetic permeability of the conductor μ_c	1
Specific resistivity of the sheath ρ_s	$1.72e-8$ Ωm
Relative magnetic permeability of the sheath μ_s	1
Relative magnetic permeability of the inner insulator μ_{i1}	1
Relative dielectric permittivity of the inner insulator ε_{i1}	2.4
Relative magnetic permeability of the outer insulator μ_{i2}	1
Relative dielectric permittivity of the outer insulator ε_{i2}	2.3
Conductor	*Al*
Sheath	*Cu*
Insulator	*XLPE*
Outer insulator	*PE*
tan δ	0.0002 to 0.0005

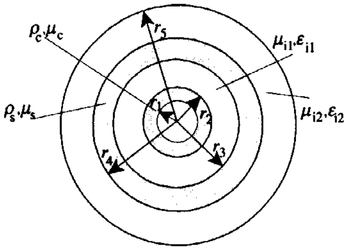

Figure 3-11: Cross section of a single-phase cable

model of the cable can be used for a wide frequency range. The calculation is performed for a 60 m long cable. Each Π-section has a length of 1 m.

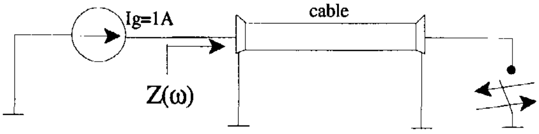

Figure 3-12: Frequency scan of a single-phase cable

Figure 3-14 shows the impedance amplitude and phase characteristics for a cable with an open receiving end, and Figure 3-15 one of which the receiving end is shorted to earth. It can be concluded that for both cases the impedance amplitude shows good agreement in the range up to a few MHz. For both cases, the impedance phase characteristic shows a slight deviation of at most 10 degrees till 1 MHz. For higher frequencies, there is slight deviation in the results as it is for the impedance amplitude characteristic. Comparison with the measurements shows that the calculated characteristics for the Π-sections give a better approximation than the ATP routine [38]. Another verification is the energisation of the cable. The cable (cable 1) is connected to a unit voltage impulse source at one side, and to a cable (cable 2) with the same parameters and equal length at the other side (see Figure 3-13). The receiving end of the last cable (cable 2) is open. Voltages at the sending and receiving end of the second cable are calculated. The single-phase cable energisation is calculated for both the ATP's frequency-dependent model and the Π-section model. The voltage responses due to energisation at the sending and at the receiving end of the cable 2 are shown in Figure 3-16 and Figure 3-17 respectively.

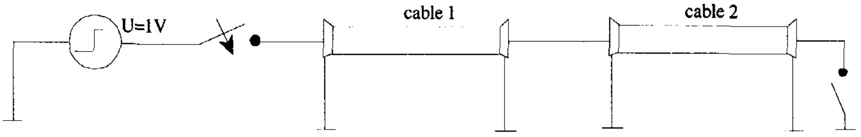

Figure 3-13: Test circuit for a voltage response study of the sending and receiving end of cable 2

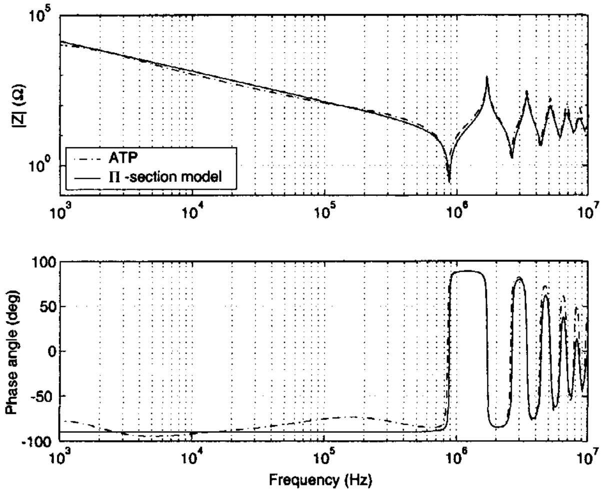

Figure 3-14: Frequency response of the impedance amplitude and phase characteristic of a cable - receiving end open according to Figure 3-12

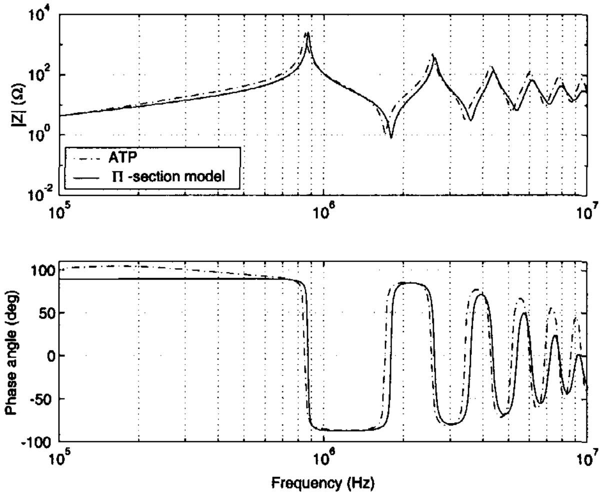

Figure 3-15: Frequency response of the impedance amplitude and phase characteristic of a cable - receiving end shorted to earth according to Figure 3-12

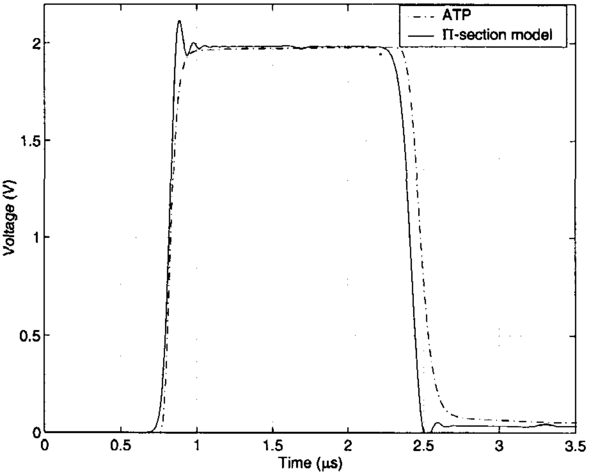

Figure 3-16: Comparison of the voltages at the sending end of cable 2 in Figure 3-13 when using ATP- and Π-section model

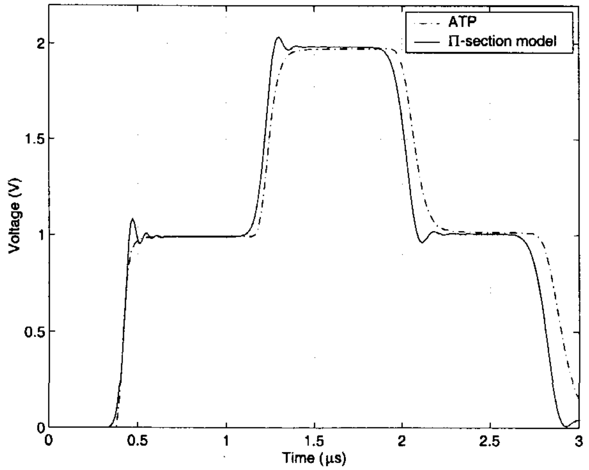

Figure 3-17: Comparison of the voltages at the receiving end of cable 2 in Figure 3-13 when using ATP- and Π-section model

An open circuit at the end of the cable means that the current at the end of the cable must be zero at any instant. After the switch has been closed and cable 1 has been connected to the voltage source, the cable is stored with an amount of energy half of which cames from the magnetic field and half from the electric field. This is because a current and a voltage wave travel along the cable, so the energy stored in the magnetic field is proportional to the square of the current, and the energy stored in the electric field is proportional to the square of the voltage. At the end of the cable, a current wave with the same value and opposite polarity is created in order to satisfy the required current zero condition at the receiving end. This means that the magnetic energy associated with the current is brought to zero at the open circuit.

If the travel time of the wave along the cable is τ, by the time the current and voltage wave reach the receiving end, an amount of energy $UI\tau$ will be stored in the cable from the source. Half of this will reside in the electric field ($UI\tau/2$) and half in the magnetic field ($UI\tau/2$). τ seconds later, energy of $2UI\tau$ has been imparted to the line. Since the current disappears, all of the energy is now stored in the electric field and it is now 4 times greater than it was τ seconds earlier, and the voltage along the line must be doubled. This process continues until the steady-state condition is reached, where the voltage along the cable is equalised to the value of the source voltage.

A parameter that increases the accuracy of the model is the number of R-L branches in one Π-section (Figure 3-9). We have used values for 50 Hz and for 1 MHz. If we use more parallel branches per Π-section for the higher frequencies, the model will also be more accurate.

Experience has shown that ATP's frequency-dependent JMarti and SEMLYEN routine can only be used with success for modelling overhead lines and single-phase cables. The use of these models for three-phase cable studies sometimes leads to instability when a complex power system with different loads is investigated. Therefore, in this thesis for calculations, the model with Π-sections is used.

3.6 Three-phase cable modelling

If a three-phase cable is designed such that each phase uses its own sheath as return current path, then the flux links only the current of its own phase and there is no mutual coupling between the three phases. The single-phase model is in that case sufficient to model the electrical behaviour of the cable. For a three-phase cable, like the belted cable (a shielded cable with an external armour that is a common sheath for all three phases) or an unshielded three-phase cable, there is no separate current return path for each phase and the flux of each phase mutually links with the other two phases. The single-phase model is not applicable any longer and modifications must be done to take inter-phase coupling into account.

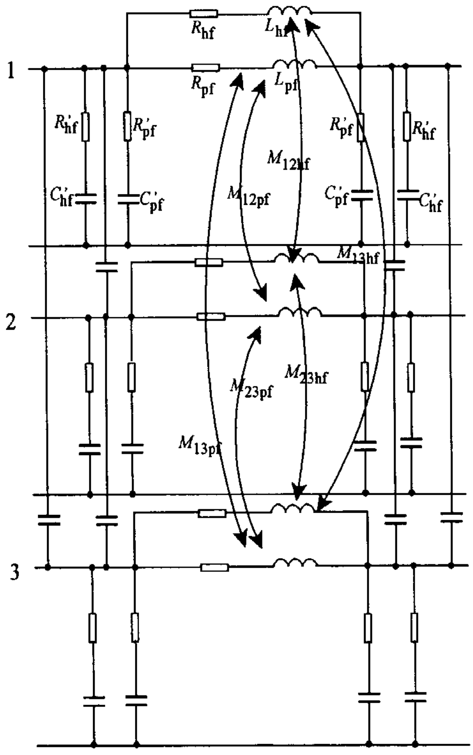

Figure 3-18: Model for an unshielded three-phase cable

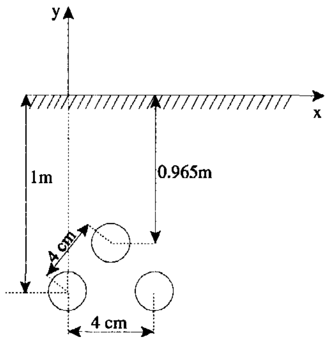

Figure 3-19: Position of the cable in soil

The ATP's cable routines can calculate the inter-phase capacitance and mutual inductance accurately for different types of cables. The three-phase model that is used in the analyses in this thesis is shown in Figure 3-18, and the cable is buried in the earth, as shown in Figure 3-19. In this cable model, the inter-phase capacitance does not have a loss component. At high frequencies, the loss component is very difficult to determine and no measured data are available.

3.7 Conclusion

Standard ATP cable models do not represent the cable for a wide range of frequencies. Based on the dimensions of the cable and its electrical and dielectric properties, these models can calculate the parameters of a cable Π-section accurately and can represent the cable up to a few tens of kHz. Although the frequency-dependent models can be used successfully for the overhead lines, the JMarti frequency-dependent model can be used only to check the behaviour of the cables impedance at different frequency. The use of this model within a more complicated circuit shows certain instabilities so the model cannot be used for three-phase cable modelling.

It should be stressed that the losses in the cable become higher as the frequency rises. These losses are caused by the skin effect in the conductors and dielectric losses expressed through cable's $\tan\delta$. A higher frequency component is subjected to more damping than a lower frequency component and the significance of the higher frequency component is smaller. One of the ways to take the frequency dependency into account is to construct a lumped Π-section which will take into account the cable's resistivity, the cable's inductance and capacitances at different frequencies. These parameters are determined by the Cable Constants model. The cable analysis shows that the capacitance of the cable weakly varies with the frequency. By increasing the frequency, the major variation exists in the cable resistance so this parameter influences the results significantly. The model shows a larger deviation at frequencies higher than 1 MHz. In order to increase the accuracy of the applied method one can use more Π-sections and increase the number of parallel R-L branches in one Π-section. Despite the research in this field, not many results are achieved and more work should be done to develop better models to represent the behaviour of the frequency dependency of the cable more accurately and to implement a frequency-dependent cable model in a transient program. Measurements done by *Helmer* and *Lindmayer* [38] show the presence of the same behaviour of the cable at high frequencies as the results presented here. So due to a lack of own measurements, the author verifies his calculations with the measurements and calculations in [38].

Chapter 4

Transformer modelling

4.1 Introduction

We have seen in the previous sections that due to switching surges caused by a vacuum circuit breaker, electromagnetic transients in a wide range of frequencies are generated. Therefore it is necessary, just like the cable, to use a transformer model that accounts for these high frequency oscillations. So far the CIGRE WG 13.02 has done extensive research on switching small inductive currents [10] based on experimental and analytical investigations. But, the transformer models used were often simplified and the transformer was mainly modelled by taking into account the transformer hysteresis or saturation and the total transformer capacitance, without paying attention to the behaviour of the transformer at different frequencies. In many cases *Boyle's* method [2, 3] was applied for calculating the maximum overvoltage. *Boyle's* method is based on estimating the effective primary inductance by means of the energy balance of the released magnetic energy. The definition of the effective primary inductance has a correlation with the hysteresis curves of the transformer. For calculating the overvoltages, the total transformer capacitance is used.

This method can be applied to compare the maximum overvoltage level of measurements and computations, but it does not take into account the history of the reignited overvoltages. A major drawback is that these models do not satisfy the transformer frequency characteristic because by using the total transformer capacitance the model does not take into account all frequency components.

An adequate model should truly represent the transformer over a wide range of frequencies. At high frequencies special attention should be given to the modelling of the transformer winding, because its impedance can vary during the transient state. But if no reignition occurs, the electromagnetic transients are in the low frequency domain and the unloaded transformer behaves as a non-linear reactor. The non-linearity is caused by the magnetic saturation and the hysteresis of the transformer core. Also because of the non-linear transformer core, inrush currents flow when a transformer is energised. Depending on the rate of saturation, the amplitude of the inrush currents can reach values a few times larger than the rated transformer current. Switching off such inrush currents can lead to a VCC in the surrounding network and that can cause severe overvoltages. We can distinguish two separate cases, when a vacuum circuit breaker reignites and when it interrupts the current without reignition.

The first case, where the vacuum circuit breaker reignites, requires the transformer model to have a wide frequency representation. At higher frequencies, fast flux variations take place and the saturation and hysteresis of the transformer core do not play a significant role and can therefore be neglected. This is supported by the theoretical investigation based on the *Maxwell* equations that demonstrate that the field distribution in the iron core laminations is not uniform for higher level harmonics. The index of non uniformity defined as the ratio of magnetic induction value at the centre to the magnetic induction value at the surface decreases considerably as the frequency increases. Due to the reduced flux penetration at a relatively higher frequency range, the performance of an iron core winding tends to be linear. However, particularly below 100 kHz, where switching transients are likely to be present, the linear assumption is not obvious.

The second case, where the vacuum circuit breaker interrupts the current without reignition, only requires the saturation and hysteresis. In order to calculate the electromagnetic transients accurately, one should take into account the residual flux. It has a significant influence on the generation of overvoltage and cannot be neglected.

The terminal impedance characteristic gives sufficient information about the wide frequency range performance not only for transformers but also for rotating machines. Such a test both for transformers and rotating machines was done by *Soysal* [80], who showed that when the transformer secondary winding is open, the presence of an iron core affects the frequency response below 100 kHz considerably by shifting the resonant frequencies and increasing the impedance magnitude. When the secondary winding is shorted, the main flux in the core is partially cancelled by the secondary ampere turns. In this case, the impedance measured on the primary winding terminals is determined by the leakage flux, and the difference observed from the presence or the absence of the core is very small. As a consequence, the linear assumption is in general acceptable over a wide frequency range if the current path of the windings linked by the same flux is closed, as it is in the case of a shorted transformer. When the transformer is at no load, the characteristic will be different as indicated by the previous observation. Table 4.1 [25] shows a description of possible models for two-winding transformers with and without surge transfer. It can be seen that, depending on the frequency, the behaviour of the transformer is different. This implies that we could accurately calculate the switching overvoltages if a different model is used for each different transient condition. However, this is not possible since there is no general transformer model that can describe the response in any operating condition.

This chapter will give details for the proposed transformer model for studying the switching surges due to a vacuum circuit breaker reignition for a wide range of frequencies.

Table 4.1: Transformer models for different frequency intervals

Transformers	*Group 1:*	*Group 2:*	*Group 3:*	*Group 4:*
	0.1Hz÷3kHz	50/60Hz÷20kHz	10 kHz÷3MHz	100kHz÷50MHz
No surge transfer	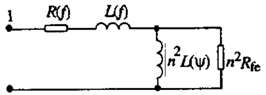 1 R(f) L(f) n²L(Ψ) n²Rfe	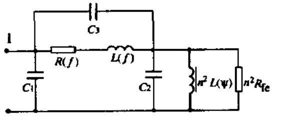 1 C3 R(f) L(f) C1 C2 n² L(Ψ) n²Rfe	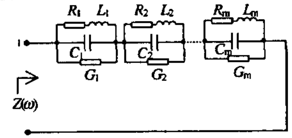 1 R1 L1 R2 L2 Rm Lm C1 C2 Cm G1 G2 Gm Z(ω)	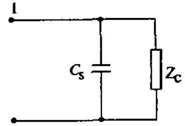
With surge transfer	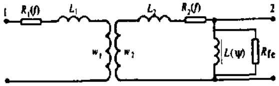 1 R1(f) L1 L2 R2(f) 2 w1 w2 L(Ψ) Rfe	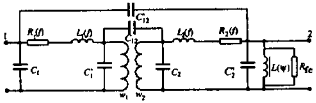 1 R1(f) L1(f) C12 L2(f) R2(f) 2 C1 C1 C2 C2 L(Ψ) Rfe w1 w2	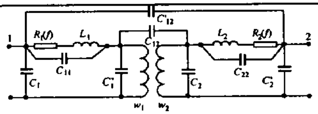 1 R1(f) L1 C12 L2 R2(f) 2 C11 C22 C1 C1 C2 C2 w1 w2	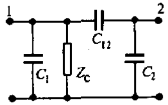 1 2 C12 C1 Zc C2
Short circuit impedance	Very important	Very important	Important only for surge transfer	Negligible
Saturation	Very important	Very important for transformer energising and load rejection with high voltage increase	Negligible	Negligible
Frequency-dependent series losses	Very important	Important	Negligible	Negligible
Hysteresis and iron losses	Important only for resonance phenomena	Important only for transformer energising	Negligible	Negligible
Capacitive coupling	Negligible	Important only for surge transfer	Very important for surge transfer	Very important for surge transfer

Examples for single-phase two-winding transformers

(index 1: primary winding; index 2: secondary winding; turn ratio $n = w_1/w_2$)

L - inductance	f - frequency	R_{fe}- hysteresis and iron losses	Z_C - characteristic impedance
R - resistance	Ψ- flux	$Z(\omega)$ - terminal impedance	
C - capacitance	$L(\Psi)$ - magnetising inductance	C_S - surge capacitance	

4.2 A terminal impedance transformer model

In our study, the model of the transformer is developed from a terminal impedance measurements (performed in LAPEM Mexico) which includes the core non linearity. The reason for this is that the magnetisation of the core is important for the generation of inrush current at energising. Therefore, when the transformer is switched on under no load, an enormous current might be drawn from the supply system because of the transformer core saturation. This current is several times larger than the nominal transformer current. So when focussing on the case of switching off the transformer shortly after energising, the magnetisation plays an important role. During switching, when a reignition occurs, the magnetising branch is no longer of great influence and the impedance of the windings can be described by RLC sections.

The first step is to find a way to determine the terminal impedance characteristic for a typical transformer if its frequency characteristic is known. Let us first assume that the system is linear and time invariant. The terminal in which the current is injected is the *driving* point terminal. If the driving point current is considered as input and the voltage as an output then the impedance can be represented as:

$$Z(s) = \frac{V(s)}{I(s)} = \frac{a_0 s^{\mathrm{m}} + a_1 s^{\mathrm{m}-1} + \ldots + a_{\mathrm{m}-1} s^1 + a_{\mathrm{m}}}{b_0 s^{\mathrm{n}} + b_1 s^{\mathrm{n}-1} + \ldots + b_{\mathrm{n}-1} s^1 + a_{\mathrm{n}}} \tag{4.1}$$

An investigation of this impedance for various types of transformers and machines prove that:

$$\lim_{\omega \longrightarrow \infty} \{|Z(j\omega)|\} = 0 \tag{4.2}$$

$$\lim_{\omega \longrightarrow \infty} \{Arg\,[Z(j\omega)]\} = -\frac{\pi}{2} \tag{4.3}$$

Due to the stray capacitance, the magnitude of the terminal impedance approaches zero for extremely high frequencies. Therefore we can assume that m=n−1 [32, 80]. Also it can be assumed that all of the poles and zeros of the impedance function are simple, and the poles are complex conjugate in the s-domain. If the last two assumptions hold, that will help to simplify the characteristic in partial fractions from which it is easy to describe the equation (4.1) with an electric circuit. In practice, for motors and transformers this always holds. If the terminal impedance is plotted as a function of frequency, a number of peaks will be observed corresponding to resonances in the winding, and there is always one local maximum more than the number of local minima [32, 80]. If we expressed the impedance characteristic as a sum of partial fractions:

$$Z(j\omega) = \sum_{i=1}^{n/2} \frac{\alpha_i s + \beta_i}{(s - \lambda_i)(s - \lambda_i^*)} = \sum_{i=1}^{n/2} \frac{\alpha_i s + \beta_i}{s^2 + 2\sigma_i s + \sigma_i^2 + \omega_i^2} \tag{4.4}$$

where:

$$\begin{aligned} \lambda_i &= -\sigma_i + j\omega_i \\ \lambda_i^* &= -\sigma_i - j\omega_i,\ (i = 1, 2, ..., n/2) \end{aligned} \tag{4.5}$$

By substituting $s = j\omega$, the terminal impedance function becomes:

$$Z(j\omega) = \sum_{i=1}^{n/2} \frac{\beta_i + j\omega\alpha_i}{\delta_i + j\gamma_i} \tag{4.6}$$

where:

$$\begin{aligned} \delta_i &= \sigma_i^2 + \omega_i^2 - \omega^2 \\ \gamma_i &= 2\sigma_i\omega \end{aligned} \tag{4.7}$$

By separating the real and imaginary parts, the impedance characteristic is:

$$Z(j\omega) = \sum_{i=1}^{n/2} \frac{\beta_i\delta_i + \alpha_i\gamma_i\omega}{\delta_i^2 + \gamma_i^2} + j\sum_{i=1}^{n/2} \frac{\alpha_i\delta_i\omega - \beta_i\gamma_i}{\delta_i^2 + \gamma_i^2} \tag{4.8}$$

Equation (4.8) contains $2n$ unknown parameters, namely α_i, β_i, σ_i and ω_i. Each pair of these four parameters determines one *RLCG* Foster section. Determining all parameters means determining the terminal impedance characteristic of a transformer represented with Foster circuits. Several methods can be used for determining these parameters. For example, a complex method based on least squares principle can be used. It is shown [80] that fitting of only the resonant frequencies, i.e., the maximum

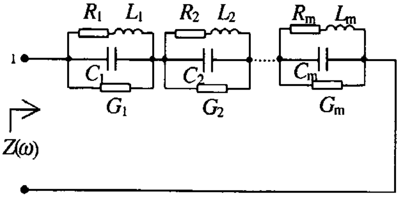

Figure 4-1: Foster circuit for representing the transformer charcteristic

and minimum points of the magnitude curve, already gives a satisfactory match for the considered frequency range. The expression (4.8) has two non-linear equations for each selected value of frequency ω_i. Also, each impedance amplitude characteristic contains $n/2$ maxima and $n/2 - 1$ minima. So, it requires only one condition more, which is normally derived from the impedance characteristic at power frequency, to satisfy the total number of equations $2n$.

Two methods have been employed for the determination of the coefficients:

- a curve fitting procedure, where a measured impedance curve is fitted with a calculated curve iteratively;
- the $2n$ equations are solved by means of Newton's method.

Both methods are based on an initial guess of a possible solution and are subsequently iteratively solved. The equations are rather complicated and if the initial guess is too far from the final solution, then the convergence fails. Therefore, there should be investigated approximately the intervals where the possible roots of the equations are. Reducing the value of σ_i in equation (4.8) makes the resonant peak sharper, whereas increasing ω_i moves the resonant peak to the right. And also, the change of α_i changes the vertical scale of the characteristic. By making use of these adjustments, it is very well possible to find an equivalent circuit the parameter values of which result in a response that closely matches any measured peak [32]. Thereafter, having found the matching parameters, Newton's or a similar method can be applied to minimize the error. The number of Foster sections is equal to the number $m = n/2$ of local maxima of the characteristics.

Table 4.2: Equivalent parameters for transformer measured characteristic from Figure 4-2

i	R_i [Ω]	L_i [H]	C_i [F]	G_i [S]	α_i	β_i	σ_i	ω_i
1	1.0e-3	1.3e-1	7.e-10	1.0e-5	1.4e+9	1.11e+7	7224	102012
2	1.0e-3	4.2e-3	1.1e-8	2.7e-5	9.1e+7	2.23e+8	1252	145903
3	2.1e-3	1.2e-4	9.8e-8	3.6e-3	1.0e+7	1.88e+8	18865	288264
4	1.1e-3	1.7e-4	3.7e-8	1.e-3	2.7e+7	1.88e+8	25865	388264
5	2.3e-5	2.5e-4	1.6e-8	1.6e-3	6.3e+7	5.92e+6	52180	495872
6	3.0e-4	1.0e-4	1.6e-8	1.8e-3	6.2e+7	1.88e+8	58652	787665
7	5.2e-5	1.6e-5	1.7e-8	2.9e-3	5.8e+7	1.88e+8	87652	1887664

From equation (4.8) the relation between the parameters and the component values of a Foster section can be derived. From Figure 4-1 the input impedance of the Foster circuit can be expressed as:

$$Z\left(j\omega\right)=\sum_{i=1}^{n/2}\frac{L_i(j\omega)+R_i}{L_iC_i(j\omega)^2+\left(R_iC_i+L_iG_i\right)\left(j\omega\right)+\left(R_iG_i+1\right)} \tag{4.9}$$

By combining equations (4-8) and (4-9) it is possible to determine the parameters of the Foster circuit that can be implemented into ATP-EMTP.

$$\begin{gathered} C_i=\tfrac{1}{\alpha_i},\, G_i=\tfrac{2\sigma_i\alpha_i-\beta_i}{\alpha_i^2} \\ R_i=\tfrac{\beta_i\alpha_i^2}{\left(\sigma_i^2+\omega_i^2\right)\alpha_i^2+(\beta_i-2\sigma_i\alpha_i)\beta_i},\, L_i=\tfrac{\alpha_i}{\beta_i}R_i \end{gathered} \tag{4.10}$$

In order to prove the validity of this approach, we will calculate a transformer impedance characteristic according to the preceding analyses, and compare the results with the measured transformer frequency characteristic. The test transformer is a generator step-up transformer Yd5, 144 MVA, 230/16 kV for which a measured characteristic was provided by LAPEM (Mexico). The calculated characteristic is represented by 7 Foster sequences with 28 components in total.

Figure 4-2 represents the comparison between the measured (see the list of published papers, reference [6, 7]) and the calculated amplitude and phase impedance transformer characteristic. There are no measurements provided for 50/60 Hz. It can be concluded that the measurements and the computations are in a good agreement with each other. At 7 kHz, the measured characteristic has a peak that deviates from the computed value.

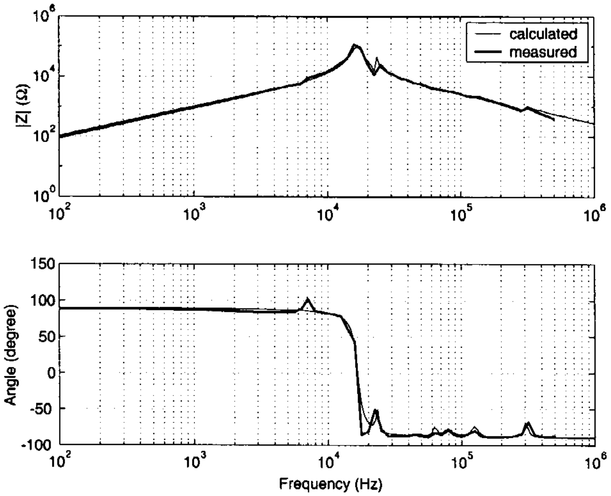

Figure 4-2: Calculated and measured amplitude and phase characteristics of a 144 MVA, 230/16 kV generator step up transformer

This local maximum does not show up in the amplitude characteristic; it is possibly a mismeasurement and not a property of the transformer characteristic. As mentioned before these kinds of characteristics always contain one more maximum than the number of minima. Table 4.2 summarises the parameters which determine these characteristics as well as the calculated values for the Foster sequence elements. The applied method represents the transformer and motor characteristics with sufficient accuracy over a wide range of frequencies if the measured characteristics are known. Having determined the parameters for the specific impedance characteristic, it is rather easy to calculate Foster section component values R_i, L_i, C_i and G_i, and subsequently implement them into ATP.

4.3 The three-phase transformer model

The previous section described how to apply the transformer frequency characteristics to represent the transformer behaviour over a wide range of frequencies. This model does not take into account the non-linearity of the core, which is important for low frequency

Table 4.3: Equivalent parameters for transformer characteristic of Figure 4-5

i	$R_i\,[\Omega]$	$L_i\,[H]$	$C_i\,[F]$	$G_i\,[S]$	α_i	β_i	σ_i	ω_i
1	1.51 e-1	variable	2.95e-10	variable	3.39e+9	variable	variable	variable
2	6.75e-1	1.29e-5	5.54e-10	7.02e-6	1.80e+9	9.43e+13	32496.91	1.18e+7
3	2.87e-1	2.56e-6	1.386e-9	2.09e-8	7.21e+8	8.05e+13	55872.1	1.68e+7
4	2.34e-2	5.20e-7	2.826e-9	2.64e-3	3.53e+8	1.59e+13	489486.4	2.61e+7
5	8.40e-4	5.63e-7	7.89e-10	3.44e-2	1.26e+9	1.88e+12	2.17e+7	4.74e+7

transients, like inrush currents due to energising of an unloaded transformer. The terminal impedance characteristic is approximated by means of linear Foster sections. This is justified when the transformer core does not play a significant role. Measurements reveal, however, that in the low frequency domain (in particular for unloaded transformers) for frequencies up to 100 kHz the transformer core does influence the terminal impedance as it moves the first local maximum to the left and shifts the impedance characteristics upward. This is caused by the non-linear inductance in such a way that the change in the current causes a change in the inductance. For a known magnetising curve, one can determine the maximal inductance from the linear part of the characteristic and its minimal value from the saturated part. Thus, it is possible to determine the boundaries of the segment of the characteristic that shifts left and upward. Because the magnetic core affects the characteristic up to a 100 kHz, this segment is determined by the first local maximum of the characteristic.

In this way, the original linear model can be upgraded by a transformer magnetising curve or hysteresis to match the actual transformer impedance. The proposed transformer model used for our further studies is a combination of the winding impedance model and a magnetising branch as shown in Figure 4-3.

The data given in Table 4.3 are for the characteristic shown in Figure 4-5. It can be seen that the component values of the first Foster section, its inductance and conductance are variable. These parameters relate to the transformer core and are dependent on the transformer saturation and its losses. The curve for $L = 0$ is the curve for which this Foster section is left out. At high frequencies this curve shows almost the same effect as other characteristics. This can be explained by the influence of transformer winding with the increase of frequency. The measured magnetising curve shown in

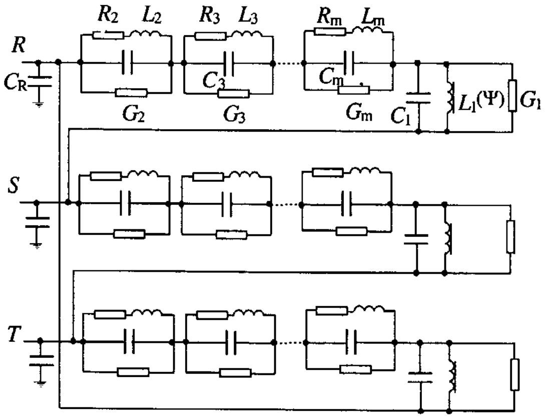

Figure 4-3: Transformer model over a wide frequency range

Figure 4-4 is fitted with a hyperbolic function (see list of published papers, reference [7]). Thus, we can calculate the magnetising inductance at any instant as a derivative of the flux ($L = \frac{d\Psi}{di}$). The transformer losses in this case correspond to parameter G_1 and their values are varied between 75.7 kΩ, 88.5 kΩ and 160 kΩ. They are also frequency dependent. The variation in the frequency-dependent losses shows an alteration when we make calculations with switching surges. The behaviour of the magnetising inductance and resistance is described by the following expression [1]:

$$Z(s) = \frac{2wN^2}{l}\sqrt{\mu_0\mu\rho s}\tanh\sqrt{\frac{\mu_0\mu s}{\rho}}\frac{d}{2} \tag{4.11}$$

where:

l - the length of the magnetic flux path,

w - the width of the lamination,

d - thickness of the lamination,

N - number of turns of the winding,

ρ - specific resistivity of the lamination.

The impedance $Z(s)$ can be developed in partial fractions [1]:

$$Z(s) = \frac{2}{\pi^2 \tau} \sum_{n=1}^{\infty} \frac{sL}{s + \frac{(2n-1)^2}{4\tau}} \tag{4.12}$$

where $L = \frac{\mu_0 \mu N^2 S}{l}$ is the low frequency inductance and $\tau = \frac{\mu_0 \mu d^2}{4\pi^2 \rho}$ is a diffusion time constant. Equation (4.12) can be used to represent the magnetic core with parallel Foster sections and their elements can be calculated as follows:

$$L_{\mathrm{km}} = \frac{L}{2};\ R_{\mathrm{km}} = \frac{k^2 L}{2\tau};\ L_{0\mathrm{m}} = L,\ k = 1, 2, 3, ... \tag{4.13}$$

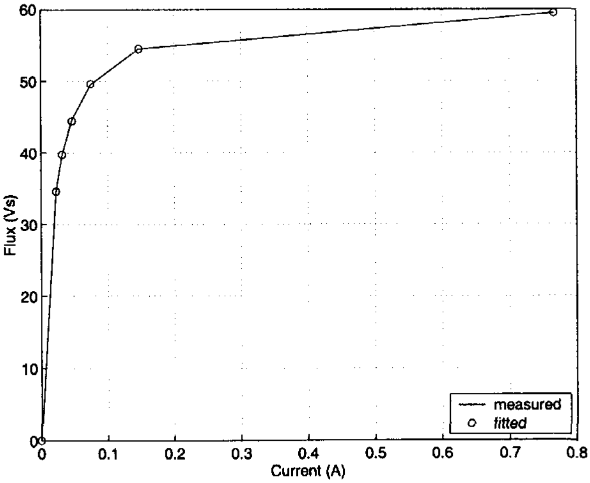

Figure 4-4: Measured and calculated transformer magnetising curve

In reality the magnetic permeability of the core is a variable. So, the inductances in the parallel R-L Foster sections are variables and expressed by the current value of the magnetising inductance. In our calculations we assume losses to be constant. To save the computation time, instead of using parallel R-L sections we estimate the frequency-dependent losses with constant losses, as shown in Figure 4-6. The calculated results are represented in Figure 4-7. The calculation is performed for a constant value of the magnetising inductance. For different inductances of the core, because of the variation

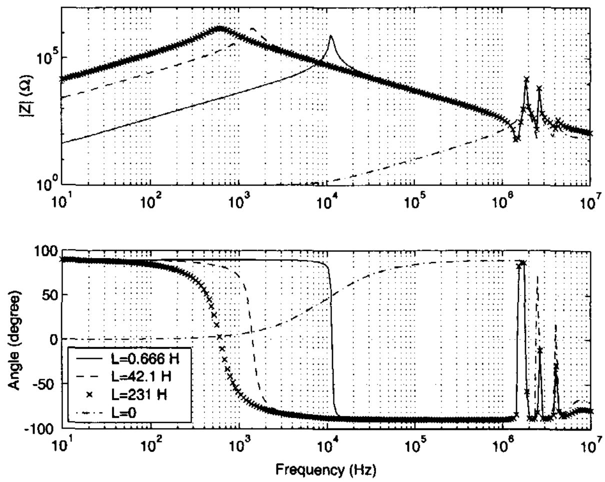

Figure 4-5: Terminal amplitude and phase characteristic of the studied transformer

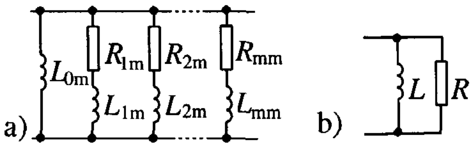

Figure 4-6: Approximation of the eddy current losses for a) frequency-dependent core losses; b) constant core losses

in the magnetic flux, a family of graphs can be made just like for the calculated terminal impedance.

If we consider the linear part of the magnetising curve in Figure 4-4, we can conclude that the computed values of the magnetic core inductance and resistance modelled by means of Foster sections show good agreement with the values in the case when losses are approximated by constant values. As mentioned, this is important to reduce the computation time and therefore we have to simplify the transformer model. Because of the transformer losses, the damping of the transient overvoltage is considerable and the overvoltage at the transformer terminals disappears shortly after the reignition ceases.

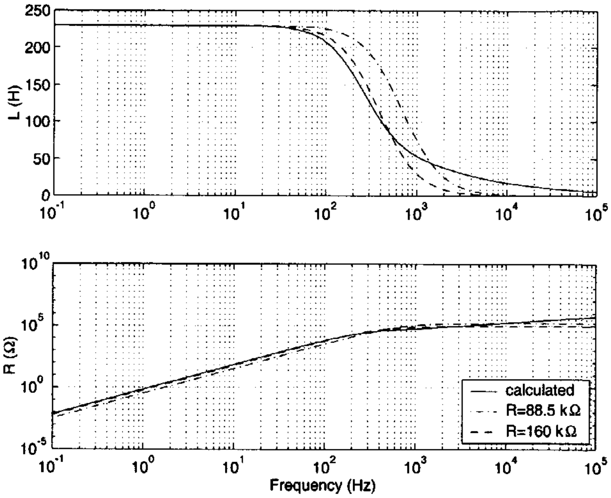

Figure 4-7: Comparison between the parameters of the core model with constant losses and frequency-dependent losses; upper trace: equivalent inductance of the core; lower trace: equivalent resistance of the core

In many practical cases, the voltage transients have the shape of a damped wave.

The phase-to-ground capacitance is the transformer capacitance having a dominant influence on the possible VCC and must therefore be taken into account. The VCC also depends on the amplitude of the inrush currents, the peak values of which strongly depend on the shape of the magnetising curve. The influence on the inrush current is in particular caused by the slope of the magnetising curve at the saturated region. Depending on the slope, higher or lower inrush currents should be expected.

The model constructed in this way is a model of an unloaded transformer and can only be applied for calculating terminal voltages. For calculating the overvoltages induced on the transformer secondary side, more data are required such as the transfer transformer capacitances, the terminal impedance at the transformer secondary side when the primary side is left open, the phase-to-ground transformer capacitances and so forth. For modelling a transformer under load, the terminal impedance characteristics are different. These characteristics are measured from the terminal of the high voltage side when the secondary side is short circuited.

4.4 The influence of the magnetic core

When switching transformer magnetising currents we can distinguish two time intervals. The first interval is for the high frequency oscillations due to the reignited current, whereas the second interval is for the low frequencies when the reignited current is interrupted. The transformer behaviour for these periods is different. Especially when a chopping without reignition occurs, the hysteresis plays an important role in the generation of overvoltages. Normally, after de-energising, not all the magnetic energy stored in the transformer coils charges the transformer capacitance, because part of this energy is used for the remanent magnetisation of the core. Typically, 20% to 60% of the energy remains in the transformer core or is dissipated as losses, and some of the remaining energy is dissipated in the surrounding network. Therefore, the magnetic flux does not follow the steady-state hysteresis curve any longer. This effect strongly influences the generated overvoltage oscillation and this overvoltage is generally smaller than the overvoltage that occurs when a linear inductance is switched off. In addition to the hysteresis, eddy current losses also contribute to fast damping of the transient oscillations.

4.4.1 The theory behind the Jiles model

The hysteresis effect of any ferromagnetic material can be described by the *Preisach* model [39] or the *Jiles* model (JM) [20, 35, 41] which uses a first order non-linear differential equation that is solved numerically to give the magnetisation M or the magnetic field H, depending on which of the parameters is known. The JM can be expressed as:

$$\frac{dH}{dM} = \frac{k\delta - a\left(M_{\text{an}} - M + k\delta c\frac{dM_{\text{an}}}{dH_{\text{e}}}\right)}{M_{\text{an}} - M + k\delta c\frac{dM_{\text{an}}}{dH_{\text{e}}}} \tag{4.14}$$

The effective magnetic field is given by:

$$H_{\text{e}} = H + \alpha M(H) \tag{4.15}$$

The parameter δ is:

$$\delta = \begin{cases} 0 \text{ if } \frac{dH}{dt} < 0 \text{ and } M_{an}(H_e) - M(H) \geq 0 \\ 0 \text{ if } \frac{dH}{dt} > 0 \text{ and } M_{an}(H_e) - M(H) \leq 0 \\ 1 \text{ for the other cases} \end{cases} \tag{4.16}$$

There are three parameters for the JM; c (dimensionless) being a ratio of the initial normal to the initial anhysteretic differential susceptibility $(\frac{dM}{dH} \approx c\frac{dM_{\mathrm{an}}}{dH})$ [41], α (dimensionless) is a mean field parameter representing the inter-domain coupling of the ferromagnetic material; and k (A/m) is a measure of hysteresis. An increase or decrease of the parameter k leads to so called hard or soft hysteresis, respectively. If $k = 0$ then no hysteresis exists. Furthermore, the shape of the hysteresis curve is determined by the anhysteretic magnetisation $M_{\mathrm{an}}(H)$, which is actually a hyperbolic function that determines the magnetisation curve when no hysteresis exists. It is given by the expression:

$$M_{\mathrm{an}} = M_{\mathrm{s}}\left[\coth\left(\frac{H_{\mathrm{e}}}{a}\right) - \frac{a}{H_{\mathrm{e}}}\right] \tag{4.17}$$

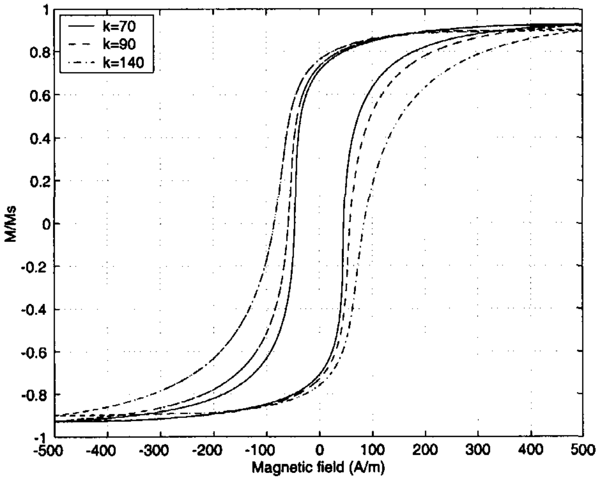

Figure 4-8: Calculated steady-state hysteresis loops

where M_{s} (A/m) is the saturation magnetisation and a (A/m) is a parameter that shows how the anhysteretic magnetisation scales with H_{e}. The equation (4.14) is solved

Table 4.4: Circuit and model parameters for the Jiles model

JM data		*Circuit data*		*TR core data*	
k	60 A/m	R_L	800 kΩ	N	792 turns
α	8.e-5	C_t	1 nF	S	388 cm^2
c	0.2	R_σ	0.1 Ω	l	3.2 m
M_s	1.34 10^6A/m	L_σ	5 mH		

by means of a fourth order Runge-Kutta method in order to calculate the magnetisation. To calculate M_{an} and its derivative numerically at small values of H_e/a ($|H_e/a| < 0.5$), a Taylor series is developed in order to avoid the problem of calculating the values around $H_e = 0$. Figure 4-8 shows the variation in the steady-state hysteresis loops for different values of the parameter k. It is clear that an increase in the parameter k leads to an increase in the hysteresis losses. Thus, different shapes of hysteresis loops can be modelled. All parameters of the JM can be calculated if a measured hysteresis curve is available. The complete procedure for the parameter extraction from the experimental data is given in reference [41].

4.4.2 The application of the JM for calculating overvoltages after chopping

So far the JM has been used for a theoretical analysis of the ferromagnetic behaviour. Because of the relation between the magnetic parameters of the hysteresis magnetisation M and the magnetic field H, the electrical parameters, being the current i through the winding and the voltage u, can be calculated, and the JM can be used for calculating the overvoltages that are generated when an unloaded transformer is switched off. When the input voltage across the non-linear inductance is known then the magnetic flux density can be calculated with:

$$B = \frac{1}{NS}\int(U_A - U_B)dt \tag{4.18}$$

where U_A and U_B are the voltages of the primary inductance nodes. The magnetisation is expressed as

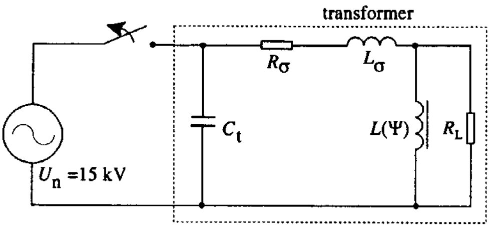

Figure 4-9: A representation of a single-phase transformer circuit for low frequency transients

$$M = \frac{B}{\mu_0} - H \tag{4.19}$$

where H is the calculated magnetic field from the previous time step. Having the value of M, equation (4.14) can be solved and the magnetic field at each time step is known. The magnetising current is calculated by

$$i = \frac{Hl}{N} \tag{4.20}$$

where l is the length of the magnetic flux path. This approach can be repeated for all non-linear inductances in the circuit.

The calculation has been done for the simplified single-phase transformer circuit shown in Figure 4-9. The parameters of the JM and transformer are given in Table 4.4. The calculation is done for different values of the parameter a in equation (4.14). For the steady-state case, the calculated results by ATP are also verified numerically. Neglecting the transformer losses we can write:

$$\frac{dB}{dt} = \frac{1}{NS}\left(U_n \cos(\omega t) - R_\sigma i - L_\sigma \frac{di}{dt}\right) \tag{4.21}$$

Taking into account equation (4.19) and (4.20), (4.14) and (4.21) can be solved. Results of the calculation are depicted in Figure 4-10. After implementation of the model in ATP, examples of switching a simplified single-phase and a three-phase unloaded transformer circuits are presented in Figure 4-11 and Figure 4-12. The circuit breaker opens

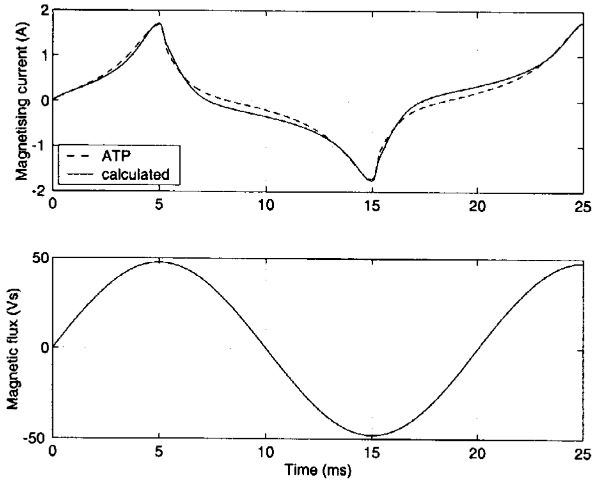

Figure 4-10: Calculated and simulated magnetising current and magnetic flux for the circuit in Figure 4-9

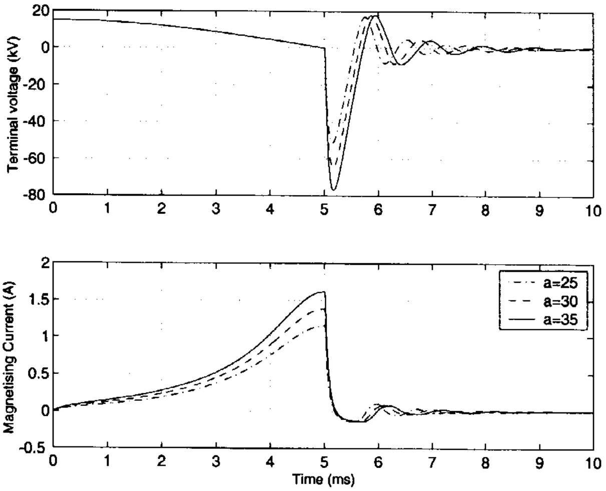

Figure 4-11: The magnetising current and terminal voltage after de-energising a single-phase transformer for the circuit in Figure 4-9

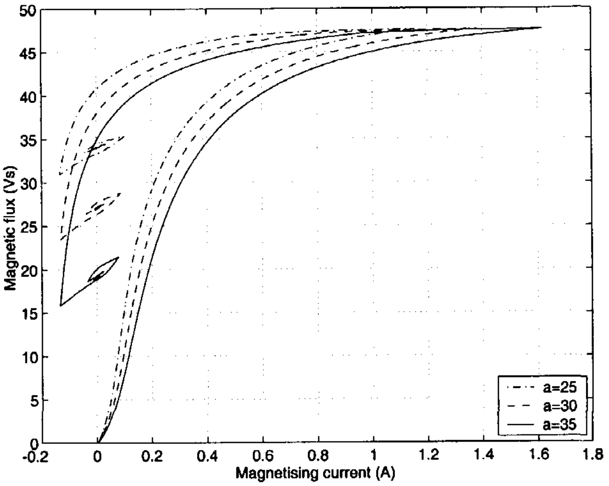

Figure 4-12: The magnetic flux after de-energising a single-phase transformer for different types of hysteresis for the circuit in Figure 4-9

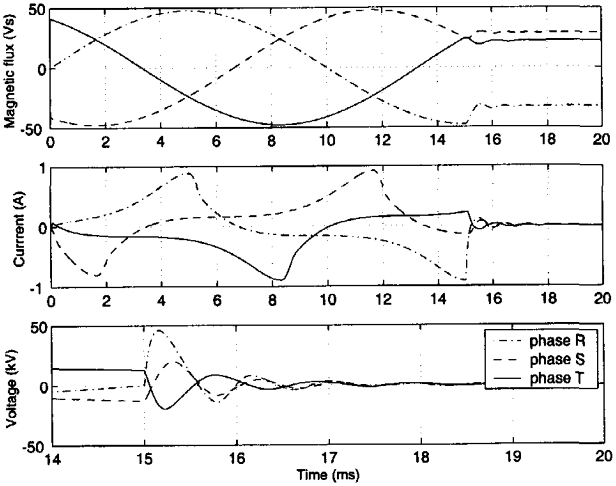

Figure 4-13: The magnetic fluxes (upper trace), magnetising currents in the leakage impedance (middle trace) and terminal voltages (lower trace) after de-energising a three-phase transformer

at peak magnetising current in order to reach the maximal voltage value. It is clear that parameter a influences the peak of the magnetising current and this results in different peak overvoltages after current interruption. Figure 4-12 shows the residual flux in the transformer core after the magnetising current has disappeared. Three-phase transformers are considered as three single-phase transformers and the same circuit from Figure 4-9 is used. The circuit breaker opens at maximum magnetising current in phase R. The results are shown in Figure 4-13. The different types of transformer ferromagnetic material have been analysed experimentally by *Berger* [4], and the calculations using the Preisach model have been performed by *Helmer* and *Lindmayer* [39]. The results of Figure 4-11 show good agreement with the results of the calculations and measurements mentioned in these references. The application of any model absolutely requires a measured hysteresis curve for calculating accurately the overvoltages that are generated after chopping without reignition of the arc in the circuit breaker. The model can be used to study not only transformer switching but also reactor switching. This is particularly useful when no restrikes in the circuit breaker occur, and the impedance of the transformer winding can be neglected.

4.5 Conclusion

Under abnormal conditions such as the occurrence of lightning impulses, energisation or de-energisation of transformers, transient oscillations in a wide frequency range occur. The transformer behaviour as a result of these transients is rather complex. For a special frequency range, dedicated transformer models should be used in order to calculate the transient overvoltages accurately. When a transformer is switched at no load with a vacuum circuit breaker, the high frequency oscillations cover a wide range of frequencies, from a few kHz (caused by the configuration of the surrounding network and its natural frequencies) up to several tens of MHz (caused by the high frequency reignition). Experience shows that when high frequency oscillations occur, the transformer core is not important due to the high flux variation and can be neglected. Significant changes in the impedance of the transformer windings take place, so it is necessary to model the behaviour of the windings in more detail. If no reignition in the vacuum circuit breaker occurs, and the current in the vacuum circuit breaker is chopped, the hysteresis is of great importance and cannot be neglected. When inrush current switching is studied, the precise calculation of the transformer inrush currents is a necessary condition to simulate the possible VCC.

In this chapter a transformer model valid for a wide range of frequencies has been discussed. The transformer is modeled by means of a measured terminal impedance from which the parameters of the Foster sections are calculated. Besides transformers, the method is also able to represent motor behaviour. For the simulation of magnetising and inrush currents, the magnetising curve is used instead of the hysteresis curve. This has been proven to be sufficient since only the reignition voltages are of interest. If no reignition in the vacuum circuit breaker occurs, the JM can be used to simulate the switching overvoltages accurately. This model is implemented into ATP in such a way that different non-linear elements can be included. It is important to notice that this includes the dynamics of the hysteresis, which cannot be neglected when the generated overvoltages are calculated.

Chapter 5

Modelling surge arresters and surge suppressors

5.1 Introduction

The study of fast front surges plays an important role for the insulation coordination analysis. When studying fast front surges, one must pay special attention to details of the circuit arrangement like the stray inductances and stray capacitances. When overvoltages are of concern, it has been common practice to apply surge arresters and surge capacitors to protect the equipment. Therefore, particular attention must also be paid to the modelling of arresters and to choosing a proper R-C surge suppression branch. Surge arresters limit the amplitude of the voltage surge but do not mitigate the rate of rise. Their primary task is to provide protection against different types of overvoltages like those from lightning strokes and switching overvoltages. Lightning strokes can create excessive overvoltages which can damage electrical motors and other reactive loads. Capacitors do reduce the rate of rise because they increase the travel time of the wave along the cable and reduce the TRV rate of rise sufficiently to prevent multiple reignitions. Therefore, surge capacitors are widely applied to protect electrical motors and transformers from unwanted overvoltages. But many users do not want to use capacitors because they can be subjected to contamination and reduce the system reliability. With overvoltages as a result of reignition and as a result of VCC produced by a switching action, experience has shown that limitation of the voltage amplitude provides adequate protection of the equipment.

In this chapter a few arrester models are discussed which cannot only be used for protecting reactive loads from switching surges, but also to protect the equipment from any kind of surge in general. A simplified model will be presented based on the measured and calculated data according to ANSI/IEEE Std. C62.11-1993. Also, the *R-C* branch as a protective device is investigated and the choice of optimal parameters is discussed.

5.2 Surge arrester models for protection against fast surges

The metal-oxide material used in surge arresters has a highly non-linear volt-ampere characteristic which depends on the wave shape of the surge current. Proper measuring of this characteristic is therefore important when analysing steep-fronted surges for insulation coordination studies. The volt-ampere characteristic depends on several factors: the shape of the current surge, the ambient temperature and the immediate history of arrester currents. Also, a spread in the production process results in arresters of the same rating having different volt-ampere characteristics. These factors make it difficult for the insulation coordination engineer to calculate the protective margins for equipment insulation accurately.

5.2.1 General properties of the metal-oxide surge arrester

The metal-oxide material from which the arresters are produced is a ceramic made by mixing ZnO with a small amount of additive materials, such as MnO, Cr_2O_3 etc. The mixture is granulated, dried and pressed into discs. The ZnO grains are small in diameter (approximately 10 μm) and have a low resistivity. They are surrounded by a granular layer of a high resistivity oxide. The disc can be represented by the equivalent circuit as shown in Figure 5-1. R_i is the non-linear resistance of the granular layers, where its specific resistivity changes from 100 MΩm for low electric field stresses to less than 0.01 Ωm for high electric field stresses. The granular layer has a relative dielectric permittivity

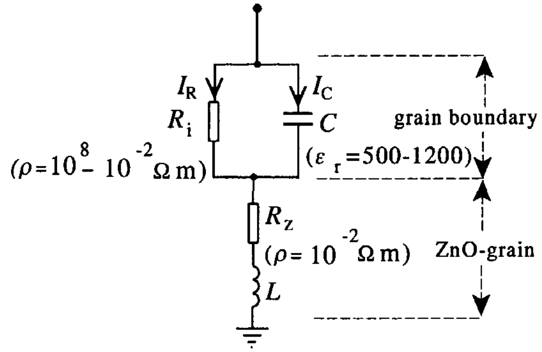
I_R
R_i
$(\rho = 10^8 - 10^{-2}\ \Omega\,m)$
I_C
C
$(\varepsilon_r = 500\text{-}1200)$
grain boundary
R_Z
$(\rho = 10^{-2}\ \Omega\,m)$
ZnO-grain
L

Figure 5-1: Equivalent circuit of a disc of metal-oxide surge arrester

between 500 and 1200, depending on the manufacturing process. R_z is the resistance of the ZnO grains with a resistivity of about 0.01 Ωm. The inductance L is an inductance of the metal-oxide disc.

Basically the volt-ampere characteristic of an arrester can be represented by the exponential function

$$I = BV^{\alpha} \tag{5.1}$$

where the multiplier B and the exponent α are constants for a specific material. If the formula is used for the resistivity component especially in a low current region, a single exponent cannot describe the complete characteristic. The corresponding exponent α depends on the conduction region and can vary from 3 to 50. An example of the typical shape of an arrester characteristic is shown in Figure 5-2.

In the regions 1 and 2 of this characteristic, the voltage applied to the arrester drops across the grain boundary as shown in Figure 5-1. The resistive current component in region 1 is usually well below 1 mA and the capacitive current component dominates. Therefore, in order to keep the power dissipation in the arrester low at the system operating voltage, the Maximal Continuous Operating Voltage (MCOV) has to be chosen in this region. The resistive current is caused by the granular layer and can be influenced by the chosen material. The protection characteristic of the arrester is determined

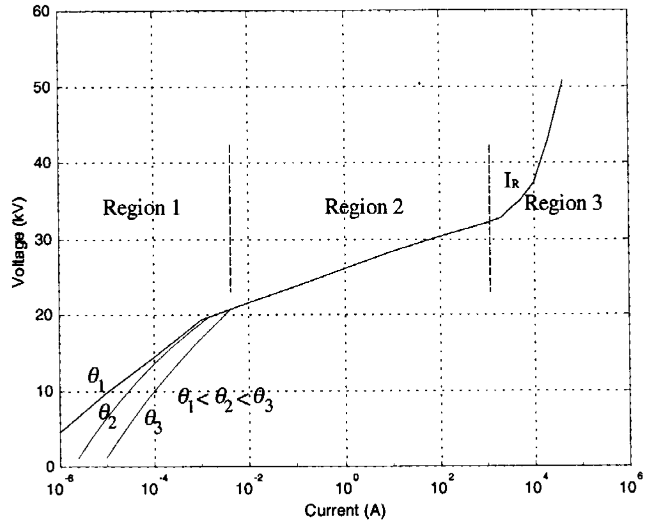

Figure 5-2: Typical volt-ampere characteristic of an arrester at different temperatures (θ)

by the volt-ampere characteristic in regions 2 and 3. In these regions, the influence of the temperature and capacitance are not present and the deviation from the linear voltage distribution along the arrester is only determined by the resistive volt-ampere characteristic.

5.2.2 A model of an arrester disk for fast surges

Based on the described theory of arresters physics, *Schmidt* et al. [78] developed an arrester model representing the arrester circuit in a similar way. This model is shown in Figure 5-3. It can be seen that the current-dependent resistance is divided in a steady-state resistance $R(i)$, a turn-on resistance A and a temperature-dependent resistance $R(\theta)$, representing the behaviour of the arrester in a low current range. For the protection performance, the temperature-dependent resistance $R(\theta)$ can be neglected. The turn-on resistance A models the dynamic charge distribution at the grain boundary layer. The dynamic behaviour depends on the voltage amplitude and the steepness of the wave

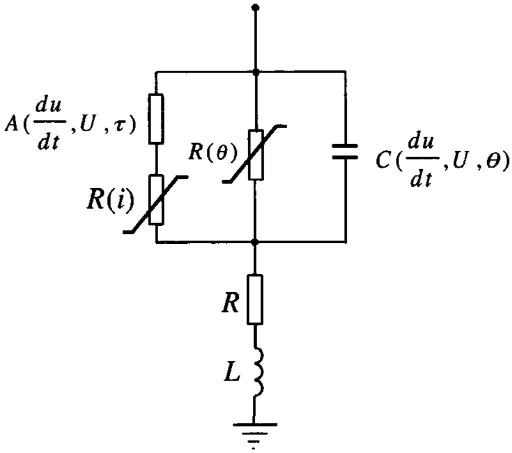

Figure 5-3: Arrester model from *Schmidt* et al. [78]

shape, as well as on the time constant for reaching equilibrium between electrons and holes at the grain boundary layer.

5.2.3 The IEEE surge arrester model

Since the early 1980s a lot of effort has been put in collecting data for surge arresters that can be of assistance in finding an arrester model that is capable of simulating the behaviour of an arrester for slow and fast surges. The outcome of these studies leads to the idea that switching surge studies can only be performed by modelling metal-oxide arresters with their non-linear volt-ampere characteristic. The test data from the IEEE surge arrester group indicate, however, that in general the metal-oxide arresters have a dynamic and a frequency-dependent characteristic which are of significance for lightning impulses and other fast wave-front surges. The importance of the dynamic characteristic is that the voltage across the metal-oxide arrester increases as the time to crest of the arrester current decreases, and that the arrester voltage reaches its peak even before the arrester current. The dynamic effect tends to become dominant for current waves with a peak at 8 μs or less. Another phenomenon that shows up when the time to crest of the arrester discharge current becomes shorter than 4 μs is the occurrence of voltage spikes.

These are voltage peaks at the front of the arrester discharge voltage wave form which can sometimes exceed the subsequent discharge voltage level for the arrester. The amplitude of these voltage spikes is strongly influenced by the stray inductance of the loops in the measuring set-up. There is no consistent agreement with respect to the realistic amplitude of these spikes, but there is some evidence that the spike does not exceed the discharge voltage for currents reaching their maximum at 0.5 μs and more. The results of the IEEE surge arrester working group are limited with respect to the surge arrester model, because other system parameters (such as arrester leads and separation distances) which are also important in studies on lightning impulses and other fast wave-front surges are ignored.

When specifying an arrester model, the model accuracy is accepted when the arrester characteristic is chosen to be consistent with the time to crest of voltage and current during system disturbances. The IEEE surge arrester working group took into account the variation in the arrester voltage as a result of the time to crest of the arrester current by adding an inductance in series with a non-linear characteristic. This approach makes sense because the voltage across the arrester, and so across the inductance, rises as the time to crest of the arresters current lowers. This type of model has proven to be successful in matching specific test results. For example, an inductance can be chosen for the model such that it results in a good match of the voltage amplitude and the wave shape of the arrester discharge current, reaching its crest at 8 μs. However, when the same inductance value but other model parameters are applied for an arrester current reaching its crest at 2 μs, the voltage amplitude has a considerable error. Therefore, a more sophisticated model is required for modelling the response of an arrester for currents with a wide range of time-to-crest values.

The model proposed by the IEEE surge arrester working group [42] is frequency dependent and the non-linear characteristic of the model is described with two non-linear resistors denoted as A_0 and A_1, as shown in Figure 5-4. The two sections are separated by an R-L filter. For slow surges, this filter has a very low impedance and the two non-linear sections of the model are connected in parallel. For surges with a steep front, the impedance of the R-L filter starts to play a role. This results in more current flowing through the non-linear section A_0 than through section A_1. Since the

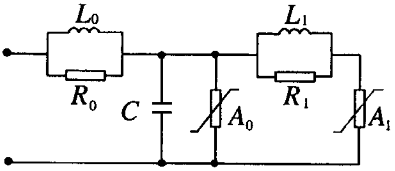

Figure 5-4: IEEE Frequency-dependent arrester model

Table 5.1: Volt-ampere characteristic for A0 and A1 with respect to Figure 5-5 and Figure 5-6

current (kA)	$A_0[p.u.]$	$A_1[p.u.]$	A_0[kV]	A_1[kV]
2.0e-6	0.810	0.623	37.4	28.8
0.1	0.974	0.788	45.0	36.4
1	1.052	0.866	48.6	40.0
3	1.108	0.922	51.2	42.6
10	1.195	1.009	55.2	46.6
20	1.277	1.091	59.0	50.4

volt-ampere characteristic of A_0 has a higher voltage for a given current than A_1, the arrester model generates a higher voltage. This model matches the overall behaviour of a metal-oxide arrester. The major difficulty with this model is acquiring information about the characteristics of the non-linear elements. They should be available from the manufacturer for a specific design. In practice, in the case of fast switching surges, the R-L filters are of great importance. The essential input for determining the parameters of the R-L filters is:

- the length of the arrester column in metres (d),
- the number of parallel columns of metal-oxide disks (n),
- the discharge voltage for a 10 kA, 8/20 μs current impulse, in kV $(V_{8/20})$,
- the switching surge discharge voltage in kV (V_{ss}).

Thus, for determining the parameters of the ZnO arresters, the following expressions can be used:

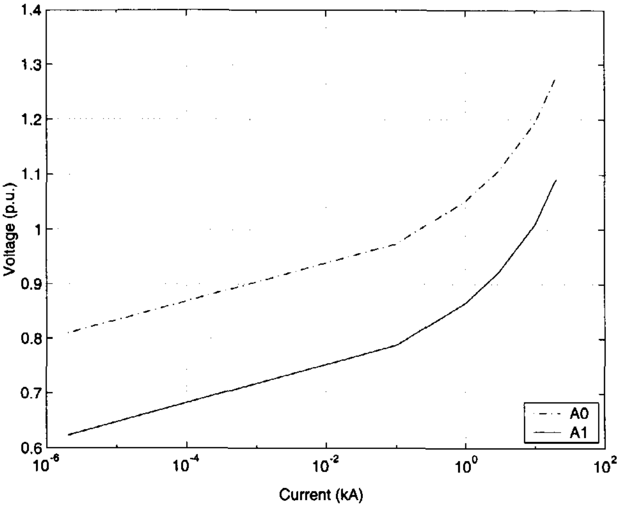

Figure 5-5: Volt-ampere relationship of a 20 kV ZnO arrester

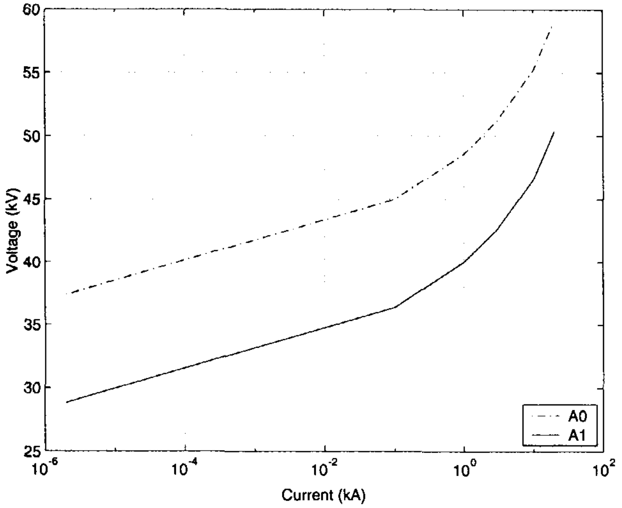

Figure 5-6: Volt-ampere relationship of a 20 kV ZnO arrester

$$L_1 = \frac{15d}{n}\ [\mu\mathrm{H}] \tag{5.2}$$

$$R_1 = \frac{65d}{n}\ [\Omega] \tag{5.3}$$

$$L_0 = \frac{0.2d}{n}\ [\mu\mathrm{H}] \tag{5.4}$$

$$R_0 = \frac{100d}{n}\ [\Omega] \tag{5.5}$$

$$C = \frac{100n}{d}\ [\mathrm{pF}] \tag{5.6}$$

These are initial parameters for the model. The final parameters should be such that the model matches the V_{ss} and $V_{8/20}$ voltages when excited by a switching surge current and an impulse current, respectively. The non-linear resistors A_0 and A_1 are modelled by means of a piecewise linear volt-ampere curve with values defined point by point. By selecting a current value and reading the corresponding relative voltage in per unit from the plot, we can compute the actual discharge voltage for the particular non-linear resistor. The expression for determining these discharge voltages is:

$$\text{discharge voltage } = A_{\mathrm{n}}(i)V_{8/20}\ [\mathrm{kV}] \tag{5.7}$$

where $A_{\mathrm{n}}(i)$, n$= 0, 1$ corresponds to the arrester voltage in per unit as calculated from the volt-ampere curves. An example of the arrester characteristics for a 20 kV ZnO arrester with $V_{8/20}$ =46.2 kV is shown in Figure 5-5. The actual characteristics with a voltage scale are depicted in Figure 5-6, while the measured data of this arrester are summarised in Table 5.1.

5.2.4 Generalised arrester model

Before the IEEE surge arrester working group adopted the model with two non-linear resistances, *Durbak* [24] had suggested a more generalised model for a surge arrester.

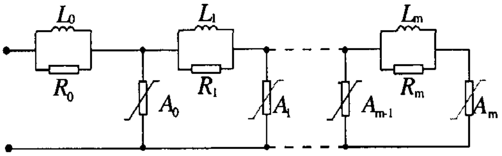

Figure 5-7: A general frequency-dependent metal-oxide arrester model

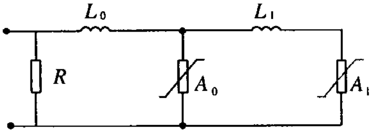

Figure 5-8: Model by *Pinceti* and *Giannettoni* [59]

A general frequency-dependent metal-oxide arrester model is made by dividing the total non-linear low frequency impedance Z of the arrester over m impedances. Each individual resistor has a non-linear low frequency impedance A_iZ, where

$$\sum_{i=1}^{m} \frac{1}{A_i} = 1 \tag{5.8}$$

These time-dependent non-linear resistances are separated by low-pass filters as shown in Figure 5-7. For waves with steep fronts, the voltage drop across the low-pass filters results in a higher percentage of current flowing through the outer resistors. It is difficult to determine the empirical parameters that can validate the model over a large range of peak currents and wave front times. For surges with less steep fronts, the R-L filters have an insignificant effect and the voltage drop on these filter sections is small, so all the resistors are connected in parallel. For insulation coordination, the major concern is the occurrence of fast front effects in the lightning impulses region, where arrester currents from 1 kA to 20 kA can occur that have a time to crest between 0.5 μs and 10 μs. For this range good results can be obtained when m=2 and this leads to the IEEE model, as has been explained in the previous section.

5.2.5 The simplified IEEE arrester model

In 1999, *Pincenti* and *Giannettoni* [59] simplified the IEEE model. Comparing Figure 5-4 and Figure 5-8 one can note that:

- The capacitance is left out, since the effects on model behaviour are hardly noticeable.
- The two resistors in parallel with the inductances are replaced by one resistance (about 1 MΩ) across the input terminals. The purpose of this resistor is to damp numerical oscillations during the calculation.

The values of the inductance can be calculated by the following expressions:

$$L_1 = \frac{1}{4}\frac{V_{1/\mathrm{T}_2} - V_{8/20}}{V_{8/20}} U_\mathrm{n} \ [\mu\mathrm{H}] \tag{5.9}$$

$$L_0 = \frac{1}{3} L_1 \ [\mu\mathrm{H}] \tag{5.10}$$

where:

U_n - is the rated arrester voltage,

V_{1/T_2} - is the residual voltage of a 10 kA fast front current surge with a shape of $1/\mathrm{T}_2$ μs. The decrease time T_2 is not given here because different manufacturers supplied different values. This does not affect the model, because the peak value of the residual voltage coincides with the rising front of the impulse.

$V_{8/20}$ - is the residual voltage for a 10 kA current surge with a 8/20 μs wave shape.

5.3 Developing an arrester model

To calculate transformer switching surges for transformers which are protected by surge arresters, one needs to use one of the models described in this chapter. However, these models require accurately measured data to match the model parameters. Due to its highly non-linear characteristics, especially the IEEE model can cause numerical problems during the calculation. Therefore we will use a simplified form of the Schmidt model shown in Figure 5-3. The branch representing the temperature-dependent resistance $R(\theta)$ and the resistance of the turn-on element are ignored for this model. The resistance $R(\theta)$ does not influence the protection performance of the arrester. The resistance of the turn-on element requires many measurements before we can calculate the variation in the turn-on resistance. The working group of CIGRE WG 33.06 designed a model with which one can easily calculate the turn-on resistance. Because this model requires measured data for the turn-on resistance as well, it is not used in our calculations.

Based on the ANSI/IEEE Std. C62.11-1993, the residual voltage level for different shapes of switching surge impulses is examined.

5.3.1 The impulse function for the representation of the current sources

In order to calculate the response of the arrester for different surges, we need to be able to describe surges of different shapes. Subsequently we must prove that the arrester responses due to these surges are in a good agreement with the data supplied by the manufacturer. An impulse function for a specific wave is described by the duration of its front and the duration of its tail. The front time T_1 is given by the following expression:

$$T_1 = \frac{T_{0.9} - T_{0.3}}{0.6} \tag{5.11}$$

where

$T_{0.9}$ - is the time when the wave reaches 90 % of the peak,

$T_{0.3}$ - is the time when the wave reaches 30 % of the peak.

The virtual time of the 50 % peak value is

$$T_2 = T_c - T_{0.3} + \frac{T_{0.9} - T_{0.3}}{2} \tag{5.12}$$

where T_c is the instant when the value of the current equals 50 % of the maximum value on the wave tail. As we can see from Figure 5-9 these times are relative according to the time instant T'. The time T' can be found when we draw a line from 90% and 30 % amplitude of the wave front. The intersection with the time axis results in T' and it can

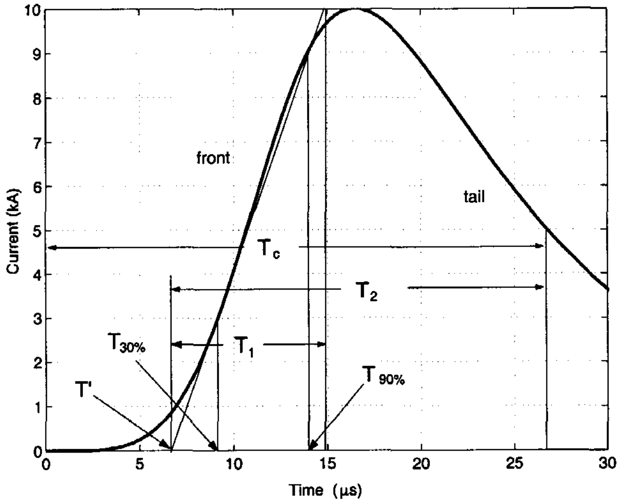

Figure 5-9: General form of a surge current impulse 10 kA, 8/20 μs

easily be calculated by:

$$T' = T_{0.3} - \frac{T_{0.9} - T_{0.3}}{2} \tag{5.13}$$

On this way can be defined a typical voltage surge waveform of an impulse generator.

We have to point out that actually the front of waveform T' of a current impulse is not defined with a line that passes through the 90% and 30% of the amplitude of the rising part like in the case of a voltage impulse, but with a line that passes through the 90% and 10% of this amplitude [47]. But, for simplicity the current impulse here is defined on the same way as the voltage impulse. Until now, the different impulse surge shapes were produced by double exponential functions prescribed by IEC as installed in ATP. But finding proper parameters for this function is not easy. Current sources with different amplitude, wave front and wave tale can accurately be described by means of the *Heidler* function [40], which is given by the following equation

$$x(t) = \frac{V_0}{\eta} \frac{(t/\tau)^n}{1 + (t/\tau)^n} \exp(-\frac{t}{\tau_1}) \tag{5.14}$$

where

Table 5.2: Calculated parameters for the Heidler function

Impulse (μs/μs)	*Amplitude* (kA)	n	τ (μs)	τ_1 (μs)	η
8/20	10	5	14.46	9.625	0.1186
1/5	10	5	1.302	4.624	0.5817
0.5/3	10	5	0.616	3.006	0.6593
1.2/50	10	5	1.118	67.94	0.9501
30/60	0.5	5	20.24	49.74	0.4800

V_0 - is the maximum peak value of either the current or the voltage impulse.

η - is an adjustment parameter.

n - is a parameter influencing the growth speed of the function. Practical values range from 1 to 10.

τ and τ_1 - are constants determined by the duration of the wave front time and wave tail time.

The major problem is to find the τ and τ_1 parameters. The impulse generators which are designed for dielectric testing of systems and components produce impulses with different shapes given according to IEC 60060-1. So the parameters τ and τ_1 must be calculated numerically in such a way that the resulting wave form satisfies the waveform which can be produced by the surge generator. The current impulses for different fronts and tails of the wave are depicted in Figure 5-10. The computed parameters of the *Heidler* function for the corresponding impulses are summarised in Table 5.2. Impulse functions defined in this way can be modelled in ATP as current or voltage sources, and can be used to simulated a lightning stroke or other switching surge source.

5.3.2 Modelling a surge arrester

The effect of multiple reignitions, of a voltage escalation and of steep-fronted surges caused by lightning or other influences can be limited and suppressed by protective devices like surge arresters. The model of an arrester that we use for transformer protection is a simplification of the *Schmidt* arrester model. The simplification is done in terms of:

- omitting the turn-on element $A(\frac{du}{dt}, U, \tau)$,

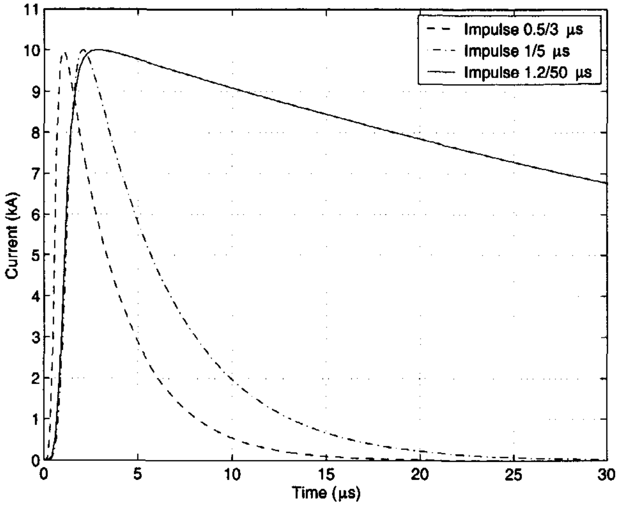

Figure 5-10: Current impulses with different shape for the parameter values in Table 5.2

- omitting the temperature-dependent resistance $R(\theta)$,
- keeping the capacitance of the arrester constant.

The simplified model is shown in Figure 5-11. Practical experience shows that the capacitance of the arrester block is in the order of 1.5 nF·kV for arresters used for distribution transformers and 5 nF·kV for arresters used for substation transformers. These values should be divided by the rated voltage of the arrester to get the total arrester capacitance (see List of published papers [7]). The inductance of the arrester is estimated to be 5 μH/m to 20 μH/m. The effective inductance is calculated by multiplying it with the distance of the connection to the protection equipment. The parameters used for modelling the arrester are chosen to be: R_a=0.6 Ω, L_a=0.5 μH and C_a=0.1 nF. The variable resistance $R(i)$ is an important parameter because it fixes the protection level of the arrester and can be calculated directly from the volt-ampere characteristic of the arrester. The arrester characteristic for a 12 kV arrester with a 10 kV Maximum Continuous Overvoltage (MCOV) is shown in Figure 5-12 with the data shown in Table 5.3. According to ANSI/IEEE Std. C62.11-1993, the maximal residual voltage for a

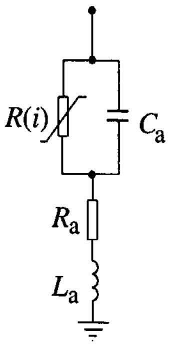

Figure 5-11: A simplified surge arrester model

Table 5.3: Measured volt-ampere characteristic of 12 kV ZNO surge arrester

current (kA)	1e-5	1e-4	1e-3	0.01	0.1	1	2	3	5	10	20	40
voltage (kV)	21.6	23.8	26.0	28.3	30.3	32.0	32.8	33.8	35.0	37.2	43.1	50.6

lightning current impulse of 10 kA with a shape of 8/20 μs, for surge impulses of 500 A with a shape of 45/60 μs or 30/60 μs, and for a front-of-wave impulse 10 kA, 0.5 μs should be compared with the maximal residual voltage as specified by the manufacturer. The comparison between the computed results and the results provided by the manufacturer are summarised in Table 5.4. The calculated voltage responses of the arrester when energised by different current impulses are depicted in Figure 5-13 through Figure 5-16. From the calculated results we can draw the following conclusions:

Table 5.4: Calculated and measured residual voltages

Amplitude of the current impulses	T_1/T_2 *of the current wave* (μs/μs)							
	8/20		1/5		0.5/3		30/60	
	c	*m*	*c*	*m*	*c*	*m*	*c*	*m*
	residual voltages (kV)							
10 kA	43.3	44.0	45.4	-	50.7	51.6	-	-
20 kA	55.4	-	59.0	-	69.3	-	-	-
0.5 kA	-	-	-	-	-	-	31.7	32.3
1 kA	-	-	-	-	-	-	32.6	-
2 kA	-	-	-	-	-	-	34.0	-
3 kA	-	-	-	-	-	-	35.5	-

- Increasing the amplitude of the current impulse leads to a rise in the arrester's maximum residual voltage.

- Steep-fronted impulses lead to higher residual voltages.

Figure 5-17 shows the dynamic voltage-current characteristic of an arrester for a nominal discharge current of 10 kA and for two impulse current shapes. The voltage in this characteristic is expressed in per unit values where 1 p.u.=44 kV, which is the residual voltage of the arrester when excited by a current impulse 10 kA, 8/20 μs (see Table 5.4).

It is evident that the characteristics differ in particular at the beginning of the current front, but that they approach each other again in the current tail. The difference in the residual voltage for the two shapes remains more or less constant in the current tail. This difference in voltage is nearly independent of the current amplitude and the curves become in fact essentially similar in the current tail. This brings us to the conclusion that for fast front surges, such as lightning overvoltages, the model has a turn-on element in series with the non-linear resistance, because this provides a further delay in time of the conduction mechanism of the arrester. The turn-on element is modelled by a set of measured curves [78] or can be approximated by a mathematical function [11]. For vacuum circuit breaker switching and for the simulation of the influence of the arrester, it is sufficient to apply this model, since the front of the reignited current impulse is not as steep as the front of the lightning impulse and its amplitude is also much lower.

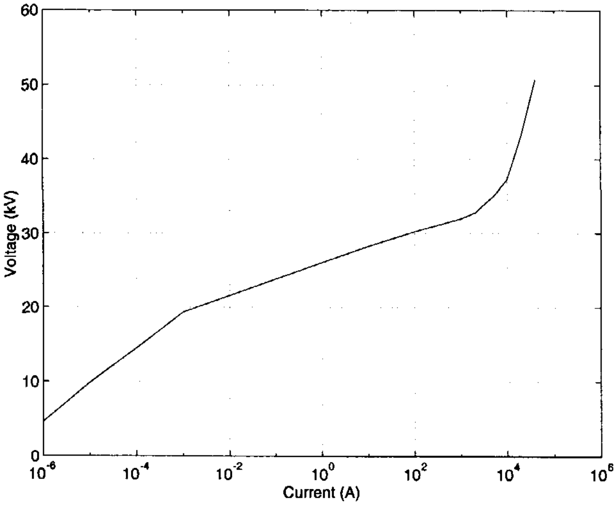

Figure 5-12: Measured characteristic of an arrester with the parameters in Table 5.3

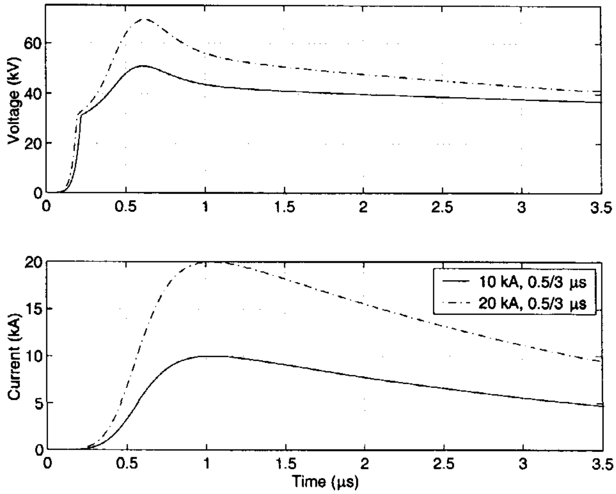

Figure 5-13: Response of the arrester (Table 5.3) after excitation by front-of-wave current impulses 0.5 μs

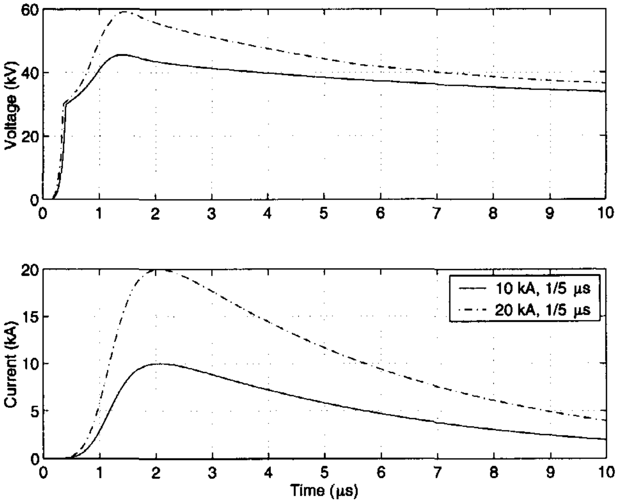

Figure 5-14: Response of the arrester (Table 5.3) after excitation by a current impulse 1/5 μs

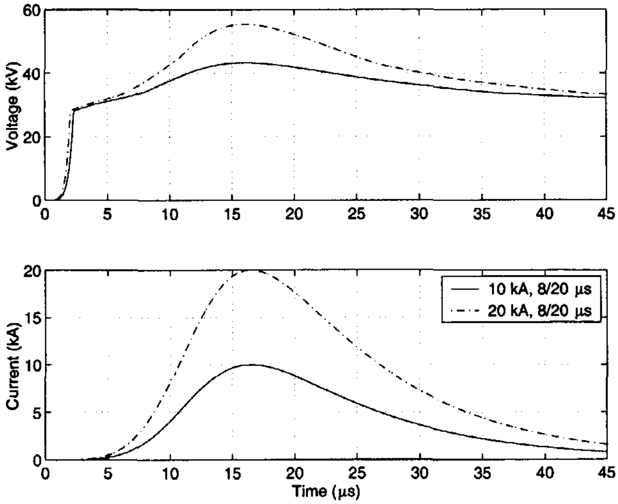

Figure 5-15: Response of the arrester (Table 5.3) after excitation by a current impulse 8/20 μs

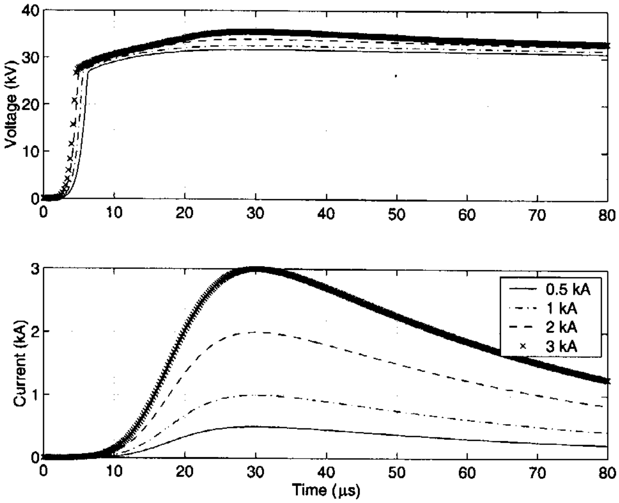

Figure 5-16: Response of the arrester (Table 5.3) after excitation by a current impulse 30/60 μs

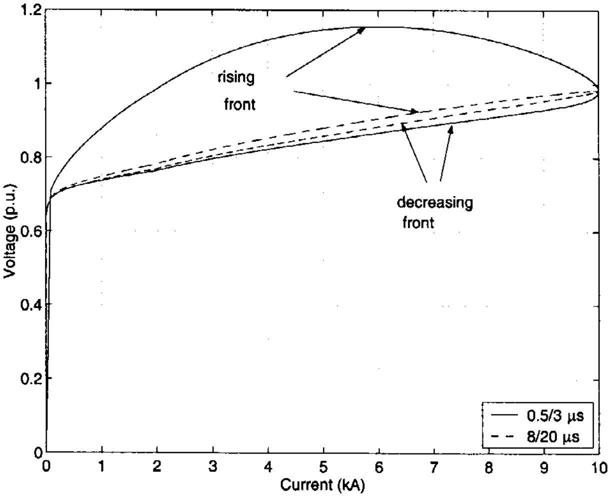

Figure 5-17: Dynamic voltage-current characteristic for current impulses 0.5/3 μs and 8/20 μs

5.4 Other methods for equipment protection

The effect of multiple reignitions can be minimised and suppressed by installing other protective equipment like:

- a surge suppression R-C series branch connected as closely as possible to the terminals of the inductive load,
- a resistor R paralleled by a ZnO varistor in series with a capacitor C *(ZORC)*,
- a ZnO varistor with a spark gap.

These three alternatives are depicted in Figure 5-18. Here we will discuss only the R-C suppression branch. The difference between the application of arresters and R-C suppression branches is that the arrester does not influence the circuit voltage under normal operation conditions. It only becomes active when the voltage exceeds the conduction level. The arrester affects the overvoltage in such a way that it limits the voltage to the value which is related to the slope and the amplitude of the surge impulse.

Unlike the arrester, the R-C suppression branch increases the total capacitance of the load side network and remains active throughout the all time. The capacitor provides absorption of the sharp voltage spikes as the voltage across the capacitor can not be changed immediately upon the arrival of the surge at the terminal of the load. The R-C branch also filters the high frequency transients and decrease the frequency of the TRV.

For surge suppression in practice, one must consider the factors that are involved in steep-fronted overvoltages:

- The high frequency reignition surge is initiated by the load side transient recovery voltage. So, if the latter is reduced to a certain maximal value, the high frequency reignition surge is reduce accordingly.
- The severity of a steep-fronted reignition decreases when its rise time is reduced.
- A steep-fronted reignition surge voltage doubles after reflection at the load terminal. In practical circuits the injected voltage surge typically increases between 50%

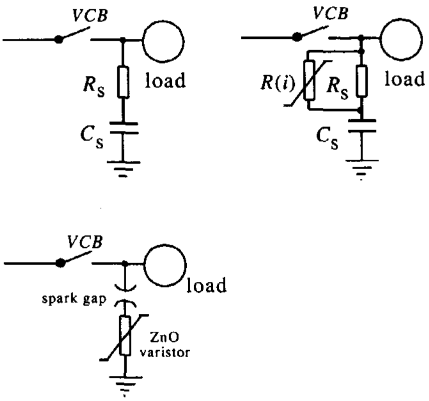

Figure 5-18: Examples of surge suppression circuits

and 70% after reflection from the load terminals since it has a finite value of the characteristic impedance.

In accordance with these three factors, the objective of surge suppression is to ensure that a surge of a given rise time does not exceed a prescribed maximal value. Therefore, the evaluation of various surge suppression techniques is based on their individual abilities to limit the amplitudes of all forms of switching surges to a prescribed maximum value. The technique of overvoltage suppression by means of R-C suppression branches is based on the fact that the capacitance reduces the slope of the surge and the resistor damps the transient oscillations. TRV transients can only be suppressed when the inserted capacitance is considerably higher than the load capacitance and the resistor is approximately equal to the circuits characteristic impedance to provide sufficient damping. While the role of the protective capacitor is to decrease the slope of the surge, the protective resistor damps the transient oscillations. There are no straightforward formulas with which we can calculate component values that give the best suppression, and therefore most of the formulas are based on practical experience. One way to determine the value of the damping resistor is to terminate the end of the cable with a resistor, so the ratio between the amplitudes of load terminal voltage and the reignition voltage is approximately [68]:

$$\frac{V_\mathrm{m}}{V_\mathrm{s}} \approx \frac{2R_\mathrm{s}}{R_\mathrm{s} + Z_\mathrm{c}} \tag{5.15}$$

where Z_c is the cable's characteristic impedance. If this ratio equals 1, the damping resistor R_s equals Z_c. Another option is to use the expression:

$$R_\mathrm{s} \geq 2\sqrt{\frac{L_\mathrm{c}}{C_\mathrm{s}}} \tag{5.16}$$

where L_c is the cable inductance. These formulas lead to values of damping resistors normally in the range between 20 Ω and 100 Ω. With respect to the suppression capacitor, *Popov* proposed a formula [63] for a transformer suppression capacitor which is based on the amount of magnetic energy released from the transformer windings to the protective capacitor:

$$C_\mathrm{s} = \frac{S_\mathrm{n} i_0}{200\pi k^2 f U_\mathrm{n}^2} \tag{5.17}$$

where is

S_n - the rated apparent transformer power in MVA,
i_0 - the magnetising current in %,
f - the power frequency in Hz,
U_n - the phase-to-phase supply voltage in kV,
k - the chopping voltage factor which limits
the overvoltage to k times phase-to-ground rated voltage.

Equation (5.17) leads to values for the surge capacitors in the range of 0.1 μF to 0.5 μF, which corresponds to the values of the capacitors used in the practical circuits. However, the method is simplified because when the transformer is unloaded, the magnetising inductance is considered to be linear, but in practice this is not the case. When applying the *R*-*C* suppression branch in practice, it is advantageous to keep the protective capacitor small. A smaller capacitance leads to a lower reignition current when the vacuum circuit breaker reignites during load current switching and subsequently there is less possibility that a VCC will occur. The resistor must carry the capacitive current continuously, so the resistor power rating will be greater in case a large protective capacitor is used. With an optimised *R*-*C* suppression branch connected to the terminals of the load, the maximal steep-fronted TRV can be reduced to less than 2.5 per unit during switching on and switching off operation. Also the R-C suppression branch prevent the reignition and reduce the steepness of the surge impulse.

5.5 Conclusion

Transformers and other loads can be protected from switching overvoltages by applying surge arresters and R-C suppression branches. When applying surge arresters in practical circuits, it is very important to know the behaviour of the arrester for surges with different shapes and amplitudes. In this chapter, we analysed the available surge arrester models with respect to the necessary data needed for their modelling. The objective of a transient overvoltage study is to provide information about the generated overvoltages, and these are also entangled with the validity of the arrester model. Thus, for temporary overvoltages caused by switching surges with a long wave front, an arrester can be modelled by choosing an applicable non-linear characteristic. For faster surges, the model must take into account the resistance and the inductance of the arrester, which have a considerable influence on the maximal residual voltage. The voltage developed across the arrester terminals for a specific discharge current increases as the time to crest of the current decreases. For discharge currents with a shorter wave front, the discharge voltage reaches its maximum prior to the maximum of the discharge current. The presented arrester model shows good agreement with the available manufacturer data. The surges generated by the vacuum circuit breaker switching and multiple reignitions have a lower amplitude and longer wave front than the surges from lightning strokes or fast transients in GIS. So, for the vacuum circuit breaker switching surges this model can be used with full success. At higher current amplitudes (>20 kA) and a short wave front, the calculated maximum residual voltages could be higher than those indicated by the manufacturer, so in this case the use of a frequency-dependent arrester model is necessary. This model could be either the IEEE proposed model or the one proposed in this thesis extended by taking into account the turn-on element in the non-linear branch.

Surge arresters limit the crest of the voltage surge in the system but they do not affect its rate of rise. For this reason, R-C branches are often applied as protective devices. The main difference is that they reduce the rate of rise of the TRV. In this way, they mitigate the TRV and prevent the vacuum circuit breaker from multiple reignitions. The major point of attention when using R-C branches is the selection of the correct parameters. There are no precise formulas available which can generally be applied for determining the optimal values for R and for C. Depending on the configuration and the type of load, it is possible to derive an approximated formula based on the stored electric and magnetic field energy. Especially when non-linear loads are used such as reactors with a core or unloaded transformers, the computation is strongly influenced by the non-linear primary inductance of the load. The values for R vary normally between 30 Ω and 100 Ω while the values of C are between 0.1 μF and 0.5 μF. Simulations for different values of R and C in order to obtain a good optimisation of the R-C branch are necessary.

Chapter 6

Switching off an unloaded transformer

6.1 Description of the problem

Having introduced the models for the system components we can apply the models in a particular system configuration and run simulations from which the generated overvoltages can be estimated. Two cases are considered:

- switching off steady-state transformer magnetising currents and
- switching off transformer inrush currents.

Since the transformer model represents its terminal impedance, only the primary phase-to-ground and phase-to-phase voltages can be observed, whilst the distribution of the surges along the turns cannot be calculated. The calculation is done for the system shown in Figure 6-1.

The transformer under no load is switched by a vacuum circuit breaker connected to the transformer by a cable. The transformer model for a broad frequency range is described in Chapter 4. The transformer data from the manufacturer are given in Table 6.1. For an accurate estimation of the generated overvoltages one must calculate the steady-state and inrush currents. It is also important to know the inrush currents for different phase angles if we want to find the time instant when the highest overvoltage

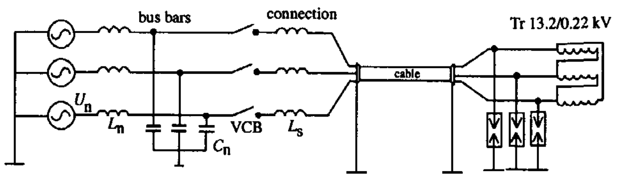

Figure 6-1: System configuration for studying transients

Table 6.1: Transformer data

Power	112.5 kVA
Voltage rating	13.2/0.22 kV
Frequency	60 Hz
Copper core losses	350 W
Winding lossses	1.247 kW
Primary/secondary leakage impedance ratio Z_h/Z_l	40/60 %
Transformer BIL	125 kV

occurs. The calculated inrush and magnetising currents are depicted in Figures 6-2 and 6-3, respectively.

The influence of the cable length on the generated overvoltages is also observed. The length of the cable is varied between 10 m and 60 m. The rated system voltage is 13.2 kV and the power frequency is 60 Hz. When switching inrush currents, different arcing times should be considered in conjunction with different scenarios of interruption.

The probability of the occurrence of overvoltages at different phase angles is calculated and expressed as percentage of the per unit voltage. Note that 1 per unit voltage is the maximum phase-to-ground voltage, being 10.75 kV. Higher overvoltage values occur and are caused by the VCC. These overvoltages are often a few times higher than the overvoltages generated at steady state. They can be very destructive with their amplitude when the transformer BIL has a rather low value as it is the case for dry-type transformers. But, the multiple reignitions are also dangerous for the insulation because of their steepness.

When switching off steady-state magnetising currents, current chopping occurs immediately after contact opening because the amplitude of the magnetising current is normally below the chopping level of the circuit breaker. This effect is not caused by the

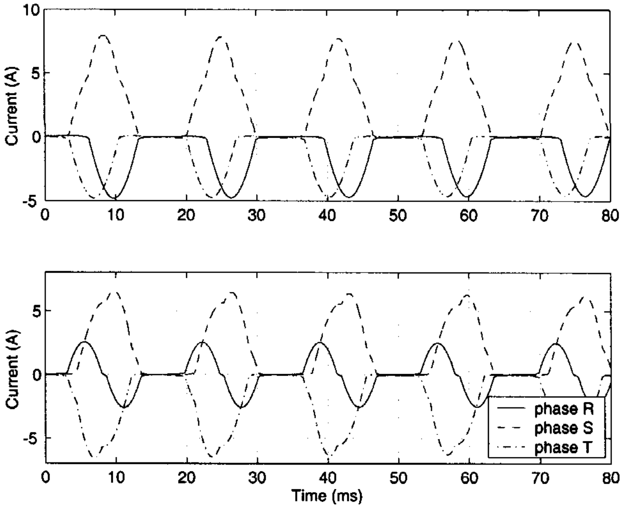

Figure 6-2: Calculated transformer inrush currents for the system in Figure 6-1, upper trace: initial phase 0^0, lower trace: initial phase 30^0

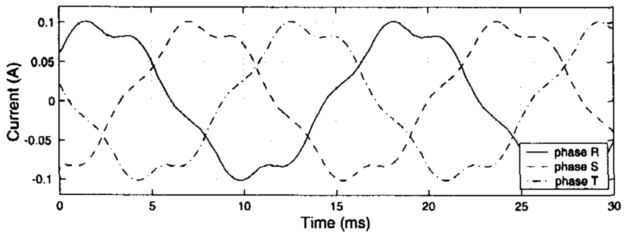

Figure 6-3: Calculated transformer magnetising currents for the system in Figure 6-1

vacuum circuit breaker contacts, but due to the level of the current being switched. For the most severe switching case, the effect of the protection equipment, surge arresters and R-C suppression branches is also studied. Regarding the practical application of the surge arresters, different arrester configurations are considered, like arresters connected phase-to-ground and arresters connected in both ways, phase-to-ground and between phases.

6.2 A statistical approach to the estimated overvoltages

The overvoltages that are generated when a vacuum circuit breaker is switched are statistical [61, 83] rather than deterministic because the crest of the generated overvoltages depends on many conditions such as: the instant of contact separation, the dielectric withstand voltage of the contact gap, the critical current slope, the chopping current and so forth. These parameters are statistically distributed and most of the time, the results vary from one switching operation to another. Therefore, in practical applications we need to estimate the overvoltages before a conclusion can be drawn about the percentage of the overvoltage level.

Apart from the vacuum circuit breaker parameters which are statistically varied, the instant of contact opening is statistically varied as well. Figure 6-4 shows the first period from the simulated inrush currents. We can conclude that from the first wave of the inrush currents, three possible intervals can be distinguished. The time intervals T_1 and T_2 are most critical with respect to the voltage escalation that might occur because there is a possibility for current chopping. One can also note that the poles begin to part immediately after energising, which is in practice rather uncommon because of the short time span between closing and opening of the vacuum circuit breaker. The main reason for this is that it saves computation time.

The statistical estimation is done in the following way. Let n be the total number of tests or energisations from which we can determine the same number of peak values of the switching overvoltage. Let v be the number of tests or energisations where some maximal value V_a from a specific measurement or calculation is $V < V_a < V + dV$. Then

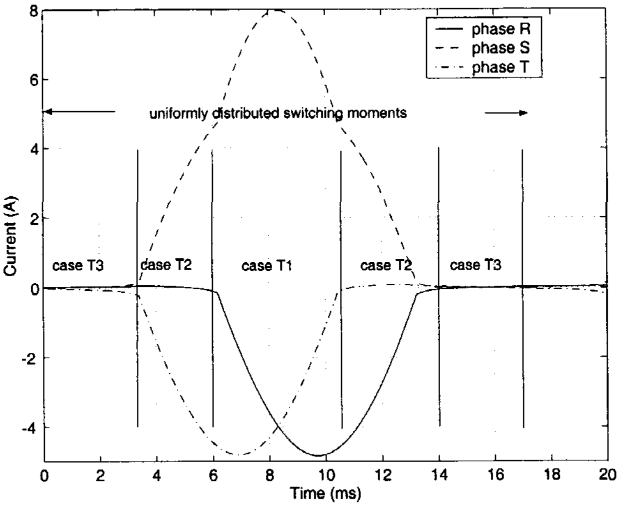

Figure 6-4: Possible switching instants during the existence of inrush currents; It describes the first period for the currents shown in Figure 6-2

ν/n is the probability of an overvoltage V_a occurring in a particular interval $[V, V + dV]$. Figure 6-5 depicts an example of how the probability versus maximal overvoltage should be expressed from the values obtained by the measurements or simulations.

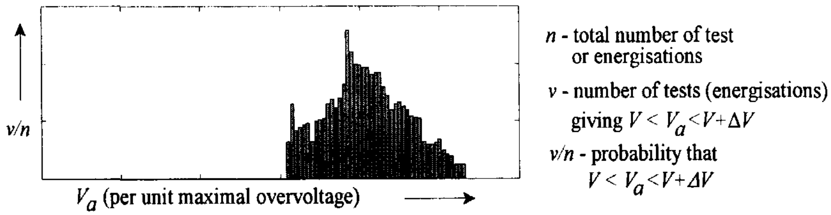

Figure 6-5: A histogram of the distribution of switching surge overvoltages

For a large number of tests and a very small dV, the histogram can be replaced with a smooth curve that can be approximated with a *Gaussian* distribution. Thus, having estimated the distribution of the switching overvoltages, one can calculate the cumulative occurrence of a particular voltage being exceeded with

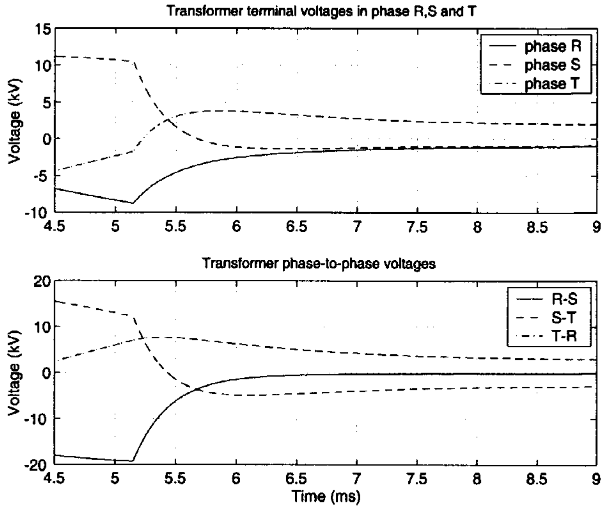

Figure 6-6: Calculated transformer terminal and phase-to-phase voltages for the system in Figure 6-1 (the circuit breaker model is A_1 and the cable length is 30 m)

$$Q(V_a) = \int_{V_a}^{\infty} f(V)dV. \tag{6.1}$$

6.3 Investigation of the switching overvoltages

a) Interrupting magnetising currents

We investigate the overvoltage level when the transformer is switched off by different vacuum circuit breakers. The models of type A, which correspond to the characteristics described in Table 2.2, are denoted as A_1 for the vacuum circuit breaker with high clearing ability, and A_2 for the vacuum circuit breaker with medium clearing ability. The calculations done with model A_1 show that no reignition occurs (Figure 6-6) and the overvoltages are below 2 per unit. This is because the withstand voltage of the vacuum circuit breaker is higher than the chopping overvoltage which in this case is rather low because of the low magnetising current. The overvoltages produced when using the low clearing ability characteristic are also low, so they are not observed here.

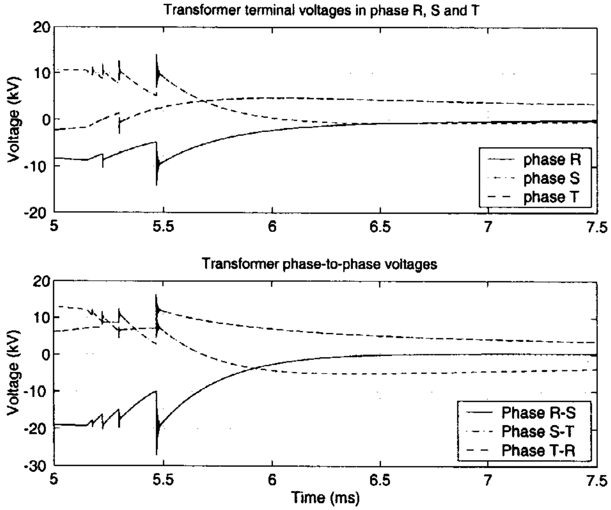

Figure 6-7: Calculated transformer terminal voltages and phase-to-phase voltages for the system in Figure 6-1 (the circuit breaker model is A_2 and the cable length is 10 m)

Unlike model A_1, model A_2 indicates that a reignition occurs but in this particular case, the overvoltages are also not so high. Figure 6-7 shows the transformer terminal voltages. The cable length for this calculation is 10 m.

With the model A_2, a statistical analysis is done. The instant of the contact opening is regarded as a stochastic value and all possible switching instants are within a time window of 5.5 ms. The probability of the instant of contact opening is uniformly distributed. This is allowed for the steady-state currents (see Figure 6-3) since we consider a three-phase balanced system. The statistical estimation of the overvoltages when using model A_2, which is presented in Figure 6-8, shows that the maximal overvoltage of about 2.2 per unit occurs for the shortest cable of 10 m. Compared to the results of the calculation with model A_1, the overvoltages are only slightly higher but due to the multiple reignitions they are rather steep. The steepness of the voltage wave is also dangerous for the transformer insulation, just as its amplitude. The low voltage transients calculated for the steady-state current switching case occur as a result of the low chopping current because in this case the magnetising currents that are switched are very low. Also transformer losses are large enough to damp the transient oscillations. The result is a low chopping overvoltage. But for other transformer classes with higher magnetising currents, in the region of 1 A to 1.5 A, the expected overvoltages can be much higher. This depends not only on the transformer parameters but also on the cable parameters and the vacuum circuit breaker characteristics. Measurements done by *Cornick* [12] show overvoltages as high as 5 per unit and a duration of the switching transients in the time range of nanoseconds.

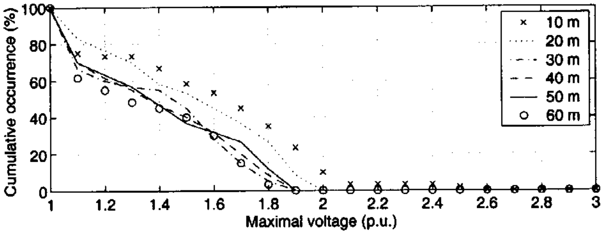

Figure 6-8: Cumulative occurrence of overvoltages during magnetising current switching for the system in Figure 6–1 (model A_2) for different cable lengths.

b) Interrupting inrush currents

Inrush currents occur while transformers are energised and find their origin in the non-linearity of the magnetic core. When the transformer is under no load, the working point of magnetising inductance follows the magnetising curve. At the saturated part, the magnetising inductance has a lower value. This implies that the inrush current in the circuit is apparently larger than the rated current, but for other transformers it might be several times higher. Inrush currents contain many DC biased decaying spikes. The first maximum has the highest value because of the saturation and each next maximum is lower than the previous one because of the hysteresis losses and the winding losses in the transformer. Thus, the total current, which is asymmetrical, tends to become symmetrical, but in practice it may take several seconds until the steady-state is reached. The inrush current is hardly damped and can therefore flow for several seconds. The inrush current duration is governed by the system X/R ratio. In circuits with rather high time constants, containing mainly unloaded transformers and reactors,

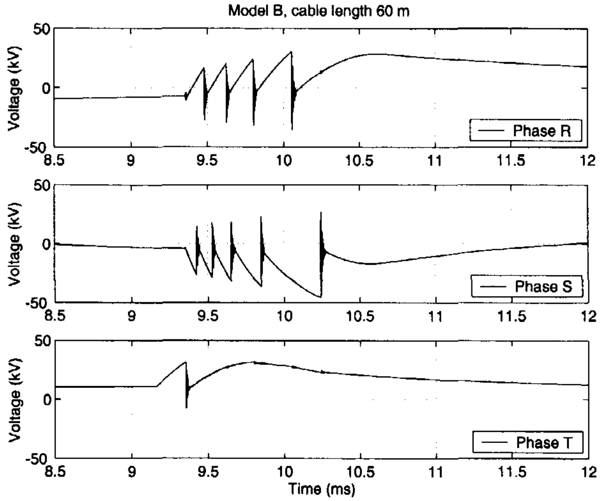

Figure 6-9: Transformer terminal voltages during the inrush current switching for the system presented in Figure 6-1 with the breaker model B; upper trace: voltage in phase R; middle trace: voltage in phase S; lower trace: voltage in phase T

the DC component can be higher than prescribed by the standards. Inrush current switching occurs in particular in arc furnace transformer networks [55, 81]. Arc furnace transformers are normally energised while the low voltage transformer winding is open. Unlike distribution transformers, where the low voltage winding is usually connected to a cable with a load, arc furnace transformers have their secondary winding open before switching. This is of importance because when a cable is connected to the secondary side of a transformer, it increases the total capacitance, and thus reduces the frequency of the overvoltages [70]. In case an arc furnace transformer is switched, for example in the course of a melting process, the transformer is energised and de-energised several times in both loaded or unloaded states. Thus, as many as hundred switching operations per day take place during the normal operation of an arc furnace. As mentioned earlier, three cases are distinguished with respect to the moment of contact opening, and the computation is done only for the first current wave, which contains the highest local maximum.

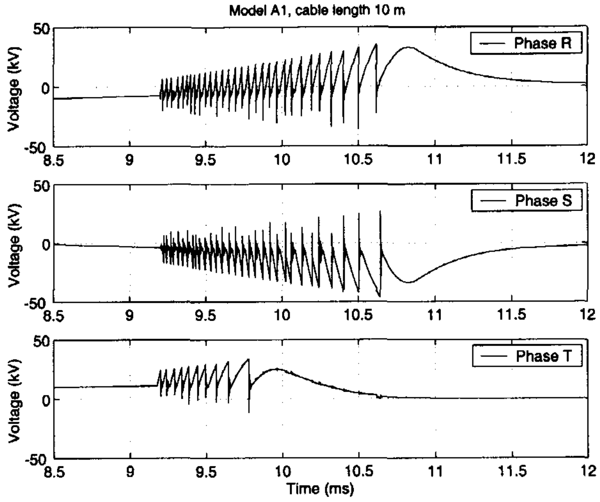

Figure 6-10: Transformer terminal voltages during inrush current switching for the system in Figure 6-1 with the breaker model A_1; upper trace: voltage in phase R; middle trace: voltage in phase S; lower trace: voltage in phase T

Figure 6-9 through Figure 6-11 show the calculated voltages at the transformer terminals for the system in Figure 6-1 where the inrush currents are switched off. The computation is done by different vacuum circuit breaker models: B, A_1 and A_2. The contacts are opened just before current zero in phase T (1.5 ms) and the value of the current at the moment of contact opening is 3.5 A. When a reignition occurs the reignited current in phase T is superimposed on the inrush currents in phase R and S and causes VCC. From the displayed pictures we can see that in phase R and phase S, the variation of the voltages have a similar shape but are of opposite polarity. Since the primary windings of the transformer are delta connected, the voltage across the transformer winding of phase R is the difference between the terminal voltages in phases R and S. So, the total voltage of the winding in phase R can reach approximately twice the value of the terminal voltage. For inrush current switching, a survey on the effect of different cable lengths was made just as in the case of magnetising current switching. The cumulative occurrence of the maximum overvoltages is calculated for the switching instants of the

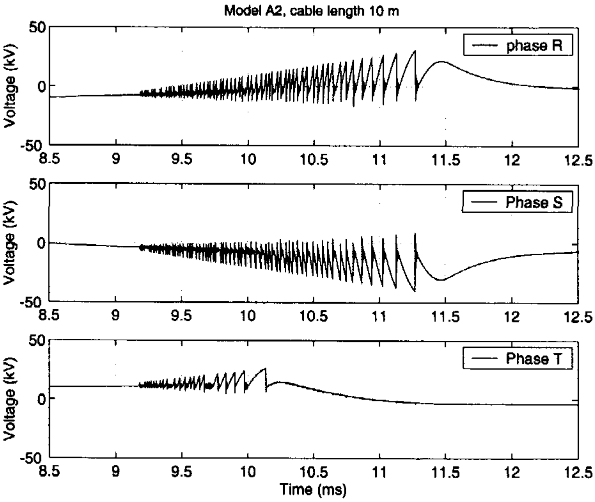

Figure 6-11: Transformer terminal voltages during inrush current switching for the system in Figure 6-1 with the breaker model A_2; upper trace: voltage in phase R; middle trace: voltage in phase S; lower trace: voltage in phase T

circuit breaker which correspond for case T_1, as shown in Figure 6-4. In this case, the maximum phase-to-phase voltage is observed, which is actually the voltage to which a transformer winding is exposed.

The virtual chopping takes place at a chopping level that is between 4 A and 8 A. In practice, the transformer inrush currents can be higher. For distribution transformers, inrush currents can even reach values of 2 kA [87]. So if a VCC takes place, the overvoltages might even be higher. The dielectric withstand capability of the vacuum circuit breaker model A_1 and B is higher than the dielectric withstand capability of the vacuum circuit breaker model A_2 and therefore the TRV across the breaker terminals exceeds the dielectric withstand capability at higher values. From Figure 6-10 and Figure 6-11 follows that the duration of reignition when using model A_2 is longer than the duration of reignition when using model A_1. Also the maximal overvoltage which occurs with the model A_2 is lower than the maximal overvoltage when the model A_1 is used. This is because the reignition with model A_2 occurs at lower TRVs than the reignition in model A_1. The cable length also influences the generated overvoltage. In general, it contributes to voltage suppression because with the increase of the cable, the travel time of the surge along the cable increases, which contributes to less steeper overvoltages upon reflection of the surge at the transformer terminal. Another fact is that the increase of the cable capacitance decreases the frequency of the TRV so the rate of rise of the TRV is reduced and there is less possibility of reignition. This is in particular important for unloaded transformers, because these are highly inductive loads with a high characteristic impedance and a capacitance which is considerably lower than that of the cable.

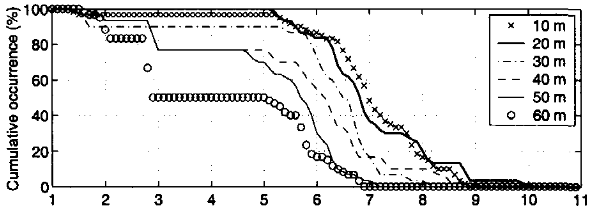

Figure 6-12: Cumulative occurrence of the maximal overvoltage during inrush current switching for the system in Figure 6-1 for different cable lengths; the switching instants are randomly chosen within interval T_1 (Figure 6-4); circuit breaker model B

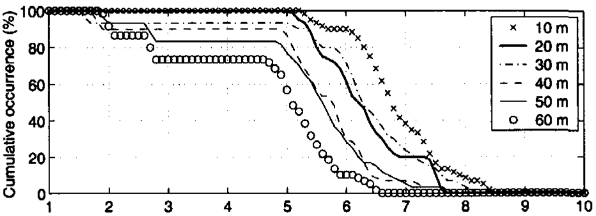

Figure 6-13: Cumulative occurrence of the maximal overvoltage during inrush current switching for the system in Figure 6-1 for different cable lengths; the switching instants are randomly chosen within interval T_1 (Figure 6-4); circuit breaker model A_1

The results of statistical calculation of the phase-to-phase overvoltages are presented in Figure 6-12 through Figure 6-14. Approximately 50 % of the overvoltages are between

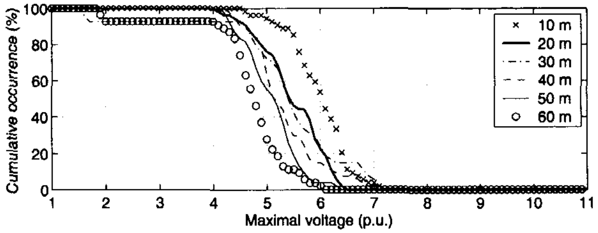

Figure 6-14: Cumulative occurrence of the maximal overvoltage during inrush current switching for the system in Figure 6-1 for different cable lengths; the switching instants are randomly chosen within interval T_1 (Figure 6-4); circuit breaker model A_2

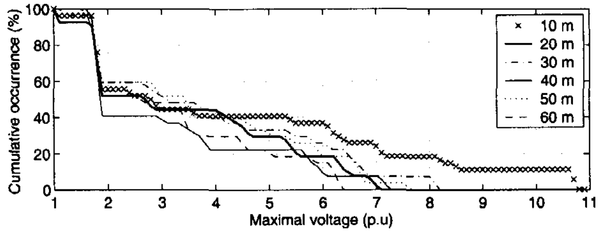

Figure 6-15: Cumulative occurrence of the maximal overvoltage during inrush current switching for the system in Figure 6-1 for different cable lengths; the switching instants are randomly chosen within the interval of the first period (Figure 6-4); circuit breaker model A_1

50 kV and 70 kV. The maximum terminal overvoltages are approximately half the value of the phase-to-phase overvoltages.

This is a rather severe switching case and when the transformer inrush currents and chopping current increase, higher VCC voltages might be expected. Generally speaking one cannot determine the probability of the occurrence of overvoltages like in case of switching off steady-state currents. The explanation for this is that there is no proper time interval that contains all possible switching instants because the inrush currents are not symmetrical. In the first period, the highest peak current occurs so that this can be considered as the worst case of switching, as shown in Figure 6-4. When the switching instant is determined in this way, the probability can be calculated. The calculated results

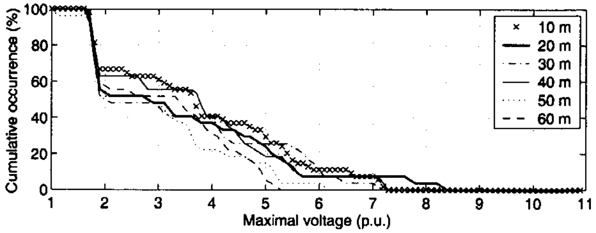

Figure 6-16: Cumulative occurrence of the maximal overvoltage during inrush current switching for the system in Figure 6-1 for different cable lengths; the switching instants are randomly chosen within the interval of the first period (Figure 6-4); circuit breaker model A_2

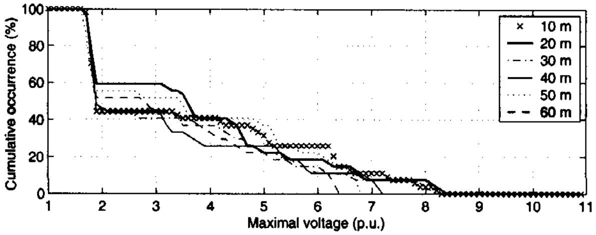

Figure 6-17: Cumulative occurrence of the maximal overvoltage during inrush current switching for the system in Figure 6-1 for different cable lengths; the switching instants are randomly chosen within the interval of the first period (Figure 6-4); circuit breaker model B

are represented in Figure 6-15 through Figure 6-17. All these results for the cumulative probability of overvoltage occurring during the inrush current switching show that the maximum overvoltages occur only when the contacts open in the intervals T_1 or T_2. The general conclusion is that the probability of occurrence is rather small.

6.4 Protection of transformers against switching surges

Repeated energisation of transformers can lead to very severe electromechanical forces as a result of the (highly distorted) inrush currents. Normally, vacuum circuit breakers operate satisfactorily under these conditions, but they also interrupt high frequency currents with the extra possibility of energy trapping and subsequently the generation of overvoltages. In order to protect the transformers from unwanted voltages, it is therefore advisable to apply surge arresters for limitating the overvoltage to a value that is determined by the parameters of the arrester.

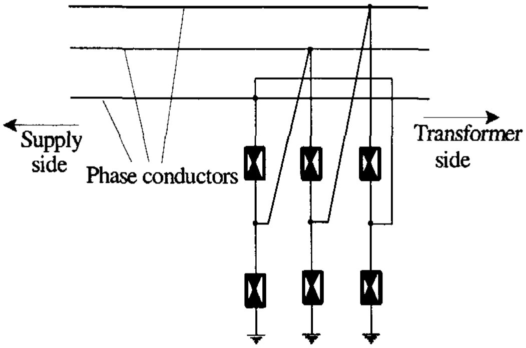

Figure 6-18: A way of protecting transformers against voltage surges

In Chapter 5 we analysed the operational effect of the surge arrester. Its residual voltage increases proportionally with the steepness of the applied surge. Since the distribution transformer windings on the primary side are mostly delta connected, the overvoltages between the phases can rise above the protection level of the arrester if the arresters are installed only phase-to-ground. This is particularly possible when VCC occurs and therefore, the surge arresters must be installed phase-to-phase and phase-to-ground (Figure 6-18).

6.4.1 Surge arresters connected phase-to-ground

Figure 6-19 shows an example of the calculated reignited overvoltages. The upper and the middle trace are the calculated voltages at the transformer terminals R and S. The

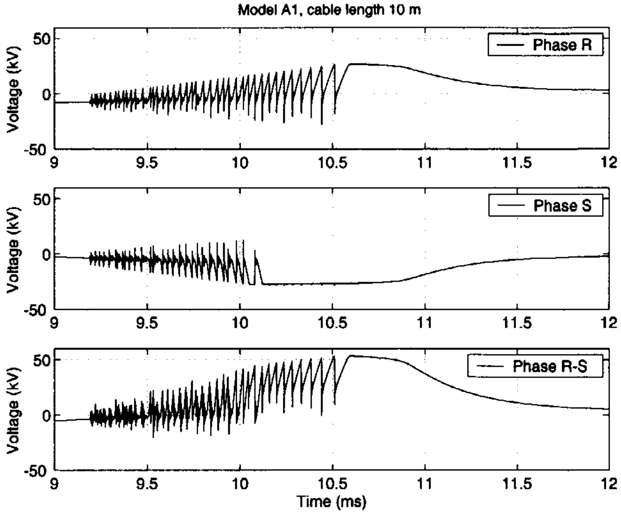

Figure 6-19: Simulation of the arrester effect when arresters are installed only phase-to-ground during inrush current switching for the system in Figure 6-1; upper trace: voltage in phase R; middle trace: voltage in phase S; lower trace: voltage between phases R and S

lower trace is the calculated voltage *between* terminals R and S, that is the phase-to-phase voltage after switching. The possibility that the voltage can rise above the protection value of arrester is now limited. When the arrester starts to operate, the reignition ceases and the voltage wave is absorbed. This is the way in which the arrester affects the voltage. In this case, although the terminal voltages are limited to the protection level of the arrester, the voltage to which the transformer winding is exposed still remains above 50 kV (4.6 p.u).

6.4.2 Surge arresters connected between phases and phase-to-ground

When the arresters are connected as shown in Figure 6-18, then the duration of the reignition is shorter and the phase-to-phase voltages are limited to the protection level of the arrester. In this case they are less than 3 per unit. This is shown in Figure 6-

20. This results in lower voltage peaks than in the case when only three arresters are installed. However, the surge arresters can only limit the overvoltage and the reignition ceases when the arrester starts to operate. Although the reignited voltage has a lower peak, it is a very steep-fronted voltage surge that suddenly stresses the transformer. The result is a very non-uniform voltage distribution along the transformer windings and this causes a high dielectric stress for the inter-turn insulation.

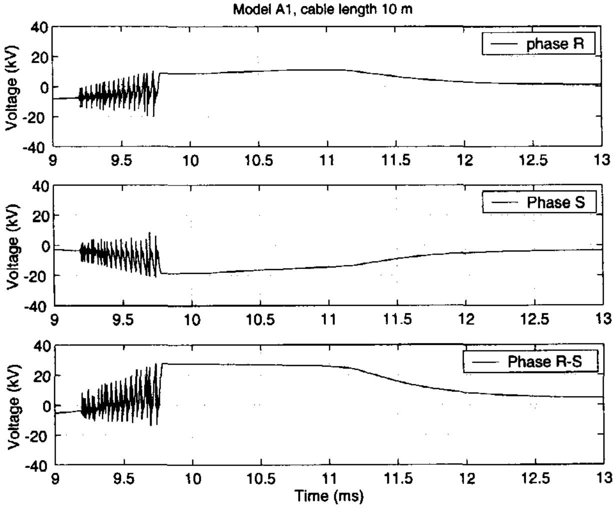

Figure 6-20: Simulation of the arrester effect when arresters are installed phase-to-ground and between each two phases during inrush current switching for the system in Figure 6-1; upper trace: voltage in phase R; middle trace: voltage in phase S; lower trace: voltage between phases R and S

6.4.3 R-C branch as a protective device

In most of the cases where frequent switching can take place, it is advisable to install *R*-*C* branches. The types that can be selected and their possible effects were explained and analysed in Chapter 5. Figure 6-21 and Figure 6-22 show the effect of *R*-*C* branch on voltage suppression. The calculations are done for cable lengths of 20 m and 50 m. The results of applying an *R*-*C* for different cable lengths are very similar and this implies that the total cable capacitance in both cases is considerably smaller than the suppression capacitance, so that it does not affect the influence of the protective branch. The damping resistor is in all cases 50 Ω. In order to quantify the influence of the various *R*-*C* combinations, we introduced a surge suppression factor:

$$K_{\mathrm{S}} = \frac{V_{\mathrm{T}} - V_{\mathrm{F}}}{V_{\mathrm{F}}} 100\% \tag{6.2}$$

with V_{T} and V_{F} being the peak values of the terminal voltage with (V_{T}) and without

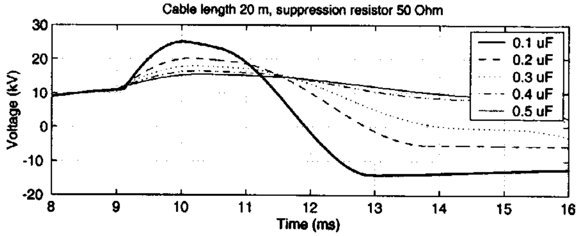

Figure 6-21: The variation of the suppressed voltage when using *R*-*C* circuit during inrush current switching for the system in Figure 6-1 and for different values of the protective capacitors

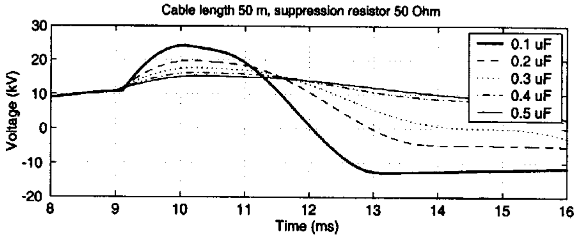

Figure 6-22: The variation of the suppressed voltage when using *R*-*C* circuit during inrush current switching for the system in Figure 6-1 and for different values of the protective capacitors

(V_{F}) the *R*-*C* suppression branch, respectively. The values of the suppression factor, calculated for different parameters of *R* and *C*, are depicted in Figure 6-23. It can be concluded that by increasing the value of the damping resistor, the suppression factor slowly increases. The major effect is the increase of the suppression capacitance. For a particular damping resistor, by changing the capacitance from 100 nF to 500 nF, the suppression factor increases approximately with 12 %. The R-C branch also decreases the steepness of the surges and in most of the cases prevents the occurrence of multiple reignitions.

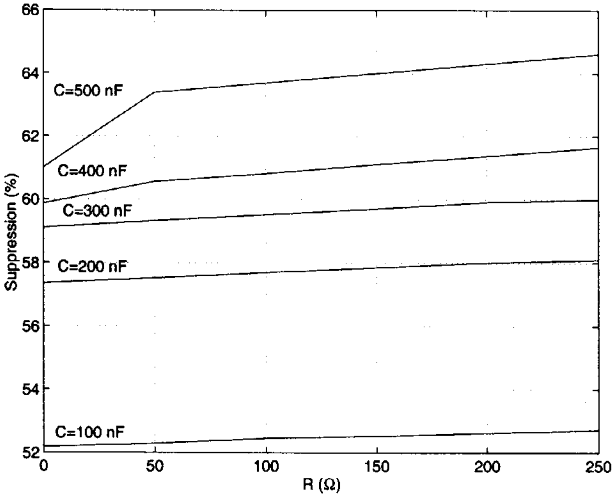

Figure 6-23: Calculated suppression factor for different parameters of R and C

6.5 Conclusion

Two scenarios have been observed during the switching with respect to the state of work of the transformer: a steady-state condition and a transient condition, which occurs during inrush current switching. The studied example is the one that is mostly used for industrial application. The transformer is connected to the vacuum circuit breaker by a cable and the results of the calculation show that the primary overvoltages generated during steady-state current switching have a maximum value between 3 per unit and 3.5 per unit. This value is below the transformer BIL. A more dangerous case is the switching of inrush currents. Inrush currents depend on the properties of the core and can reach values several times the transformer rated current. Switching off high inrush currents can lead to VCC as explained in this chapter. The generated overvoltages after inrush current switching can be as high as 10 per unit and this is supported by the measurements performed by *Daalder* and *van den Heuvel* [87].

The length of the cable influences the overvoltage in such a way that it increases the total load capacitance. The study is done for cable lengths of 10 m, 20 m, 30 m, 40 m, 50 m and 60 m. Calculations show that in general short cables cause higher overvoltages because of the increase of the TRV and its rate of rise. An increase of the cable length reduces the overvoltages significantly. Another important factor which influences the overvoltage level is the arcing time. This is especially important for inrush current switching. The statistical overvoltage distribution correlates with the randomly chosen switching instants. From Figure 6-8 it can be seen that for steady-state switching, the distribution of overvoltages is close to normal distribution. For inrush current switching, the overvoltage has a normal distribution only within specific intervals denoted as T_1, T_2 and T_3 (Figure 6-4), while the distribution for the 16.6 ms interval deviates from the normal distribution. When switching takes place in the intervals T_1 or T_2, VCC can occur in the investigated transformer. When the switching takes place during the interval T_3, the situation is similar to the case of steady-state switching.

Chapter 7

Calculation of the Probability of Reignition

7.1 Introduction

If one wants to estimate accurately the overvoltage amplitude and its variation while de-energising a low inductive current circuit, it is necessary to model the network and system components quite precisely. This is rather difficult since a large number of parameters play a role. The frequency dependency of the system elements is important and for such an analysis, a lot of data and many characteristics are needed for studying the transient phenomena. These data are not always available to engineers, so the study of overvoltages in engineering applications is confronted with many difficulties, particularly when these data must be provided. By using the system parameters that are available, the probability of reignition can be calculated and an approximation of the overvoltages for the 3 per unit and 5 per unit level can also be found with depending on the cable length, the motor power and the switching angle.

This chapter focuses on the practical estimation of overvoltages when stalled electric motors are switched off. A similar approach can be applied for studying the switching of loaded transformers or any other low inductive circuit. In practice motors are more frequently exposed to high overvoltages than unloaded transformers and transformers are not tested dielectrically that severely.

7.2 Influence of the circuit parameters

Experience shows that one of the switching operations that results in a significant overvoltage is when a motor is switched off at its start up. The probability of the occurrence of both reignition and VCC strongly depends on the parameters of the surrounding circuit and the breaker. Circuit parameters that are of influence are the motor power, the busbar configuration, the type of cable and its length, the system voltage and the number of connected cables. The important circuit breaker parameters are the speed of contact separation, the dielectric withstand capability, the current chopping level and the high frequency interruption ability. These parameters are essential for modeling the vacuum circuit breaker reignitions (see Chapter 2). A simulation study was carried out in order to quantify the influence of parameters on the probability of the occurrence of a multiple reignition and VCC for each switching operation.

7.2.1 Probability of a reignition

A reignition of the vacuum circuit breaker occurs because the TRV exceeds the momentary dielectric withstand capability of the vacuum circuit breaker gap. For the specific TRV (which can be calculated from the circuit parameters), the dielectric recovery curve of the gap and the speed of contact opening, a critical time window (of length T_{reig}) around the natural power frequency current zero can be defined as follows: a contact separation outside the time window does not lead to a reignition, while a contact separation within the interval T_{reig} does lead to a reignition, as can be seen in Figure 7-1. There are 6 current zero crossings per 20 ms in a 50 Hz three-phase system. For a randomly opening vacuum circuit breaker in a 50 Hz three-phase circuit the probability of reignition P_{reig} is therefore [73, 76]:

$$P_{\mathrm{reig}} = \frac{T_{\mathrm{reig}}}{3.3} \tag{7.1}$$

Whether or not the reignition leads to VCC also depends on the circuit and the vacuum circuit breaker parameters. A reignition resulting in a VCC can be associated with an effective time window T_{VCC} and a probability P_{VCC} defined in a similar way as P_{reig}. This probability is always less than or equal to the probability of reignition P_{reig} because

$T_{\mathrm{VCC}} \leq T_{\mathrm{reig}}$.

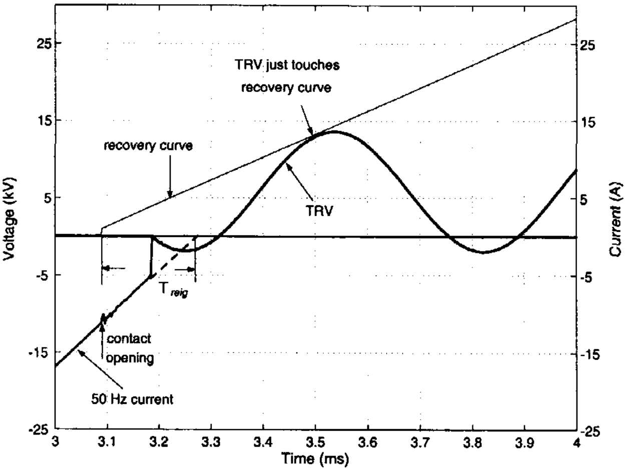

Figure 7-1: Time window of a reignition in relation to current chopping and the TRV

In practical applications, a variety of motor circuits are in use. Since the worst-case situation dictates whether or not a protection is necessary, the motor test circuit is modelled by the standard motor scheme according to IEC 61233 shown in Figure 7-2.

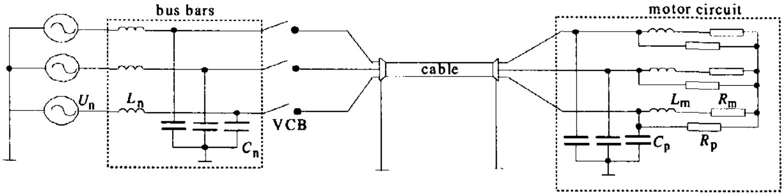

Figure 7-2: Standard motor circuit according to IEC 61233

For this circuit, the reignition and VCC probabilities can be calculated by varying the parameters of both the circuit and the vacuum circuit breaker. These computations have to be done by varying circuit parameters such as motor power and cable length, and vacuum circuit breaker parameters such as the slope of recovery curve and the chopping current. For this analysis only model *B* for the vacuum circuit breaker was used because the idea is to investigate how the parameters of the network (particularly cable length and motor power) and chopping current influence the probability of reignition.

The self- and mutual inductance of the busbars are 6 μH and 3 μH respectively. The cable is a belted cable modelled by the distributed parameter routine in ATP. The parameters of the cable's positive component R_1=0.0837 Ω/km, L_1 = 0.0912 mH/km and C_1=0.3 μF/km. Zero sequence component has the following parameters: R_0=1.37 Ω/km, L_0 = 0.138 mH/km and C_0=0.3 μF/km. The motors inductance is assumed as 1/6 of the nominal motor's inductance in order to take into account the inrush current during the start up of the motor. The system voltage is 7.2 kV.

7.3 Computation methodology

In order to estimate the reignition probability one needs to find the time window for which the recovery curve touches the TRV. Therefore many simulations for a specific circuit and for fixed vacuum circuit breaker data must be done to determine this time window. The method of computation is depicted in Figure 7-3.

The set of all ATP data cases are for a specific motor power, a certain chopping current and fixed parameters for the vacuum circuit breaker. The data cases differ in cable length. The observed cable lengths are 10 m, 40 m, 70 m, 100 m, 200 m, 300 m, 400 m, 500 m up to 1 km. For each data case the main program runs the ATP-EMTP program in batch processing. At the end of each simulation, a separate subroutine verifies whether a reignition has occurred or not. If the reignition did occur the batch file continues with the next program file where for the chosen system data, the probability of the reignition is computed. This program also checks if it is reignition or VCC. If no reignition occurs, the instant of contact opening is increased and the ATP-EMTP data case is run again. When each of the data cases is worked out, the motor and vacuum circuit breaker parameters are changed and the program represented by the flow chart in Figure 7-3 is run again to calculate the probabilities for the new data.

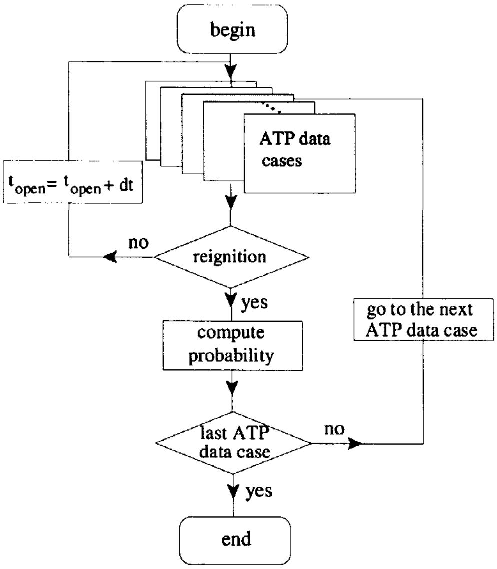
begin
ATP data cases
$t_{open} = t_{open} + dt$
no
reignition
yes
compute probability
go to the next ATP data case
last ATP data case
no
yes
end

Figure 7-3: Flow chart for reignition probability computation

7.3.1 Results

If one wants to use these results in practice, one should consider [73, 74, 76] that:

- The calculated probabilities correspond to switching off a motor at start up and the relatively high values of the probability of reignition do not occur during normal motor operation,
- a synchronous opening of the vacuum circuit breaker poles is considered for this analysis.

Figure 7-4 through Figure 7-15 show the calculated probability of the total reignition P_{reig} and the reignition with VCC P_{VCC} versus the motor power for different cable lengths. The other parameters (system voltage, busbars length, type of the cable, circuit breaker parameters and the maximal inrush current) are kept constant. Generally speaking, the results show that small motor powers in combination with short cables have a high probability of reignition. So, larger motor powers in combination with longer cables minimize the probability of reignition and VCC. Figure 7-16 shows the variation of the probability depending on the chopping current of the vacuum circuit breaker. This result shows clearly that the higher chopping current increases the probability of reignition. The graphs which describe the probability of the total reignition P_{reig} and the probability of reignition P_{VCC} with the occurrence of VCC have a similar shape. The opinion is that this is influenced by the parameters of the cable and busbars and if different parameters are involved the curves of probability can have different shape. However, P_{reig} is always higher than the P_{VCC} because it corresponds to a longer time window. Generally, with the increase in the motor power the probability decreases.

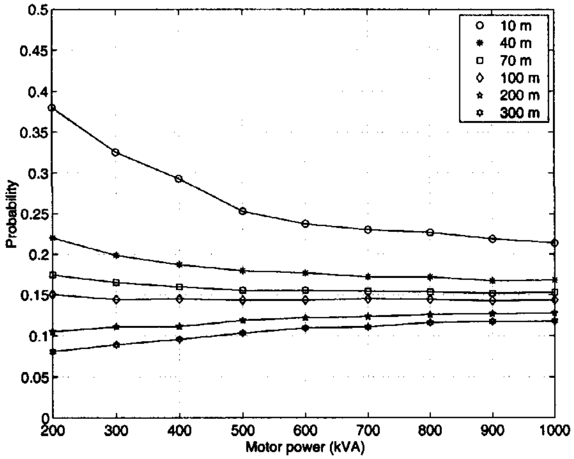

Figure 7-4: Probability of total reignition P_{reig} as a function of the motor power and the cable length; the slope of the recovery curve is 20 V/μs and the chopping current is 3 A

According to the data used for the system in Figure 7-2, even for high motor powers and long cables both P_{reig} and P_{VCC} probabilities are close to each other. This implies that for short arcing time, when reignition occurs, reignition automatically leads to VCC or the time window of VCC is only slightly shorter than the time window of the total reignition. Also for small motor powers and cable lengths longer than 300 m due to numerical problems with the determination of time window, the probability is not calculated.

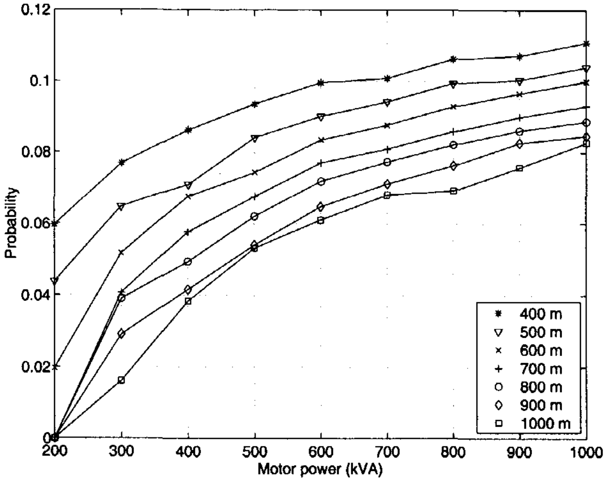

Figure 7-5: Probability of total reignition P_{reig} as a function of the motor power and the cable length; the slope of the recovery curve is 20 V/μs and the chopping current is 3 A

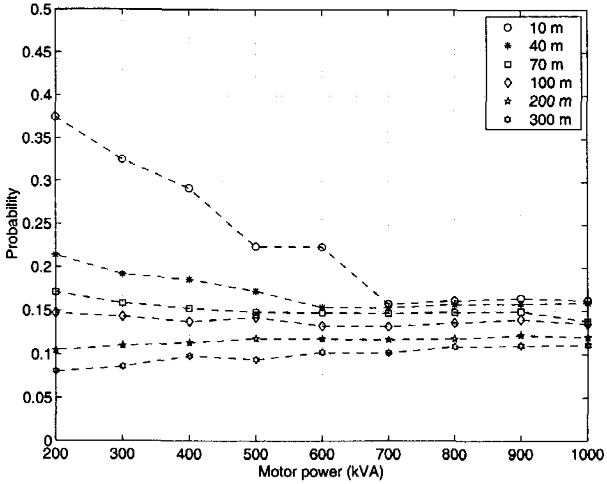

Figure 7-6: Probability of reignition with a VCC P_{VCC} as a function of the motor power and the cable length; the slope of the recovery curve is 20 V/μs and the chopping current is 3 A

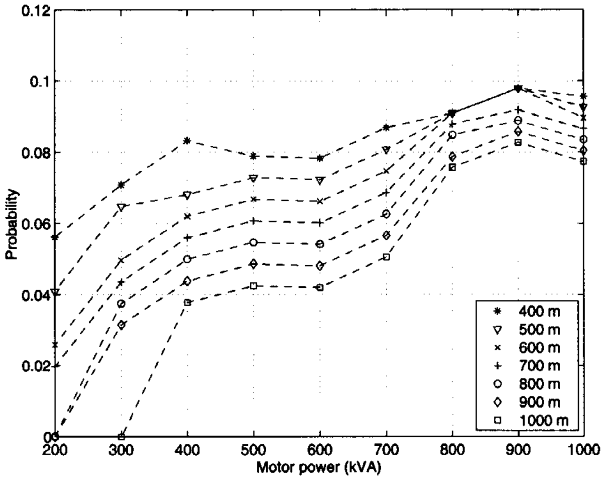

Figure 7-7: Probability of reignition with a VCC *P*vcc as a function of the motor power and the cable length; the slope of the recovery curve is 20 V/μs and the chopping current is 3 A

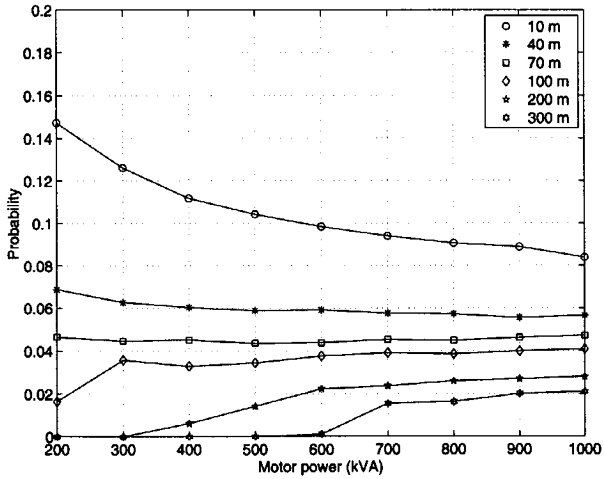

Figure 7-8: Probability of total reignition P_{reig} as a function of the motor power and the cable length; the slope of the recovery curve is 50 V/μs and the chopping current is 3 A

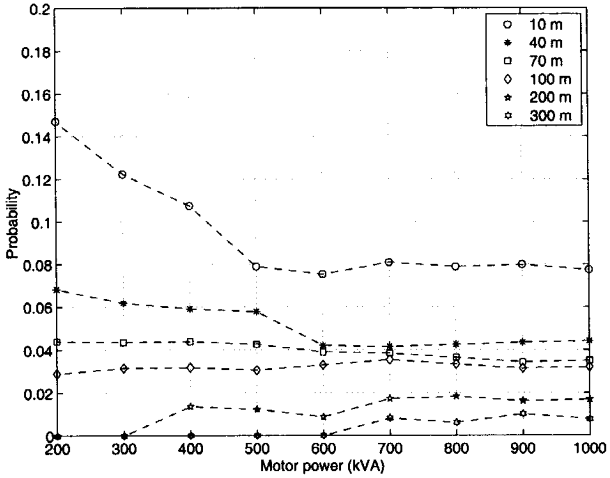

Figure 7-9: Probability of reignition with a VCC $P_{\rm VCC}$ as a function of the motor power and the cable length; the slope of the recovery curve is 50 V/μs and the chopping current is 3 A

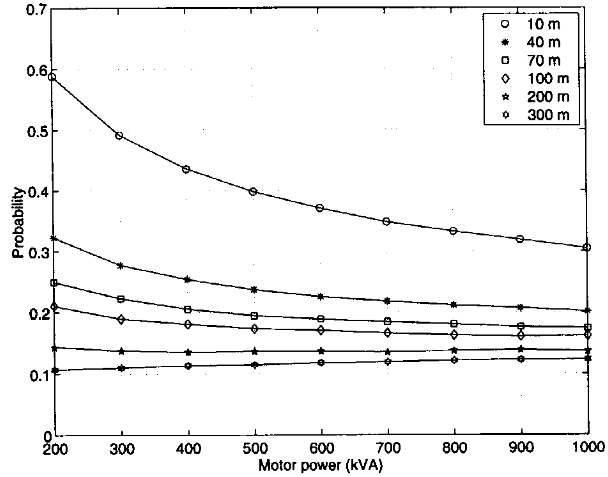

Figure 7-10: Probability of total reignition $P_{\rm reig}$ as a function of the motor power and the cable length; the slope of the recovery curve is 20 V/μs and the chopping current is 5 A

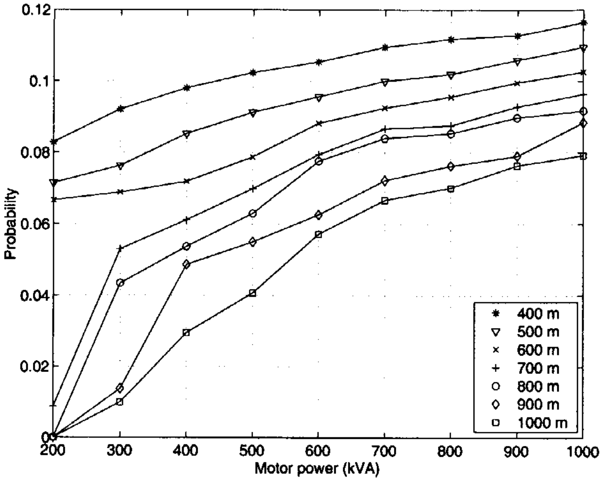

Figure 7-11: Probability of total reignition P_{reig} as a function of the motor power and the cable length; the slope of the recovery curve is 20 V/μs and the chopping current is 5 A

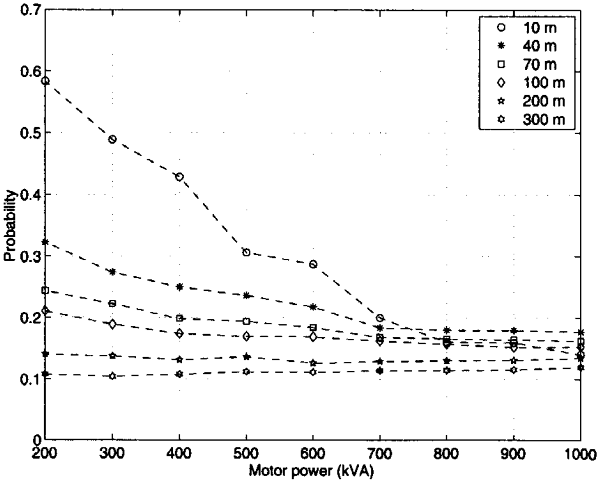

Figure 7-12: Probability of reignition with the VCC P_{VCC} as a function of the motor power and the cable length; the slope of the recovery curve is 20 V/μs and the chopping current is 5 A

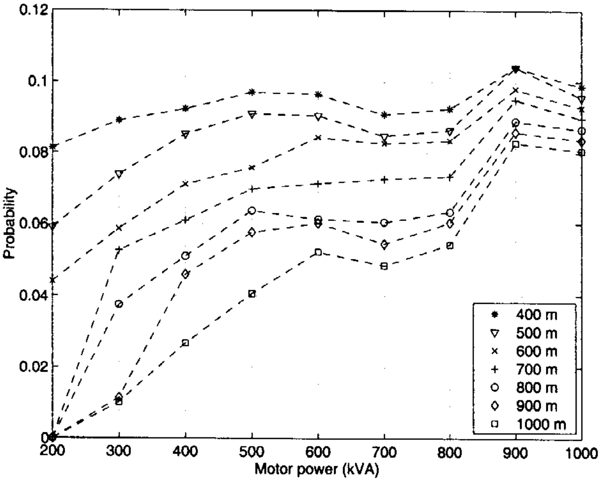

Figure 7-13: Probability of reignition with the VCC P_{VCC} as a function of the motor power and the cable length; the slope of the recovery curve is 20 V/μs and the chopping current is 5 A

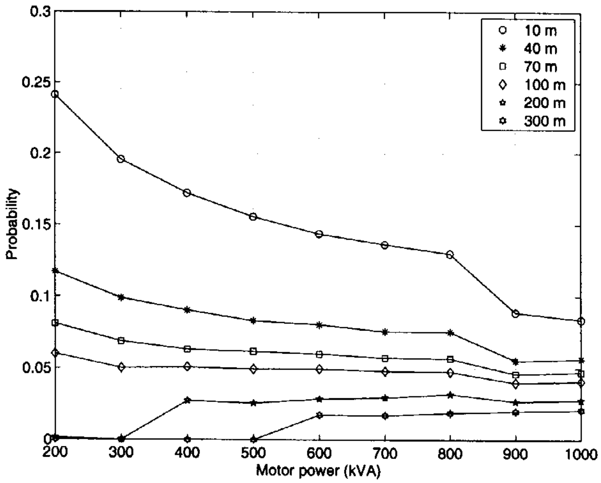

Figure 7-14: Probability of total reignition P_{reig} as a function of the motor power and the cable length; the slope of the recovery curve is 50 V/μs and the chopping current is 5 A

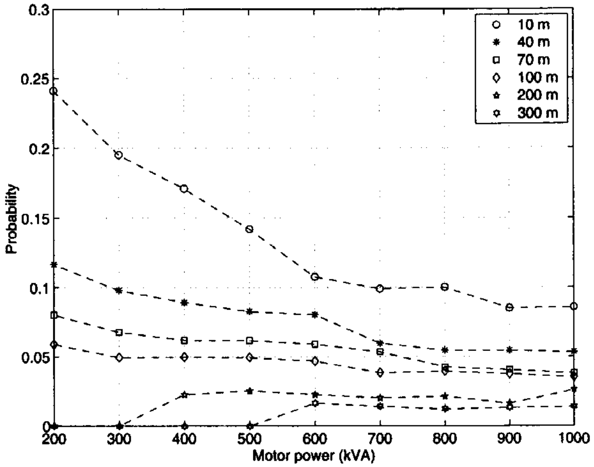

Figure 7-15: Probability of reignition with the VCC P_{VCC} as a function of the motor power and the cable length; the slope of the recovery curve is 50 V/μs and the chopping current is 5 A

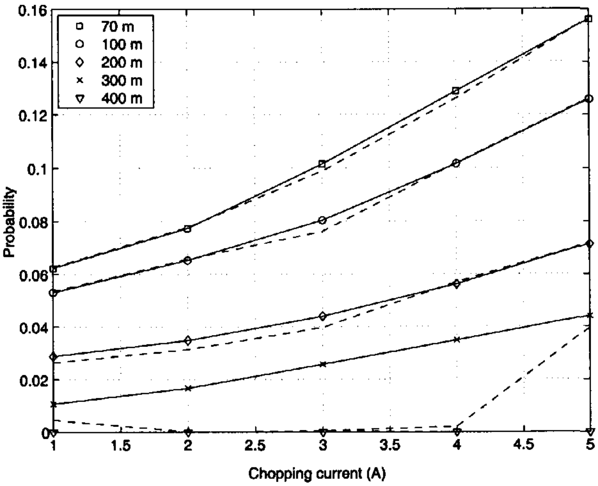

Figure 7-16: Probability of total reignition (solid line) P_{reig} and the reignition with the VCC (dashed line) P_{VCC} as a function of the chopping current and the cable length; the slope of recovery curve is 30 V/μs and the motor power is 200 kW

7.4 Determination of the overvoltage curves

Despite the large number of data necessary to estimate the variation of overvoltages in steepness and amplitude during the switching of small inductive currents, one can determine how the overvoltage level varies by changing the motor power and cable length. By using the power frequency data for cables and motors in a similar way, like in the case of reignition probability estimation, the overvoltage can be estimated for different cable lengths. The goal of the computation is determining the 3 per unit and 5 per unit overvoltages. For a fixed motor power, the computations are performed starting with the longest cable value which in our case is 2.5 km. Normally for very long cables, because of the large cable capacitance, the overvoltages are rather low. Then, we decrease the cable length until the overvoltage reaches 3 per unit the rated system voltage, on at least one motor terminal. This identifies one point in the cable length versus motor power diagram. In the same way the 5 per unit line is determined and the same procedure is used to determine the 3 per unit and 5 per unit curves when VCC occurs.

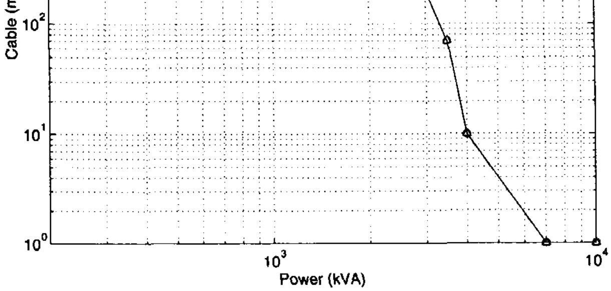

Figure 7-17: The geometrical place of the combination between cable length and motor power resulting in an overvoltage of 3 p.u. or 5 p.u.

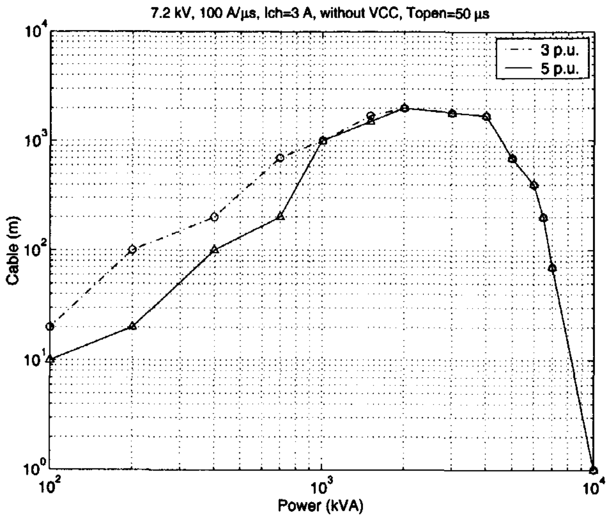

Figure 7-18: The geometrical place of the combination between cable length and motor power resulting in an overvoltage of 3 p.u. or 5 p.u.

When observing the situation in which VCC occurs, in most of the cases, the critical motor power is between 500 kVA and 2 MVA. For short arcing times in 95 % of all cases due to the VCC, the voltage exceeds 5 per unit. That is why 3 per unit and 5 per unit curves overlap. For motor powers between 200 kVA and 2 MVA the graphics are similar to those with VCC, while for motor powers greater than 5 MVA due to the high start-up current, VCC almost disappears. Therefore the arc is re-established and cleared in the next current zero. This contributes to lower overvoltages. Furthermore, the system voltage has a large impact on these curves. The analysis involves two system voltages: 7.2 kV and 3.6 kV. In general, the increase of the system voltage leads to higher overvoltages and the cable versus motor power diagram covers higher surface of 3 per unit and 5 per unit lines. These lines are determined for different arcing times of 50 μs, 100 μs, 200 μs and 500 μs, different chopping currents 1 A, 3 A and 5 A and different clearing abilities of the vacuum circuit breaker of 50 A/μs, 75 A/μs and 100 A/μs. Figure 7-18 through Figure 7-23 is only a selection of the results showing the calculated curves for different arcing time. The results show that the clearing ability is of modest influence on the amplitude of the overvoltage, while the chopping current, the arcing time and the dielectric capability are very important and show high sensitivity to the variation of the overvoltage. For a wide range of cables and motor powers, the arcing times between 50 μs and 200 μs cause high overvoltage with a large number of restrikes. According to the presented results, they cover high surface in the cable-motor power diagram. The switching instant of 500 μs is for all cases not as severe as the other switching instants. The critical area of 3 per unit is small and may exist mainly up to 1 MVA. Above this motor power there is practically no high overvoltage. The 5 per unit area almost vanishes and it only exists for low motor powers in combination with short cable lengths.

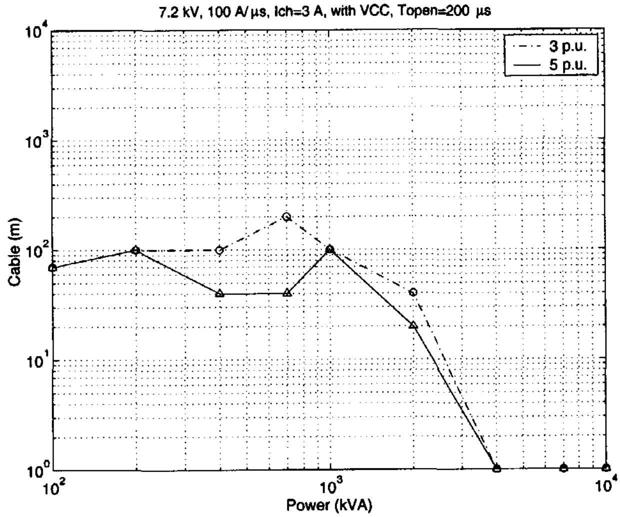

Figure 7-19: The geometrical place of the combination between cable length and motor power resulting in an overvoltage of 3 p.u. or 5 p.u.

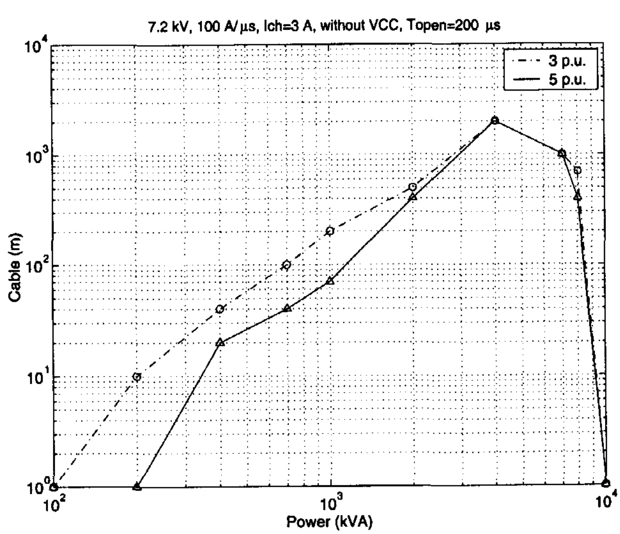

Figure 7-20: The geometrical place of the combination between cable length and motor power resulting in an overvoltage of 3 p.u. or 5 p.u.

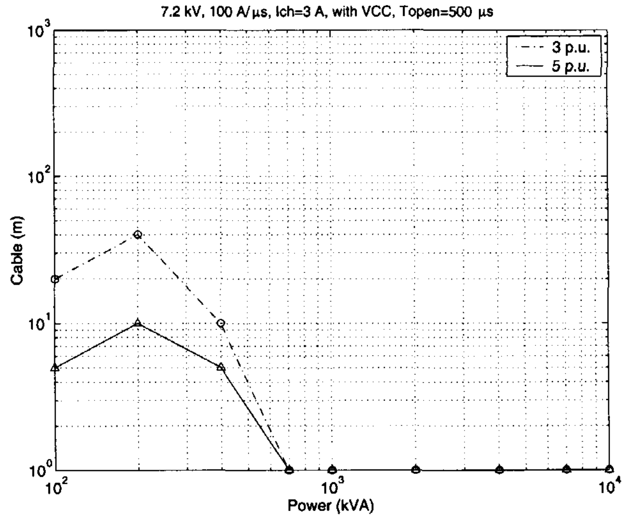

Figure 7-21: The geometrical place of the combination between cable length and motor power resulting in an overvoltage of 3 p.u. or 5 p.u.

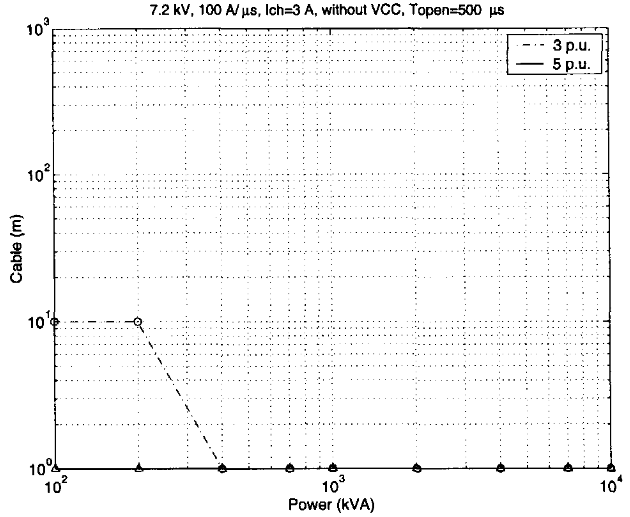

Figure 7-22: The geometrical place of the combination between cable length and motor power resulting in an overvoltage of 3 p.u. or 5 p.u.

7.5 Conclusion

The presented method is a suitable tool for predicting the tendency of overvoltages in motor circuits and circuits with loaded transformers. The calculation of the resulting overvoltages and their variation over time required very detailed models, the parameters of which are very hard to find. However, for calculation the probability of reignition, the simplified models are enough because we need only the instant when the reignition occurs. For the worst case of switching, it is found that:

- the slope of recovery curve is the most important parameter that influences the reignition in the vacuum circuit breaker,
- the chopping current also influences the probability of reignition but it dominates only for low motor powers and for short cable lengths,
- depending on the chosen parameter, the probabilities of P_{VCC} and P_{reig} occurring at high motor powers are close to each other. This is because the reignition which occurs during short arcing times and high motor powers is followed by high frequency currents which can easily cause VCC. The reignition and VCC strongly depend on the capacitive and inductive coupling of the system parameters.

The circuit under study contains no busbars between the vacuum circuit breaker terminals and the cable at the load side. When busbars are present they should be taken into account because during the reignition, the inductance of the busbars plays an important role. The frequency of the TRV depends on this inductance, and it determines the number of reignitions, but for short busbars this factor is irrelevant.

The analysis also concludes with the calculation of the amplitude of overvoltages for different motor powers and cable lengths. The opening time also changes and different curves are drawn depending on the fixed value of this parameter. These curves are in particular important for locations where different motor powers are in use. According to the calculated geometrical place of the combination between the motor power and the cable length it is possible to choose a cable length so the occurrence of the overvoltages during switching motors and loaded transformers can be lower than 3 per unit or 5 per unit.

Chapter 8

General Conclusions and Future Possible Work

8.1 Conclusion

The thesis was motivated by the objective of modelling and finding the conditions under which high overvoltages can be generated through voltage escalation while interrupting a no-load transformer. It was also desired to determine the effect of each circuit element and the interaction of the vacuum circuit breaker with the network. The aim was also to estimate the probability of reignition in low inductive current circuits.

Because of a shortage of field tests and because of complicated circuit conditions particularly with frequency-dependent circuit properties, the approach adopted in this thesis is to simulate the generated overvoltages by a digital computer. The thesis consists of two major parts. First, the model of each system component is presented and its properties are examined and compared with recent investigations. Second, the models are implemented into ATP and applied to simulate different switching conditions.

The cable was represented by means of a currently used model with lumped parameters. This model takes into account the frequency dependency of the cable by applying the conductor and dielectric losses. The use of a lumped inductance for a short busbar for the switching transients study was validated by comparing it with a transmission line model. The transformer model was improved by taking into account the dependency of the transformer in a broad frequency range and it clearly shows the influence of the transformer winding at high frequencies and the influence of the non-linearity of the transformer at low frequencies. Apart from the traditional IEEE surge arrester model, a new simplified surge arrester model is used and it was shown that for the purpose of transients caused by switching surges, this model can be used successfully. Two types of circuit breaker models are applied in this thesis. The first one uses the arc resistance applied by the volt-ampere characteristic when the arc burns, and the second model is based on the withstand capability and clearing ability of the vacuum circuit breaker.

The results of the calculations show that the transformers, which basically have a high BIL, only under special network and switching conditions can be stressed by switching overvoltages that pass that level. Under normal circumstances, the occurrence of high overvoltages is rare, but steep-fronted surges, even ones with a low amplitude can be dangerous for the insulation because of the highly non-linear distribution along the transformer winding. This can accelerate the deterioration of the insulation and result in a shorter lifetime of the transformer. The effect of the surge propagation into the winding was not observed here and it will be a subject for further work.

In general, the problem occurs not because of the imperfection of the vacuum circuit breakers and the load that is being switched, but because of the incompatibility of the circuit breaker and the transformer (or any inductive load) in a specific network arrangement. After the chopping, the transformer as a highly inductive load traps an amount of magnetic energy and this energy results in higher TRV after each reignition. The TRV is always limited by the withstand capability of the circuit breaker if it tends to rise above it. This leads to a gradual build up of higher and steeper overvoltages after each high frequency reignition due to the increase of current in the highly inductive load during the preceding high frequency current. Once a reignition in the circuit breaker occurs, a steep voltage surge proceeds to the transformer terminals that partly reflects and partly enters the transformer winding. A repetitive reignition in the circuit breaker causes a sequence of surges that stresses the transformer winding.

The thesis focuses on a specific system configuration and on specific parameters for the system components, and therefore the results cannot be applied for systems with a similar topology because many parameters influence the reignition overvoltages. No general rule can be given that tells us which of the parameters influencing the possible overvoltage are the most important. Many parameters must be considered in order to come to a reliable conclusion for the overvoltage level in a specific system layout. However, in the last chapter, it was shown that the type of the load and its power plays a significant role. The vacuum circuit breakers are vulnerable to multiple reignitions when they are used to switch motors, and the probability of reignition in general is higher for motors with lower power. Due to the complex modelling of an unloaded transformers and not having data for unloaded transformers for different powers, such analysis was not done.

The analysis of switching overvoltages is very important for insulation coordination. These overvoltages have different origins and an insulation failure can either be caused by the amplitude of the overvoltage, by its rise time or by both. With respect to the protection of the transformer, *R-C* branches provide suppression of both multiple reignitions and overvoltages and also decrease the rise time of the overvoltage, while surge arresters limit the overvoltage to a certain maximum value which is determined by the arrester characteristics.

8.2 Suggestions for future work

The thesis deals with the computation of overvoltages which are generated when switching unloaded transformers under specific network conditions. The possible source of high overvoltages in this and similar network configurations like reactor or motor switching are the multiple reignitions and overvoltages caused by virtual current chopping. Overvoltages caused by multiple reignitions are not as high as the overvoltages due to virtual current chopping because the amplitude is limited by the dielectric recovery of the vacuum gap. However, when reignition occurs, the TRV drops with a very high du/dt to zero. This effect causes a highly non-linear distribution of the voltage along the transformer winding that can damage the transformer insulation. Surge arresters can limit only the amplitude of the overvoltages and steep-fronted switching surges with lower amplitude can still enter the transformer. It can be dangerous when the frequency of the surge matches some of the natural frequencies of the transformer. This causes an internal resonance and it is not a rare case because transformers have many natural frequencies.

The effect of the internal resonances is twofold. Firstly, the voltage at some winding can grow higher than the voltage at the transformer terminal so a flashover from the winding to the core can occur [70]. Secondly, the inter-turn voltage between adjacent windings becomes much higher than the maximal allowable voltage (see list of published papers [9]). Therefore, it is important more work to be done to investigate the propagation of switching surges in transformer windings. A detailed model of the transformer windings capable to represent the distributed overvoltage in distributive transformers is needed. This implies that the transformer parameters should be calculated accurately and the capacitive and inductive coupling between the coils and windings should be taken into account. The inter-turn voltage between adjacent turns should be measured with respect to the frequency in order to find the resonance frequencies. Also, the transformer model must be capable to represent the frequency characteristic of the transformer.

Appendix A

Statistical variation of the breaker parameters

For a normal distribution, the probability of the breakdown voltage V can be represented by equation (A.1) in which the variable V has been transformed into the normalised variable (z):

$$p = \frac{1}{\sqrt{2\pi}\sigma} \int_{-\infty}^{z} \exp(-\frac{z^2}{2}) dz \tag{A.1}$$

where

$$z = \frac{V - \overline{V}}{\sigma} \tag{A.2}$$

$$\overline{V} = \frac{\sum V}{n} \tag{A.3}$$

$n=$ number of tests or energisations

$$\sigma = \left[\frac{\sum \left(V - \overline{V} \right)^2}{n} \right]^{1/2} \tag{A.4}$$

The standard deviation σ is a measure of the scatter or dispersion of the observations (V) about the mean value $(\overline{V})$, while $\sigma/\overline{V}$ is the coefficient of variation (or per unit standard deviation).

If no measured data from a large number of tests are available as in our case, the expression (2.5) or any other expression that should be statistically varied represents the mean value at any instant. For a standard deviation σ =10 %, the calculated probability by expression (A.1) is shown in Figure (A-1).

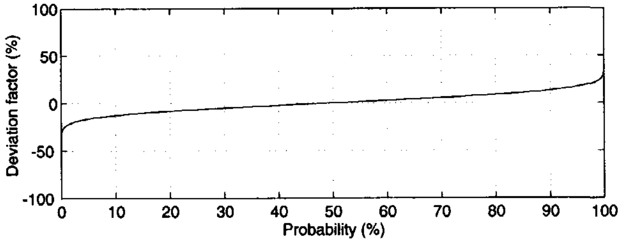

Figure A-1: Normal distribution of the withstand voltage

This curve gives the probability that a deviation factor δ (%) is less than the determined value. So the withstand voltage can be calculated as:

$$V_b = \left(1 + \frac{\delta}{100}\right) \overline{V}_b \tag{A.5}$$

In the calculation, the probability is randomly chosen by means of a random generator that seeds uniformly distributed numbers for the interval [0,1]. Subsequently from Figure (A-1) the corresponding deviation factor δ can be determined and substituted in expression (A.5).

Appendix B

Comparing different breaker models

The vacuum circuit breaker can be modelled by model A or B to study overvoltages due to reignitions. The system under study is depicted in Figure B-1. The 110 kV network is represented by an ideal voltage source, a positive sequence impedance of 4.6 Ω and a zero sequence impedance of 19.37 Ω. The supply is connected via a 20 MVA substation power transformer TR. The transformer supplies a 6.3 kV motor with a power of 1.5 MVA. The transformer and motor are connected by two cables. The first cable has a length of 2.56 km. The second cable is 70 m long and connects the motor to the vacuum circuit breaker. Both cables are separated by a vacuum circuit breaker and 7 m long busbars. The transformer TR is modelled by the BCTRAN routine whilst the long cable is modelled by 16 lumped Π-sections each with a length of 160 m. The short cable is modelled by two 35 m long lumped Π-sections. The parameters of the system components are shown in Table B.1.

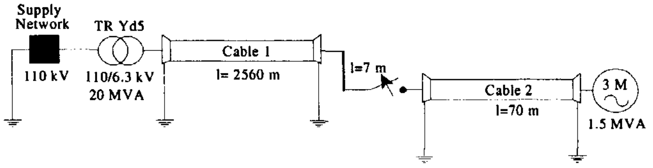

Figure B-1: Three-phase system configuration used for the vacuum circuit breaker model validation

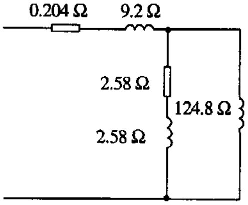

Figure B-2: Representation of the motor by a lumped element

Table B.1: Parameters for the system components

vacuum breaker	chopping current 4 A quenching capability 75 A/μs gap distance 5 mm critical electric field 20 kV/mm speed of contacts 1 m/s	*busbars*	length 7 m R=4 mΩ L=1 μH/m
cable 1	R=0.115 Ω/km L=2.34 mH/km C=0.636 μF/km	*cable 2*	R=0.115 Ω/km L=2.34 mH/km C=0.636 μF/km

The cable parameters are given for each Π-section. The data of the motor parameters at 50 Hz are separately shown in Figure B-2. The dielectric withstand capability of the vacuum circuit breaker is zero at the instant of contact separation. The calculation is done in the following way. The vacuum circuit breaker contacts begin to part at instant t_0, 200 μs before the current chops. At the instant of contact separation, the value of the current to be interrupted is 29 A. The current flows through the arc channel and decreases until the chopping level is reached. When the current is actually chopped the TRV across the vacuum circuit breaker contacts oscillates with a high rate of rise. The rate of rise of the TRV is proportional to the amplitude of the chopping current. At a certain instant, it equals the dielectric withstand capability of the gap and a breakdown occurs. The reignition current through the arc channel contains high frequency components superimposed on a 50 Hz component that flows again from the source side to the load. The results of the calculated load side voltages at the motor terminals and currents through the vacuum circuit breaker poles for models A and B are shown in the Figure B-3 through Figure B-5. At first glance it appears that the TRVs and the

Table B.2: Calculated maximum overvoltages

	phase R	*phase* S	*phase* T
U_A [kV]	10.54	7.97	6.15
U_B [kV]	10.62	8.01	6.28

currents are similar. The current and voltage traces depicted in Figure B-6 and Figure B-7 are enlargements of the previous calculation on a longer time scale. We can see that their shapes are almost the same, and this is because the same network was used for both calculations. The enlarged figures show that there is a slight displacement of the reignited currents and voltages. Figure B-8 shows the reignited voltage in phase R that is a result of the current that clears first. It consist of a chopping overvoltage, being the voltage after interruption of the 50 Hz current, and a restrike overvoltage caused after the reignited current is interrupted. The reignition overvoltage is more severe than the chopping overvoltage because it has a higher amplitude and a steeper rate of rise. In Table B.2, the calculated values of the maximum overvoltages in both phases are presented. The overvoltages for phases S and T are considerably lower than the ones in phase R. The current in the phases S and T is interrupted later and because at that instant, the gap has fully opened, the dielectric capability of the vacuum circuit breaker is large enough to withstand the TRV, so only the chopping overvoltage exists. The other values correspond to the high frequency components which are superimposed on the 50 Hz voltage at the moment when the first phase clears. These traces are shown in Figure B-8.

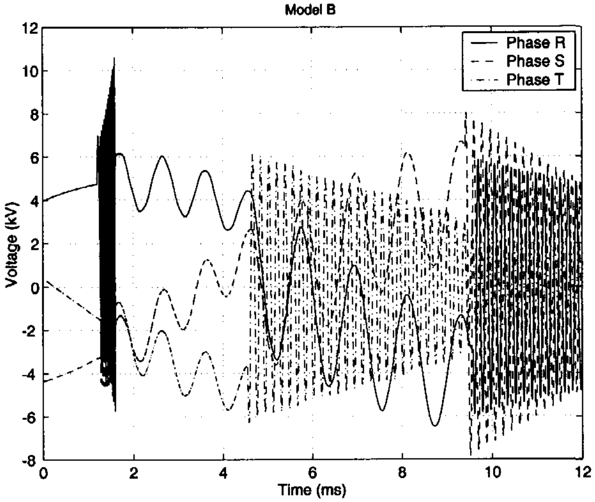

Figure B-3: Voltage at the motor terminals for the system in Figure B-1

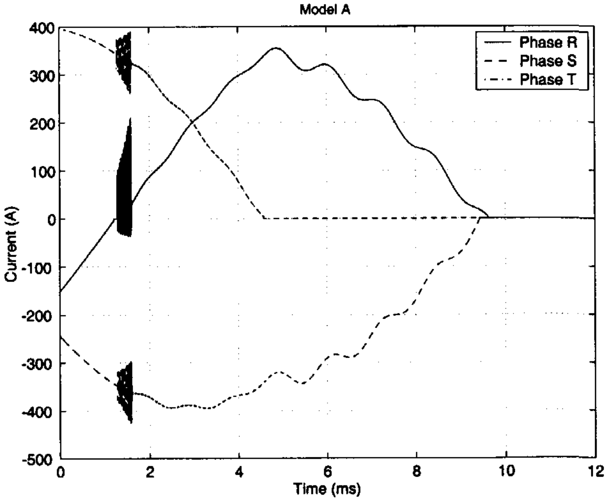

Figure B-4: Current through the circuit breaker for the system in Figure B-1 using model A

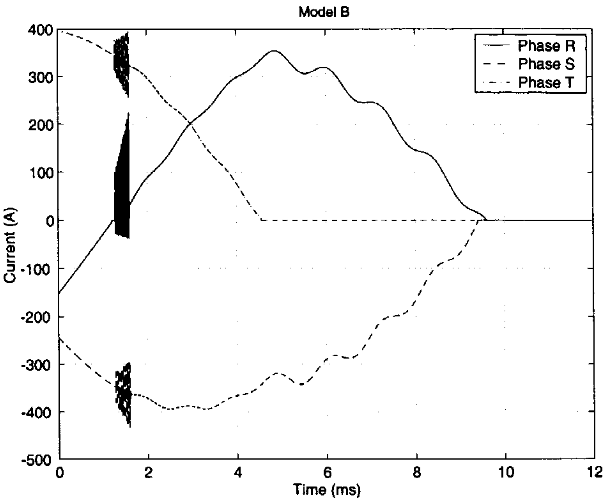

Figure B-5: Current through the circuit breaker for the system in Figure B-1 using model B

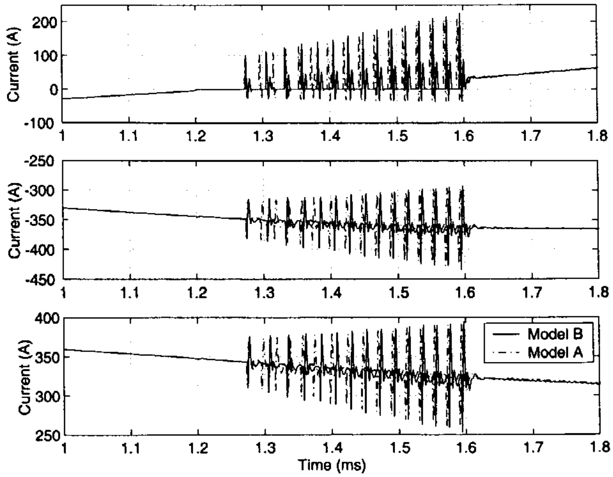

Figure B-6: Reignited breaker's currents for models *A* and *B* for the system in Figure B-1; upper trace: Phase R; middle trace: Phase S; lower trace: Phase T

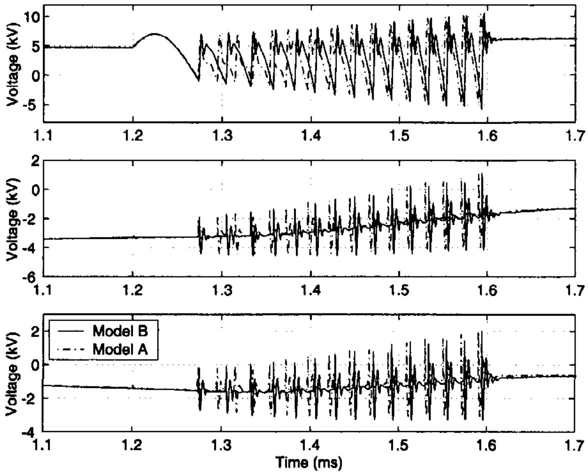

Figure B-7: Motor voltages for models A and B; upper trace: voltage in phase R; middle trace: voltage in phase S; lower trace: voltage in phase S

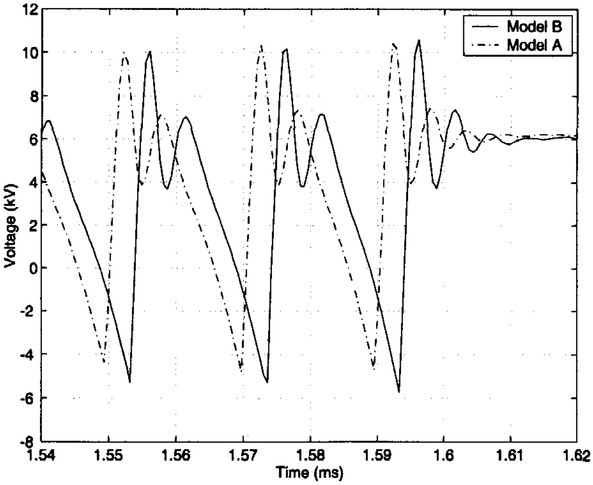

Figure B-8: Motor terminal voltage in phase R from Figure B-7 (last three reignitions)

Bibliography

[1] Avila-Rosales J., Alvarado L.F.: Non-linear Frequency Dependent Transformer Model for Electromagnetic Transient Studies in Power Systems, *IEEE Trans. on Power Apparatus and Systems*, Vol. PAS-101, No. 11, pp. 4281-4288, November 1982.

[2] Boyle D.: Interruption of Currents in No-load, Internal Working Document 24 of CIGRE WG 13.02, *Electra*, 1982.

[3] Boyle D.: Current Chopping Overvoltages Following the Interruption of Transformer No-load Current, *Electra,* No. 133, 1990, pp. 99-107.

[4] Berger M. K.: Switching of Small Inductive Currents, Cigre Colloquium WG 13.02, 1964, pp. 454-460.

[5] CIGRE WG 13.02: Interruption of Small Inductive Currents, Chapter 3, Part A, *Electra* No. 75, pp. 5-30.

[6] CIGRE WG 13.02: Interruption of Small Inductive Currents, Chapter 3, Part B, *Electra* No. 95, pp. 31-44.

[7] CIGRE WG 13.02: Reactor Switching, Limitation of Overvoltages and Testing, *Electra* No. 113, pp. 51-74.

[8] CIGRE WG 13.02: Switching of Reactor-Loaded Transformers, *Electra* No. 138, pp. 51-65.

[9] CIGRE WG 13.02: Interruption of Small Inductive Currents, Chapter 5: Switching of Unloaded Transformers, *Electra*, No. 133, 1990, pp. 79-97.

[10] CIGRE WG 13.02: Part 2, Three-Phase Transformer Interruption, Reignition Phenomena, Test Results and Conclusions, *Electra,* No. 134, pp. 23-44.

[11] CIGRE WG 33.06: Part 5, Metal Oxide Surge Arresters in AC Systems, *Electra,* No. 133, pp. 133-143, 1990.

[12] Cornick K., Kunji A.M.: Nanoseconds Switching Transients Recorded in a Mining Transformer Installation, *IEEE Trans. on Power Delivery,* Vol. 8, No. 3, July 1993, pp. 1130-1137.

[13] Cornick K.J.: Factors Governing the Severity of Prestriking Transients in Motor Systems, *IEE Proceedings,* Vol. 137, Pt. B, No. 1, January 1990, pp. 14-24.

[14] Czarnecki L., Lindmayer M.: Influence of Contact Material Proparties on the Behavior of Vacuum Arcs Around Current Zero, *International Conference on Electrical Contacts, Electromechanical Components and Their Applications,* Nagoya, Japan, July 15-18, 1986.

[15] Czarnecki L., Lindmayer M.: Measurements and Statistical Simulation of Virtual Current Chopping in Vacuum Switches, *XI-th International Symposium on Discharges and Electrical Insulation in Vacuum,* Berlin, GDR, September 1984.

[16] Czarnecki L.: *Einflus Des Kontaktwerkstoffes Auf Stromabris Und Loschung Des Vakuumbogens,* Ph.D. Thesis, TU Braunscheweig, 1986.

[17] Colombo E., et al.: Results of Investigation on the Overvoltages Due to a Vacuum Circuit Breaker when Switching an HV Motor, *IEEE Trans. on Power Delivery,* Vol. 3, No.1, January 1988, pp. 205-213.

[18] Dube L., Bonfanti I.: MODELS: A New Simulation Tool in the EMTP, *ETEP* Vol. 2, No. 1, January/February 1992, pp.45-50.

[19] Dube L.: How to Use MODELS-Based User-Defined Network Components in ATP, *European ATP-EMTP Meeting,* Budapest, 1996.

[20] Dean J.H.B.: Modelling the Dynamics of Nonlinear Inductor Circuit, *IEEE Trans. on Magnetics,* Vol. 30, No. 5, September 1994, pp. 2795-2801.

[21] Damstra G.C.: Virtual Chopping Phenomena, Switching 3-Phase Inductive Circuits, *Colloquium of CIGRE* SC*13*, Helsinki 1981.

[22] Damstra G.C.: Current Chopping and Overvoltages in Relation to System Parameters, CIGRE SC13, Paris, 1964.

[23] Damstra G.C.: Influence of Circuit Parameters on Current Chopping and Overvoltages in Inductive MV Circuits, CIGRE SC13, Paris, 1976.

[24] Durbak W. D.: Zinc-Oxid Arrester Model for Fast Surges, *EMTP Newsletter*, Vol. 5, No. 1, January 1985.

[25] EEUG User Group: *EMTP Course on Overvoltages and Insulation Coordination Studies*, Barcelona, November 12-14, 1997.

[26] Eichenberg, J.P., et al.: Multiple Restrike Phenomenon when Using Vacuum Circuit Breakers to Start Refiner Motors, *Proceedings of IEEE IAS Conference 1998*, pp.266-273.

[27] Fu Y.H., Damstra G.C.: Switching Transients During Energizing Capacitive Load by a Vacuum Circuit Breaker, *IEEE Trans. on Electrical Insulation*, Vol. 28, No. 4, August 1993, pp. 657-665.

[28] Gibbs J.D., Koch D., et al.: Comparision of Performance of Switching Technologies on a Cigre Motor Simulation Circuit, *IEEE Trans. on Power Delivery*, Vol. 4, No. 3, July 1989, pp. 1745-1750.

[29] Gibbs J.D., Koch D., et al.: Investigation of Prestriking Effect and Current Chopping in Medium Voltage SF6, Rotating Arc and Vacuum Switchgear, *IEEE Trans. on Power Delivery*, Vol. 4, No. 1, January 1989, pp. 308-316.

[30] Glinkowski M. et al.: Voltage Escalation and Reignition Behavior of Vacuum Generator Circuit Breakers During Load Shedding, *IEEE Trans. on Power Delivery*, Vol. 12, No. 1, January 1997, pp. 219-226.

[31] Glinkowski M., et al.: Capacitance Switching with Vacuum Circuit Breakers - a Comparative Evaluation, *IEEE Trans. on Power Delivery*, Vol. 6, No. 3, July 1991, pp. 1088-1094.

[32] Greenwood A. *Electrical Transients in Power Systems*, John Wiley & Sons, Inc., ISBN 0-471-62058-0.

[33] Greenwood A., Glinkowski M.: Voltage Escalation in Vacuum Switching Operations, *IEEE Trans. on Power Delivery*, Vol. 3, No. 4, October 1988, pp. 1698-1706.

[34] Greenwood A.: *Vacuum Switchgear*, The IEE Press, 1994.

[35] Grčev L., et al.: Shielding Characteristics of Hysteresis Ferromagnetic Tubular Shields, *Proceedings of International Symposium on EMC*, Rome, Italy, September 17-20, 1996.

[36] Hall W.: *Vacuum Interrupter Technology*, Rerolle - Rolce Royce Report.

[37] Helmer J., Lindmayer M.: Mathematical Modeling of the High Frequency Behavior of Vacuum Interrupters and Comparison with Measured Transients in Power Systems, *XVII-th International Symposium on Discharges and Electrical Insulation in Vacuum*, Berkley, California, USA, July 21-26, 1996, pp. 1-9.

[38] Helmer J.: *Hochfrequente Vorgange-Zwischen Vakuum - Schaltstrecken Und Dreiphasigen Kreisen*, Ph.D. Thesis, TU Braunscheweig, 1996.

[39] Helmer J., Lindmayer M.: A Hysteresis Model for Transient Calculations, *European ATP-EMTP Meeting*, November 7-8th 1994, Hannover.

[40] Hevia O.: Sources of Type Inpulse in the ATP, *European EMTP User Group (EEUG) News*, November 1998.

[41] Jiles D.C., et al.: Numerical Determination of Hysteresis Parameters for Modeling of Magnetic Properties Using the Theory of Ferromagnetic Hysteresis, *IEEE Trans. on Magnetics*, Vol. 28, No. 1, January 1992, pp. 27-35.

[42] IEEE WG 3.4.11: Modelling of Metal Oxide Surge Arresters, *IEEE Trans. on Power Delivery,* Vol. 7 No. 1, January 1992, pp. 302-309.

[43] Ihara S., Panek J. Tuohy E.J.: Chopping of Transformer Magnetizing Currents, Part II: Three-Phase Transformers, *IEEE Trans. on Power Apparatus and Systems,* Vol. PAS-102, No. 5, May 1983, pp. 1106-1114.

[44] Itoh T., et al.: Voltage Escalation in the Switching of the Motor Control Circuit by the Vacuum Contactor, *IEEE PES Winter Meeting, T-72 053-2,* New York, Jan. 30 - Feb. 4, 1972.

[45] Koreman C.G.A.: Determination of the Magnetizing Characteristics of Three-Phase Transformers in Field Tests, *IEEE Trans. on Power Delivery,* Vol. 4, No. 3, July 1989, pp. 1779-1785.

[46] Kosmač J., Žunko P.: A Statistical Vacuum Circuit Breaker for Simulation of Transient Overvoltages, *IEEE Trans. on Power Delivery,* Vol. 10, No. 1, January 1995, pp. 294-300.

[47] Kind D., Feser K.: *Hochspannungs-Versuchstechnik,* Friedr. Vieweg&Sohn Verlagsgesellschaft mbH, Braunschweig/Wiesbaden, 1995, ISBN 3-528-43805-3.

[48] Legros W., et al.: Vacuum Circuit Breaker Modeling at Interruption of Small Inductive Currents, *European ATP-EMTP Meeting,* October 17-18, 1988, Leuven.

[49] Ma Z., et al.: An Investigation Of Transient Overvoltage Generation when Switching High Voltage Shunt Reactors by SF6 Circuit Breaker, *IEEE Trans. on Power Delivery,* Vol. 13, No. 2, April 1988, pp. 472-479.

[50] Murano M., Yanabu S., et al.: Current Chopping Phenomena of Medium Voltage Circuit Breakers, *IEEE Trans. on Power Apparatus and Systems,* Vol. PAS-96, No. 1, Jan/Feb 1977, pp. 143-149.

[51] Ma Z.: *Reactor Current Switching With Gas Blast Circuit Breakers,* Ph.D. Thesis, Stafford University, March 1996.

[52] Matsui Y., et al.: Reignition Current Interruption Characteristics of the Vacuum Interrupter, *IEEE Trans. on Power Delivery*, Vol. 3, No. 4, October 1988, pp. 1672-1677.

[53] Meyer S., Liu T.H.: *ATP Rule Book*, BPA, 1992.

[54] Marti J.: Accurate Modelling of Frequency-Dependent Transmission Lines in electromagnetic Transient Simulations, *IEEE Trans. on Power Apparatus and Systems*, Vol. PAS-101, No. 1, January 1982, pp. 147-157.

[55] Moore A.H., Blalock T.J.: Extensive Field Measurements Support New Approach to Protection of Arc Furnace Transformers Against Switching Transients, *IEEE Trans. on Power Apparatus and Systems*, Vol. PAS-94, No. 2, March/April 1975, pp. 473-481.

[56] Nishikawa H., et al.: A Method of Evaluating a Circuit Breaker for a Capacitor Bank and Supression of Restrike Overvoltage, *IEEE Trans. on Power Apparatus and Systems* , Vol. PAS-102, No. 6, June 1983, pp. 1574-1581.

[57] Ohashi H. et al: Application of Vacuum Circuit Breaker to Dry Type Transformer Switching, *IEEE PES Winter Meeting*, New York, A76 174-3, 1976.

[58] Ohashi H. et al: Switching Surge and Application of Vacuum Contactors and Vacuum Circuit Breakers, *IEEE PES Winter Meeting*, New York, A76 174-3, 1976.

[59] Pinceti P., Giannettoni M.: A Simplified Model for Zinc Oxide Surge Arresters, *IEEE Trans. on Power Delivery*, Vol. 14, No. 2, pp. 393-397, April 1999.

[60] Panek J., Fehrle K.G.: Overvoltage Phenomena Associated with Virtual Current Chopping in Three Phase Circuits, *IEEE Trans. on Power Apparatus and Systems*, Vol. PAS-94, No. 4, July/August 1975, pp. 1317-1325.

[61] Perkins J.F.: Evaluation of Switching Surge Overvoltages on Medium Voltage Power Systems, *IEEE Trans. on Power Apparatus and Systems*, Vol. PAS-101, No. 6, June 1982, pp. 1727-1733.

[62] Popov M. et al.: An Analyses of Transient Phenomena due to Switching off Low Inductive Currents with a Vacuum Circuit Breaker, *UPEC '97, Manchester, UK,* pp. 170-173.

[63] Popov M., Acha E.: Overvoltages due to Switching off an Unloaded Transformer with a Vacuum Circuit Breaker, *IEEE Trans. on Power Delivery,* Vol. 14, No. 4, October 1999, pp.1317-1326.

[64] Popov M.: A Vacuum Circuit Breaker Arc Model for Digital Simulation of Transient Phenomena, *Proceedings of the Faculty of Electrical Eng.*, Skopje, 1998, pp. 47-53 (in Macedonian).

[65] Popov M.: Digital Simulation of Low-Inductive Current Switching with a Vacuum Circuit Breaker, *2^{nd} Meeting of MAKO CIGRE,* 23-25 September, Struga, 1998 (in Macedonian).

[66] Popov M.: *SF6 and Vacuum Circuit Breaker Arc Models for Analyses of Transient Phenomena when Switching off Different Loads,* M.Sc Thesis, Faculty of Electrical Engineering, Skopje, 1998 (in Macedonian).

[67] Popov M.: Switching off an Unloaded Transformer with a Vacuum Circuit Breaker, *2^{nd} Meeting of MAKO CIGRE,* 23-25 September, Struga, 1998 (in Macedonian).

[68] Pretorius R.E.: Optimised Surge Suppression on High Voltage Vacuum Contactor Controlled Motors, *IEE Publication 210,* pp.65-70, 1982.

[69] Pretorius R.E., Eriksson A.J.: Field Studies of Switching Surge Generation in High Voltage Vacuum Contactor Controlled Motors - Results of Extensive Practical Investigations, *IEE Publication 210,* pp.59-65, 1982.

[70] Paap G. C., Alkema A. A., van der Sluis L.: Overvoltages in Power Transformers Caused by No-load Switching, *IEEE Trans. on Power Delivery,* Vol. 10, No. 1, pp. 301-307, January 1995.

[71] Roguski T. A.: Experimental Investigation of the Dielectric Recovery Strength Between the Separating Contacts of Vacuum Circuit Breaker, *IEEE Trans. on Power Delivery,* Vol. 4, No. 2, pp. 1063-1069, April 1989.

[72] Reininghaus U.: *Schaltverhalten Unterschiedlicher Kontaktwerkstoffe in Vacuum*, Ph.D. Thesis, TU Braunschweig, 1983.

[73] Smeets R.P.P., et al.: Essential Parameters of Vacuum Interrupter and Circuit Related to the Occurrence of Virtual Current Chopping in Motor Circuits, *International Symposium on Power and Energy*, Sapporo, Japan, 1993.

[74] Smeets R.P.P., Kardos R.C.M.: Overspanningen bij Het Schakelen Van Motoren Met Vacuumschakelaars, *Energietechniek* 2, jaargang 72, Februari 1994, pp. 104-111 (in Dutch).

[75] Smeets R.P.P.: *Low Current Behavior and Current Chopping of Vacuum Arcs*, Ph.D. Thesis, University Of Eindhoven, 1987.

[76] Smeets R.P.P.: Switching Surges Associated With Vacuum Interrupters in Motor Circuits, *CEPSI Conference*, Kuala Lumpur, 1996.

[77] Smeets R.P.P., van der Wen W.J., Watanabe K.: Vacuum Arc Lifetime Extension at Small Gaplength: Beneficial for Low-Surge Circuit Interruption, *International Conference on Gas Discharges and Their Applications*, Tokyo, 1995.

[78] Schmidt W., et al.: Behaviour of MO-Surge-Arrester Blocks to Fast Transients, *IEEE Trans. on Power Delivery*, Vol. 4, No. 1, pp. 292-300, January 1989.

[79] Slade G. P.: Vacuum Interrupters: The New Technology for Switching and Protecting Distribution Circuits, *IEEE Trans. on Industry Application*, Vol. 33, No. 6, November/December 1997, pp.1501-1511.

[80] Soysal A. O.: A Method for Wide Frequency Range Modelling of Power Transformers and Rotating Machines, *IEEE Trans. on Power Delivery*, Vol. 8, No. 4, October 1993, pp. 1802-1810.

[81] Soysal A. O.: Protection of Arc Furnace Supply Systems From Switching Surges, Proceedings of 1999 *IEEE PES Winter Meeting*, 31 January-4 February 1999, New York, NY, Vol. 2, pp. 1092-1095, ISBN 0-7803-4893-1.

[82] Tuohu E.J., Panek J.: Chopping of Transformer Magnetizing Currents, Part I: Single Phase Transformer, *IEEE Trans. on Power Apparatus and Systems*, Vol. PAS-97, No.1, January / February 1978, pp. 261-268.

[83] Ueno N., et al.: Monte-Carlo Simulation of Overvoltage Generation in the Inductive Current Interruption by Vacuum Interrupters, *IEEE Trans. on Power Apparatus and Systems*, Vol. PAS-103, No. 3, March 1984, pp. 498-505.

[84] Van den Heuvel W.M.C.: Overvoltages After Current Chopping in Three-Phase Inductive Circuit with Isolated Neutral, *IEEE Trans. on Power Apparatus and Systems*, Vol.-100, No.12, December 1981, pp. 4795-4801.

[85] Van den Heuvel, et al.: Interaction between Phases in Three-Phase Reactor Switching, Grounded Reactors, Part I, *Electra,* No. *91*, pp. 11-50.

[86] Van den Heuvel W.M.C., et al.: Interaction between Phases in Three-Phase Reactor Switching, Ungrounded Reactors, Part I, *Electra* No. *112*, pp. 57-81.

[87] Van den Heuvel W.M.C., et al.: Interruption of a Dry Type Transformer in No-Load by Vacuum Circuit Breaker, *EUT-Report 83-E-141* (1983), TU Eindhoven.

[88] Van den Heuvel W.M.C., Damstra G.C.: Current Chopping and Overvoltages in MV and HV inductive circuits, *Colloquium of CIGRE SC13*, Sarajevo 1989.

[89] Van der Sluis L.: *Transients in Power Systems*, John Wiley & Sons Ltd, ISBN 0-471-48639-6.

[90] Von S. Wenger: Versuche Zur Ermittlung Von Uberspannungen beim Schalten von Hochspannungsmotoren, *ELIN-Zeitschrift 1986, Heft* $\frac{1}{2}$, pp. 8-16.

[91] Veuhoff F.W., Elwardt J.: Vacuum Circuit Breaker Model in ATP-EMTP for the Examination of Multiple Reignitions in Inductive Circuits, *European ATP-EMTP Meeting*, November 8-10th 1999, Gizzeria Lido, Italy, pp. 47-54.

List of published papers

1. Popov M., van der Sluis L., Paap G. C., Schavemaker P.H.: On a Hysteresis Model for Transient Analysis, *IEEE Power Engineering Review*, Vol. 20, No. 5, May 2000, pp. 53-54.
2. Popov M, van der Sluis L., Paap G. C., Schavemaker P.H. : On the Calculation of Transients in Circuits with Stiff Non-linear Elements, *ICEM*, Espoo, Finland, August 28-30, 2000, pp. 267-271.
3. Popov M, van der Sluis L.: Comparison of Two Vacuum Circuit Breaker Models for Small Inductive Current Switching, *XIX Symposium on Discharges and Electrical Insulation in Vacuum*, Xi'an, China, September 18 - 21, 2000.
4. Popov M., van der Sluis L., Paap G. C.: A Simplified Transformer Model for the Simulation of Fast Surges and Adequate Protection Measures, *IEEE PES Winter Meeting 2001*, 2001WM038, 27 January - 1 February, Columbus OH.
5. Popov M., Acha E.: Overvoltages due to Switching off an Unloaded Transformer with a Vacuum Circuit Breaker, *IEEE Trans. on Power Delivery*, Vol. 14, No. 4, October 1999, pp.1317-1326.
6. Popov M., van der Sluis L.: Improved Calculations for No-load Transformer Switching Surges, *IEEE Trans. on Power Delivery,* Vol. 16, No. 3, July 2001, pp. 401-408.
7. Popov M., van der Sluis L., Paap G.C.: Investigation of the Circuit Breaker Reignition Overvoltages Caused by No-Load Transformer Switching Surges, *European Transactions of Electrical Power (ETEP)*, Vol.11, No.6, November/December 2001, pp. 413-422.
8. De Herdt H., Lopez-Roldan J., Sels T., van Dommelen D., Popov M., van der Sluis L.: Analysis, Simulation and Testing of Transformer Insulation Failures Related to Switching Transients Overvoltages, *CIGRE* 2002, Paris.
9. Popov M., van der Sluis L., Paap G.C., de Herdt H.: Computation of Very Fast Transient Overvoltages in Transformer Windings, Paper TPWRD-00109-2002 (to be published in *IEEE Trans. on Power Delivery*)

Summary

Electrical power systems are subjected to many types of disturbances that result in electrical transients such as lightning, clearing faults or routine switching operations like line energisation and de-energisation, the opening of disconnectors and switching of inductive and capacitive loads.

When a sudden change of state occurs, for instance a system fault or an operation of a circuit breaker, the electric and magnetic energy stored in the capacitive and inductive elements of the network is redistributed. This redistribution of energy cannot occur instantaneously and the power system must go through a transient state before it reaches a new steady state. In principle, it is possible to explain the transients qualitatively and to calculate them quantitatively by the classical laws of electromagnetism and by applying circuit analysis. There are many circumstances which can effectively influence the transients. These factors can originate from the actual values of the circuit elements, the characteristics of the equipment, the network configurations, and from the interaction between the circuit elements themselves. In medium voltage and high voltage circuits, the transients caused by operation of the circuit breaker sometimes produce overvoltages which can even be several times higher than the nominal voltage of the system. An overvoltage is a phenomenon the occurrence of which is sometimes inevitable. It is an unwanted phenomenon because it can cause considerable problems for the insulation and the system in general. Therefore, it is necessary to study its origin and to find ways to prevent and eliminate it. Overvoltages can be with different shapes, and an insulation failure can be caused either by the transients amplitude, the transients rise time or both.

This thesis deals with the calculation and estimation of the switching overvoltages which are produced during the interruption of a transformer with a vacuum circuit breaker. For this purpose, the system components are analysed and adequate models

are developed. Due to the switching surges, the response of the network is different for different frequencies of transient oscillations, so the system is modelled such that it takes into account the frequency-dependent behaviour of the components.

The thesis shows that for this particular transformer, the interruption of magnetising currents does not create problems that are too severe. Because of the very low magnetising currents ($\sim$0.1 A), the chopping overvoltage hardly rises fast enough to cause a reignition in the vacuum circuit breaker. However, in general, the numerical analyses show that when the magnetising currents of the transformer are higher, depending on the residual flux of transformer core and its dynamic hysteresis, overvoltages can reach a value of even 5 per unit. This occurs in particular when the transformer is disconnected at the peak of the magnetising current. The interruption of transient currents can result in virtual current chopping. This means an interruption of a current due to reignition of a current in a different phase. When this happens, the characteristics of the vacuum circuit breakers are important. A vacuum circuit breaker with a typical high dielectric withstand capability might cause high overvoltages at the transformer terminals and across the contacts when reignition takes place. There are many parameters influencing the transient oscillations after current interruption. Therefore, an analysis is undertaken on a statistical basis. The cumulative probability of overvoltage occurrence and of reignitions for different vacuum circuit breaker characteristics are calculated as well.

In this thesis, an overview of the available surge arrester models is given. With the help of a digital surge arrester model, simulations are done with surge arresters connected to the transformer terminals in different ways. The protection by means of R-C suppression circuit is analysed as well, and an optimal choice of the resistance and capacitance is studied.

Samenvatting

Elektriciteitsvoorzieningssystemen worden regelmatig blootgesteld aan veel typen storingen die resulteren in elektrische transiënten ten gevolge van bijvoorbeeld blikseminslag, afschakelen van een fout of ten gevolge van een routinematige schakelhandeling zoals het schakelen van inductieve en capacitieve belastingen.

In geval van een wijziging van de topologie van het net vindt een herverdeling plaats van de energie die is opgeslagen in capacitatieve en inductieve netwerkelementen. Deze herverdeling van energie kost tijd en voordat het systeem de nieuwe stationaire toestand bereikt, vinden overgangsverschijnselen plaats. De transiënten kunnen kwalitatief worden begrepen en kwantitatief worden berekend door gebruikmaking van de klassieke wetten van het elektromagnetisme en van de netwerktheorie. Het verloop van transiënten is afhankelijk van de beginvoorwaarden en de parameters van het netwerk met zijn componenten.

In midden- en hoogspanningscircuits produceren de transiënten als gevolg van de schakelhandeling overspanningen die kunnen oplopen tot een veelvoud van de nominale bedrijfsspanning. Het optreden van overspanning is soms onvermijdelijk. Het is een ongewenst verschijnsel dat aanzienlijke problemen kan veroorzaken voor de isolatie en voor het systeem in algemeen.

Het is daarom noodzakelijk om de oorsprong van een overspanning te bestuderen en het optreden ervan indien mogelijk te voorkomen of de gevolgen te beperken. De vorm van de overspanning varieert en zowel de duur als de amplitude van overspanning kunnen leiden tot beschadiging van de isolatie.

Het proefschrift behandelt het berekenen en schatten van de overspanning die wordt geproduceerd tijdens het afschakelen van een transformator met een vacuümschakelaar. Voor dit doel worden de componenten van het systeem geanalyseerd en geschikte modellen ontwikkeld. Afhankelijk van het schakelverschijnsel varieert de respons van het netwerk voor de verschillende frequenties van de transiente oscillaties. Daarom wordt het systeem op een zodanige wijze gemodelleerd dat rekening gehouden wordt met de frequentieafhankelijkheid.

Uit het proefschrift blijkt dat voor de hier onderzochte transformator de onderbreking van de magnetiseringsstroom niet leidt tot grote problemen. Aangezien de magnetiseringsstroom klein is (~0.1 A), stijgt de overspanning niet snel genoeg om een herontsteking in de vacuümschakelaar te doen optreden. Uit numerieke berekeningen blijkt dat wanneer de magnetiseringstroom groter is, overspanningen kunnen optreden met een amplitude tot 5 per unit. De hoogte van deze overspanningen hangt af van de remanente flux en de dynamische hysterese van de kern van de transformator. Het onderbreken van transiente stromen kan leiden tot virtuele chopping. Dit is onderbreken van een stroom ten gevolge van de herontsteking van de stroom in een andere fase. Bij het optreden van dit verschijnsel zijn de karakteristieken van de vacuümschakelaar van groot belang. Een vacuümschakelaar met een hoge diëlektrische sterkte kan hoge overspanningen veroorzaken op de klemmen van de transformator en de kontakten van de schakelaar wanneer herontsteking plaats vindt. Er zijn veel parameters die de transiënte oscillaties na stroomonderbreking beïnvloeden. Daarom worden statistische methoden toegepast om de cumulatieve waarschijnlijkheid van het optreden van overspanningen en herontstekingen voor verschillende karakteristieken van vacuümschakelaars te berekenen.

In dit proefschrift wordt een overzicht van de bestaande hoogspanningsafleiders gegeven. Met behulp van een digitaal model van een hoogspanningsafleider zijn simulaties uitgevoerd, waarbij de hoogspanningsafleiders op verschillende manieren op de klemmen van de transformator zijn aangesloten. Het onderdrukken van de overspanning met een serieschakeling van een weerstand en een capaciteit is eveneens onderzocht en de optimale waarde voor de weerstand en de capaciteit van het R-C circuit zijn vastgesteld.

Abstrakt

Elektroenergetskite sistemi se izloženi na najrazlični vidovi perturbacii kako što se udar na molnja, isklučuvanje na kusi vrski ili vklučuvanje i isklučuvanje na prekinuvači i rastavuvači, kako i isklučuvanje na induktivni i kapacitivni optovaruvanja koi rezultiraat vo električni tranzienti.

Pri pojava na nenadejna promena na sostojbata vo mrežata, na primer kusa vrska ili isklučuvanje (vklučuvanje) na prekinuvač, doađa do preraspredelba na električnata i magnetnata energija koncentrirana vo kapacitivnite i induktivnite elementi na mrežata. Preraspredelbata na energija ne može da nastane momentalno i energetskiot sistem mora da pomini niz tranzienten proces pred da ja postigne novata stacionarna sostojba. Tranzientite e možno da se objasnat kvantitativno i presmetat kvalitativno so primena na klasičnite zakoni na elektromagnetika i analizata na kola. Postojat mnogu faktori koi vlijaat na tranzientite. Tie proizleguvaat od vrednostite na elementite na mrežata i nejzinata konfiguracija, karakteristikite na opremata, kako i od interakcijata pomeđu poedini elementi vo mrežata. Vo srednonaponskite i visokonaponskite mreži, tranzientite koi se predizvikani od isklučuvanje na prekinuvač možno e da predizvikaat prenaponi koi se i nekolku pati pogolemi od nominalniot napon na mrežata. Prenaponite se fenomeni čija pojava e ponekogaš neizbežna. Toa se nepoželni fenomeni koi može da predizvikaat značajni problemi vo izolacijata na sistemot. Zatoa, potrebno e da se ispita nivnoto nastanuvanje kako i da se najde način toa da se spreči i eliminira. Prenaponite može da imaat najrazlična forma i probiv na izolacijata može da bide predizvikan kako od nivnata amplitudata taka i od nivnata brzina na porast.

Ovaa disertacija glavno dava prilog vo presmetuvanje i ocenuvanje na prenaponite pri isklučuvanje na transformator so vakuumski prekinuvač. Za ovaa cel, analizirani se komponentite na sistemot i razvieni se adekvatni modeli. Pri postoenje na komutacioni

prenaponi, energetskiot sistem reagira različno pri različni frekvencii na tranzientnite oscilacii, pri što sistemot e modeliran taka što ja zema vo predvid frekventnata zavisnost na komponentite.

Ovaa disertacija pokažuva deka za istražuvaniot transformator, isključuvanjeto na strui na magnetiziranje ne predizvikuva golemi problemi. Poradi mnogu malite strui na magnetiziranje (~0.1 A), povratniot napon ne rasti dovolno brzo za da predizvika povtorno palenje na lakot vo prekinuvačot. Kako i da e, numeričkite analizi pokažuvaat deka koga struite na magnetiziranje na transformatorot se pogolemi, zavisno od remanentniot fluks vo jadroto na transformatorot i negoviot dinamički histerezis, prenaponite može da dostignat vredonosti i do 5 pati pogolemi od nominalniot napon. Ova posebno se slučuva koga strujata se isključuva vo momentot koga ima maksimalna vrednost. Isključuvanje na tranzientni strui (strui na puštanje) može da predizvika virtuelno otsečuvanje na strujata. Ova znači prekinuvanje na strujata vo edna faza poradi povtorno palenje na lakot vo prekinuvačot vo druga faza. Pri ovaa pojava, karakteristikite na prekinuvačot se od golema važnost. Vakuumski prekinuvač so golema dielektrična cvrstina može da predizvika golemi prenaponi na klemite od transformatorot kako i na kontaktite od prekinuvačot pri pojava na povtorno palenje. Postojat mnogu parametri koi vlijaat vrz tranzientnite oscilacii po prekinuvanjeto na strujata. Zatoa e realizirana statistička analiza i e presmetana kumulativnata verojatnost na pojava na prenaponi i povtornoto palanje na lakot za različni karakteristiki na vakuumski prekinuvači.

Vo ovaa disertacija, napraven e pregled na dosegašnite razvieni modeli na odvodnici na prenapon. So pomoš na digitalen model na odvodnik na prenapon, napraveni se simulacii so odvodnici na prenaponi povrzani na klemite od transformator na različni načini. Zaštitata od prenaponi so pomoš na R-C granka e isto taka analizirana, i ispituvan e optimalniot izbor na soodvetnata otpornost i kapacitet na grankata.

Acknowledgements

Since this is neither a speech for a Nobel price nor an Oscar nomination, the acknowledgements to the persons who mostly contributed to this work should not be short.

First of all I want to express my gratitude to the only existing God for giving me the health, power and luck required to fulfill this work. I want to thank my supervisor Prof. ir. Lou van der Sluis for providing me a Ph.D position at TU Delft and being a great adviser.

Many thanks go to all employees in the Power Systems group for their support and help which was always available, and for the pleasant working atmosphere in the group. Infinite thanks go to Dr. G. C. Paap for the enthusiastic and heated discussions about how to model the transformer, for co-authoring some of my papers as well as for giving many other ideas during this work. I want to thank Mr. G. Schoonenberg and Holec-Hengelo who offered a project for vacuum circuit breaker switching and partly supported this work financially. Thanks to Mrs. Mirjam Nieman for proofreading the thesis.

Numerous thanks to Mr. Francisco Javier Peñaloza Sánchez from the Lab branch (LAPEM) of Mexico's CFE for providing some measurement data for my models. Lots of thanks to Prof. Orlando Hevia from the Universidad Tecnologica National, Facultat Regional Santa Fe, Argentina, for helping me resolve all possible existing problems with the ATP and suggestions how to implement some models. I highly appreciate some suggestions from Prof. dr. R.P.P. Smeets from KEMA labs; a great person ready to share research views in this field.

Many thanks to two persons. To Dr. Janko Kosmač from Electroinstitute "Milan Vidmar", Slovenia, for suggesting me to start using ATP and offering me help in modelling system components, and to Prof. Michael T.C. Fang from the University of Liverpool, for his recommendation to join TU Delft and for his words *"work hard and prove that* *my recommendation was right".*

I want to thank my colleagues at the University of Skopje, Faculty of Electrical Engineering. Special thanks go to the Institute of Power Plants and Substations and the Laboratory of Relay Protection where I worked for 5 years and acquired a lot of knowledge in electrical engineering.

My endless gratitude goes to my parents, my brother and my parents-in-law for all their love, support, encouragement throughout all these years, for making me morally strong and for being great advisers that show the right way at any time. Incomparable and infinite thanks to my wife Elizabeta for her great understanding during the time while I was apart from her, and for her superhuman energy that inspired everything I have done so far. Last but not least, warmest thanks to my daughter Veronika for making me the happiest father just before this project was completed. This thesis is dedicated to them.

Curriculum vitae

Marjan Popov was born on April 30, 1969 in Kavadarci, Macedonia. He finished his primary and secondary education in his place of birth and in 1988 he enrolled at the Department of Electrical Engineering of the University of Skopje. During his studies, Mr. Popov's outstanding achievements were acknowledged. He finished his undergraduate program in 1993 with his final project "Computation of Fault Currents Responsible for Modelling of Grounding Systems in High Voltage Substations". Until 1998, he worked as a teaching and research fellow at the Faculty of Electrical Engineering, in the group of Power Plants, Substations and Relay Protection. He taught courses like fundamental electrical engineering, and high-voltage substation and relay protection. At the same time, he did part time postgraduate studies in the field of transients in power systems and high voltage substations and in 1998 he graduated with the thesis "Modelling of SF6 and Vacuum Circuit Breakers for an Analysis of Transients During Switching off Different Types of Loads". In 1997 he was a research assistant at the University of Liverpool performing research and receiving training in the field of SF6 arcs. From 1998 he has been with the TU Delft, to work on his Ph.D. project and to give lectures and instruction in Linear Algebra and Grounding and Protection in Power Systems. He has been an IEEE member since 1995.

Avtobiografija

Marjan Popov e roden na 30 April 1969 godina vo Kavadarci, Makedonija. Osnovno i sredno obrazovanie ima završeno vo rodnoto mesto, a vo 1988 se zapišuva na Elektrotehničkiot fakultet vo Skopje. Za vreme na studiite e sekogaš nagraduvan za postignati odlicni rezultati vo tekovnata godina. Na elektrotehničkiot fakultet diplomira vo 1993 godina so diplomska rabota "Strui na kusi vrski merodavni za dimenzioniranje na zazemjuvači vo razvodni postrojki ". Do 1998 godina raboti na elektrotehničiot fakultet na rabotno mesto pomlad asistent i izveduva vežbi po predmetite elektrotehnika, razvodni postrojki i relejna zaštita. Vo isto vreme, posetuva post-diplomski studii od oblasta na tranzienti vo energetski sistemi i razvodni postrojki i vo 1998 godina magistrira so magisterski trud "Modeliranje na SF6 i vakuumski prekinuvači za analiza na preodnite pojavi pri isključuvanje na različni optovaruvanja". Vo 1997 godina raboti kako asistent iztražuvač na univerzitetot vo Liverpool kade raboti na poleto na modeliranje na SF6 lak. Od 1998 godina e vraboten na tehničkiot univerzitet vo Delft kade raboti na doktorskata disertacija i izveduva nastava po linearna algebra i zazemjuvanje i zaštita. Člen e na IEEE od 1995 godina.